JOURNAL OF APPLIED PHYSICS

JOURNAL
OF
APPLIED PHYSICS

Vol. 16, No. 6 JUNE, 1945

In This Issue

Page

Contributed Original Research

Mechanics of the Metal Cutting Process. II. Plasticity Conditions in Orthogonal Cutting M. EUGENE MERCHANT 318

Frictional Properties of Some White Metal Bearing Alloys: The Role of the Matrix and the Hard Particles D. TABOR 325

High Temperature, High Pressure Rheometer for Plastics H. K. NASON 338

Relationship Between the Rheological Properties and Working Properties of Printing Inks ROLF BUCHDAHL AND JOAN E. THIMM 344

Electromagnetic Field Inside a Cylinder with a Gap C. C. WANG 351

Convection Currents in a Porous Medium C. W. HORTON AND F. T. ROGERS, JR. 367

Pigment Dispersion Methods for Electron Microscopy H. C. O'BRIEN, JR. 370

In Every Issue

News from Here and There 315

New Booklets 317

New Books 317

Index to Advertisers xxx

BOARD OF EDITORS

ELMER HUTCHISSON, *Editor*

Associate Editors

R. B. BARNES
OTTO BEECK
W. F. BUSSE
S. H. CALDWELL
CLARK GOODMAN
SELIG HECHT
W. J. LYONS
MORRIS MUSKAT
THOMAS H. OSGOOD
PAUL E. SABINE
FREDERICK SEITZ
J. R. TOWNSEND

Publication of the
American Institute of Physics

ADMINISTRATIVE STAFF

HENRY A. BARTON, *Director*

MADELINE M. MITCHELL, *Publications Manager*

JOHN T. TATE, *Adviser on Publications*

GOVERNING BOARD

PAUL E. KLOPSTEG, *Chairman*

WALLACE WATERFALL, *Secretary*

GEORGE B. PEGRAM, *Treasurer*

T. D. COPE
R. B. DOW
L. A. DUBRIDGE
FLOYD A. FIRESTONE
HARVEY FLETCHER
R. C. GIBBS
K. S. GIBSON
HERMANN MARK
A. G. WORTHING
JOHN T. TATE
L. W. TAYLOR
N. W. TAYLOR
WALLACE WATERFALL

The JOURNAL OF APPLIED PHYSICS, published monthly at Prince and Lemon Sts., Lancaster, Pa., is devoted to physics in its role as the science basic to other natural sciences and to the arts and industries. Previous to 1937 this publication was known as PHYSICS. The JOURNAL OF APPLIED PHYSICS publishes editorials, news of physicists, and reviews, as well as technical papers of applied physics.

Manuscripts should be submitted to Elmer Hutchisson, Editor Case School of Applied Science, Cleveland 6, Ohio.

Subscriptions and orders for back numbers should be addressed to Prince and Lemon Streets, Lancaster, Pa. or to the American Institute of Physics, 57 East 55 Street, New York 22, N. Y.

Subscription Price

	U. S. AND CANADA	ELSEWHERE
To members of scientific societies	$5.00	$5.70
To all others	7.00	7.70

Back Number Prices

Complete set: Vol. 1, July, 1931–Vol. 15, 1944—$94.50
Yearly back number rate: $7.70
Single copies: $0.70 each.

Changes of address and proofs should be addressed to the Publications Manager.

Advertising rates supplied on request. Orders, advertising copy, and cuts should be sent to the American Institute of Physics.

Entered as second class matter January 22, 1937, at the Post Office at Lancaster, Pennsylvania, under the Act of March 3, 1879
Accepted for mailing at the special rate of postage provided for in the Act of February 28, 1925, authorized May 2, 1932.

Copyright 1945, by the American Institute of Physics.

Journal
of
Applied Physics

Volume 16, Number 6 June, 1945

News from Here and There

Personnel Changes in the American Institute of Physics

MISS MADELINE M. MITCHELL has resigned her position as Publications Manager to take effect on June 30. She is to be married and while her interest in the affairs of physics and the Institute is undiminished, she will not find it possible to continue the strenuous work and bear the exacting responsibilities that go with the position she has held. She has actually been more than Publications Manager, as she has acted as general office manager and manager of the physics building as well.

It would have been, in any case, necessary to divide the work which has until now been under Miss Mitchell's direction. It is too much for one person, having increased as the importance of physics and the circulation of the physics journals have increased.

Miss Margaret S. Griffin, heretofore Miss Mitchell's general assistant, has been appointed to the position of Publications Manager to take over on July 1 the duties particular to that function when they are released by Miss Mitchell.

There has been established, further, the position of Assistant Treasurer and Business Manager to include supervision of all accounts and finances, sales of journals and reprints, management of the building, and other matters of business. To this position Mr. Theodore Vorburger has been appointed as of May 16. Mr. Vorburger was formerly in charge of auditing the Institute's books quarterly for the firm of Pasley & Conroy, the Institute's auditors. He is therefore well equipped by profession and acquaintance with the affairs of the Institute for his new position. It is an unusually fortunate circumstance that such a man is available, especially at the present time.

The Director of the Institute, Dr. Henry A. Barton, will continue in general charge, but it is hoped that he can delegate most of the "internal" responsibilities to Mr. Vorburger and Miss Griffin.

Dr. Paul E. Klopsteg, director of research at the Technological Institute of Northwestern University, has been re-elected chairman of the governing board of the American Institute of Physics for a fifth consecutive term.

Pryor Lindsay Watts, an RCA theater service engineer in the New York area before the war, and more recently an airborne radar specialist in the Government Group of the RCA Service Company, was killed March 5 in a plane crash at Orlando, Florida, where he was preparing for an overseas assignment in connection with important military equipment. Mr. Watts was a member of the Institute of Radio Engineers, the American Institute of Electrical Engineers, and the Society of Motion Picture Engineers.

New Appointments

Dr. W. B. Pings, organic chemist, has recently joined the staff of Arthur D. Little, Inc., Cambridge, Massachusetts, industrial research organization. Dr. Pings was previously at the Experimental Station of E. I. du Pont de Nemours and Company, Wilmington, Delaware.

Predoctoral Fellowships in the Natural Sciences

The National Research Council has announced that it is the recipient of a grant of $335,000 from the Rockefeller Foundation for the establishment of a temporary, nation-wide program of predoctoral fellowships for graduate study in the natural sciences. The fellowships are designed to encourage resumption of graduate study by young men who have had to interrupt their education to engage in war work, by enabling them to devote essentially full time to the completion of their work for the doctor's degree. In view of the uncertainty of the duration of the war it is not expected that the program can be inaugurated immediately. This preliminary announcement is made so that young men now in war work will realize that perseverance in their present important tasks will not prejudice their opportunity to pursue their formal education later, and that it may be inadvisable to make commitments at present for post-war employment.

Plans for administration of the fellowships and methods for the selection of candidates are not yet worked out in detail, but it is intended that stipends will be fixed at rates to compare favorably with most other fellowships at this stage of training.

The Council and the Foundation have developed this program to help alleviate the very serious set-back to American scientific competence resulting from the war's

interference with normal educational processes. The almost complete cessation of consecutive professional training which has occurred in scientific fields will make impossible for some time the normal accession of additional highly trained personnel. These losses, in the face of sharply increasing demands for such personnel, will inevitably retard to the danger point the resumption of scientific progress after the war. The resulting handicap to post-war industrial recovery, public health, and military security is a matter of national concern.

It should be realized, however, that this generous grant is sufficient to furnish financial assistance to only a moderate fraction of all graduate students who should resume study for advanced professional degrees in the natural sciences and that, therefore, other types of assistance heretofore available should not be curtailed. The program is planned also not to divert too many qualified candidates from part-time teaching positions, since it is expected that colleges and universities will, after the war, be overburdened with undergraduate students in these fields.

The National Research Council will continue to administer its post-doctoral fellowship program, which has been such an outstanding factor in building up the scientific competence of the country, and which has thereby contributed essentially to the effort in meeting the present crisis.

Noise Abatement Awards

In 1945 the National Noise Abatement Council will make, in addition to its four city-population class awards, a Grand National Award, to be given to the one city of all United States cities whose achievements in noise abatement are adjudged most outstanding. Material submitted as supporting evidence to claims for the awards must be received not later than July 1, 1945, by the National Noise Abatement Council, 9 Rockefeller Plaza, New York 20, New York.

United Air Lines Scholarships

Six United Air Lines scholarships will be awarded to teachers enrolled in the course, "Physics for Teachers," at the 1945 University of New Hampshire Summer School. Selection will be based on evidence of teaching and leadership ability, interest in aviation, and apparent ability to contribute to education for the age of flight by developing aids for teachers of physics in secondary schools. Applications and recommendations for the scholarships should be sent to A. Monroe Stowe, chairman, Summer School Committee, Durham, New Hampshire.

Research Board for National Security

A joint statement issued by Henry L. Stimson, Secretary of War; James Forrestal, Secretary of the Navy; and Frank B. Jewett, President of the National Academy of Sciences, announces the establishment by the National Academy of the Research Board for National Security. The Secretaries of War and Navy said: "A recommendation from the Committee on Post-war Research has been received for the establishment by Congress of an independent agency to deal with the matter, but pending action on this recommendation and to assist in providing for continued civilian participation in the longer term scientific problems of national security when the Office of Scientific Research and Development proceeds to liquidate its activities as a temporary wartime agency, the National Academy of Sciences is hereby requested to establish promptly a Research Board for National Security."

The objective of the Board will be to continue, pending final consideration by Congress on creation of an independent agency, the close cooperation between civilian scientists and the Armed Services which has proved to be such a vital element in the prosecution of the war. The charter of the new Board provides for up to twenty civilians selected with the advice of the Chairman of the National Research Council and the Council of the National Academy of Sciences; also up to ten high ranking officers each from the Army and the Navy, nominated by the respective Secretaries; all to be appointed by the President of the Academy. Five members of this Board shall constitute its Executive or Operating Committee. The members of the Board serve as such without compensation. The research activities are to be carried out under contracts whereby existing laboratories and facilities will be used wherever practicable.

The initial membership of the Executive Committee consists of Karl T. Compton, president, Massachusetts Institute of Technology, Chairman; Roger Adams, head, Department of Chemistry, University of Illinois; A. R. Dochez, professor of Experimental Medicine and Surgery, College of Physicians and Surgeons, Columbia University; Brigadier General W. A. Borden, director, New Developments Division, War Department Special Staff; Rear Admiral J. A. Furer, coordinator of Research and Development, Navy Department.

Radio Receptor Company Scholarships

Science reports that the Radio Receptor Company, Inc., has placed a scholarship of $2500 at the disposal of the department of physics of the Washington Square College of New York University. The recipient of this scholarship will be a student working for the doctorate, and the research which the scholarship is designed to promote will be the subject of the thesis for the degree. Applications with credentials should be directed to the Chairman of the Physics Department, Washington Square College of Arts and Science, New York University, Washington Square, New York 3, New York.

Conference on Ultracentrifuge

Under the joint auspices of the Polytechnic Institute of Brooklyn, the Society of Rheology, and the Metropolitan Section of the American Physical Society, a one-day conference was held at the Polytechnic Institute of Brooklyn June 2 on "The Ultracentrifuge in High Polymer Research." The conference dealt with the most recent applications of the ultracentrifuge to the study of the shape and size of large molecules. James B. Nichols, research chemist of the Experimental Station of the DuPont Company, presided. The researches reported at the Institute dealt with the physical-chemical properties of gelatine, which has been proposed as a blood substitute, starch, and synthetic high polymers.

Bakelite Technical Films

Bakelite Corporation has announced the release of the first two films in its Technical Film Library: "Bakelite Plastics—Selecting the Right Thermosetting Molding Material," and "Bakelite Plastics—Product Design and Molding Technique for Thermosetting Plastics." These motion pictures are designed as guides to the understanding of the proper uses of thermosetting plastics. Sixteen-millimeter prints are available without cost to executives, industrial organizations, engineers, designers, and educational institutions upon request to Technical Film Library, Bakelite Corporation, 300 Madison Avenue, New York 17, New York.

Mathematical Biophysics

The *Bulletin of Mathematical Biophysics* has the following table of contents for June:

A Note on the Physiological Arrangement of Tissues—M. F. MORALES AND R. E. SMITH.
Dynamics of Quadrupedal Locomotion—ALSTON S. HOUSEHOLDER.
A Theory of Photosensitivity of Some Lower Animals—RICHARD RUNGE.
Outline of a Mathematical Approach to the Cancer Problem—N. RASHEVSKY.
Neural Mechanisms for the Concepts of Difference and Similarity—H. D. LANDAHL.
A Heterarchy of Values Determined by the Topology of Nervous Nets—WARREN S. MCCULLOCH.
Book Review—**Alston S. Householder and Herbert D. Landahl,** *Mathematical Biophysics of the Central Nervous System*—HERMAN BRANSON.

The University of Chicago Press, Chicago, Illinois, Volume 7, Number 2.

New Booklets

How to calculate, design, and install radiant heating systems for buildings ranging from monumental type structures to small industrial buildings is described in the new handbook, *Byers Wrought Iron for Radiant Heating*, issued recently by A. M. Byers Company, Pittsburgh, Pennsylvania. Chief purpose of the 52-page book is to serve as a working manual. Detailed procedure is listed for figuring heat losses and piping requirements, designing the coils, and supply and return mains. Factual data are presented on the relative merits of locating the coils in floor and ceiling. Included is a full-page drawing of a floor-type radiant heating system for a representative industrial building in which both sinuous coils and grids are used to advantage. The book records in picture and text 23 typical installations covering a wide range of structures, including six churches, two medical buildings, a library, and three factory buildings.

The first issue of Westinghouse *Newsfront*, a new publication by the Westinghouse Electric Corporation, appeared in April. Featured in the issue were a round-up on the company's annual report to stockholders, a story on a new application of the Precipitron air-cleaner for the removal of fly-ash, and a picture page illustrating recent Westinghouse developments. This new four-page monthly, printed in two colors and illustrated with drawings and photographs, will contain short articles describing the latest achievements by the company in the fields of scientific research, engineering, and production. Requests to be placed on the mailing list should be addressed to the Editor, Westinghouse *Newsfront*, 306 Fourth Avenue, Box 1017, Pittsburgh, Pennsylvania.

A new electric timer bulletin, No. 1100, has been released by the C. H. Stoelting Company, Industrial Division, 424-P North Homan Avenue, Chicago 24, Illinois. It describes table model stop clocks, wall model stop clocks, precision chronoscopes, combination timers and impulse counters, stop watch controllers, and spring wound x-ray timers. These devices have wide application in industrial and laboratory testing, such as in measuring start-to-stop intervals of relays and instruments and for checking sequence operations. Circuit diagrams are included to show correct methods of connecting the various timers in test circuits.

Walker-Jimieson, Inc., radio and electronic distributors at 311 South Western Avenue, Chicago 12, Illinois, have published a new edition of their *Industrial Availability Booklet*, which shows items available on priority for immediate delivery from stock. It contains 48 pages. This monthly catalogue is free to any engineers or purchasing agents requesting it.

New Books

Colloid Chemistry—Theoretical and Applied, Volume V. Theory and Methods; Biology and Medicine

Collected and edited by Jerome Alexander. Reinhold Publishing Corporation, New York, 1944. Price $20.00.

Exactly 84 years ago Thomas Graham published a paper on liquid diffusion applied to analysis. In this paper he discusses the difference in diffusion and solubility of chemical compounds and states that the comparatively "fixed" class as regards diffusion is represented by chemical substances marked out by the absence of the power to crystallize. Among these he mentions gelatine, and then states, "As gelatine appears to be its type, it is proposed to designate substances of this class as colloids, and to speak of their peculiar form of aggregation as the colloidal condition of matter. Opposed to the colloidal is the crystalline condition. Substances affecting the latter form will be classed as crystalloids."

Since then the science of colloids has progressed tremendously, because taking Graham's original definition, colloids embrace not only reactions within the realm of classical chemistry, but also of biology, botany, geology, medicine, and many other branches of science and technology. Although many textbooks have been published on fundamental colloid chemistry, Jerome Alexander was the first to edit a compendium on the development of colloid chemistry. During the years 1926 to 1932, four volumes were edited which still today must be considered the most comprehensive compilation of colloidal phenomena and methods for their study. Now Volume V, published 16 years after Volumes I and II, brings us up to date in regard to advancements made in the field of the theory and methods of colloid chemistry and its importance and application in biology and medicine.

This volume is composed of 25 chapters on theory and methods, and 35 chapters pertaining to biology and medicine. It must not only be considered as a timely and necessary addition to the previous set, but the selection of authors and the name of the editor make this book a monument in the literature of colloid chemistry which cannot be overlooked by anyone interested in this field.

ERNST A. HAUSER
Massachusetts Institute of Technology

Heating Ventilating Air Conditioning Guide

Published by the American Society of Heating and and Ventilating Engineers, New York. Pp. 1216. Price $5.00.

American Society of Heating and Ventilating Engineers, 51 Madison Avenue, New York 10, New York, has published the 23rd edition of the *Heating Ventilating Air Conditioning Guide*. The Guide contains 48 chapters of technical data and information grouped under the general sub-divisions: principles; heating and cooling load calculations; combustion and consumption of fuels; steam and hot water heating; air heating, cooling and conditioning; automatic controls, instruments and motors; special applications; and miscellaneous. A 15-page detailed index, a single-page quick reference table of contents, and a brief summary of chapter contents under each chapter heading provide easy reference to the subjects treated in the book.

Mechanics of the Metal Cutting Process. II. Plasticity Conditions in Orthogonal Cutting*

M. Eugene Merchant
Research Department, The Cincinnati Milling Machine Company, Cincinnati, Ohio

(Received November 15, 1944)

The analysis of the mechanics of orthogonal cutting with a type 2 chip as presented in the first paper of this series can be extended by introducing those physical properties of the work material which control its plastic behavior. One evident plasticity condition is the equality of the shear stress on the plane of shear to the shear strength of the metal. If it is also assumed that the shear strength of the work material is a constant and is the only quantity controlling its plastic behavior, then a very simple additional plasticity condition is obtained by application of the principle of minimum energy. This condition is $2\phi+\tau-\alpha=90°$, where ϕ is the shear angle, τ the friction angle, and α the rake angle. This condition, however, is found by experiment to be a poor approximation in the case of polycrystalline metals. A very good approximation is obtained, though, if use is made of the fact that the shear strength of the polycrystalline metal is actually a function of the compressive stress on the shear plane. The resulting plasticity condition is $\cot(2\phi+\tau-\alpha)=k$, where k is the slope of the linear curve relating shear strength and compressive stress, and is thus a constant of the work material.

Such a plasticity condition establishes a relationship between the force system and the geometry of chip formation, so that, if k and the shear strength be known for a given material, all forces involved in cutting it can be calculated with reasonably good accuracy directly from measurements of chip geometry only, without use of a tool dynamometer. This is of importance in the analysis of practical machining operations.

INTRODUCTION

IN the first paper of this series, relationships were presented which make possible the analysis of an orthogonal cutting process in terms of basic mechanical quantities, from measurements of forces on the tool and the geometry of chip formation. However, it is evident that the force system controls the geometry of chip formation in a manner dictated by those physical properties of the work material which determine its plastic behavior. The results of an initial theoretical and experimental study of plasticity conditions in cutting, to determine the relationship between forces and geometry, serve as the basis for this second paper of the series. The study is by no means complete, but does result in a good first approximation. The analysis is again limited, in theory at least, to orthogonal cutting with a tool having a single straight cutting edge and a plane face, and generating a type 2 chip, as defined in the previous paper. However, as before, minor deviations from these conditions result in little error.

The force system acting in the case of orthogonal cutting with a type 2 chip, as discussed in the first paper of this series, is shown in Fig. 1. The important force relationships derivable from the geometry of this figure, as previously discussed, are:

$$\mu=F/N=\tan\tau=(F_t+F_c\tan\alpha)/(F_c-F_t\tan\alpha), \quad (9)$$

$$F=F_t\cos\alpha+F_c\sin\alpha, \quad (10)$$

$$F_s=F_c\cos\phi-F_t\sin\phi, \quad (11)$$

$$S_s=F_s/A_s=(F_c\sin\phi\cos\phi-F_t\sin^2\phi)/A_0, \quad (12)$$

$$S_n=F_n/A_s=S_s\tan(\phi+\tau-\alpha), \quad (13)$$

$$W_f=F/A_c, \quad (14)$$

$$W_s=S_s\epsilon, \quad (15)$$

$$W_c=W_s+W_f; \quad (16)$$

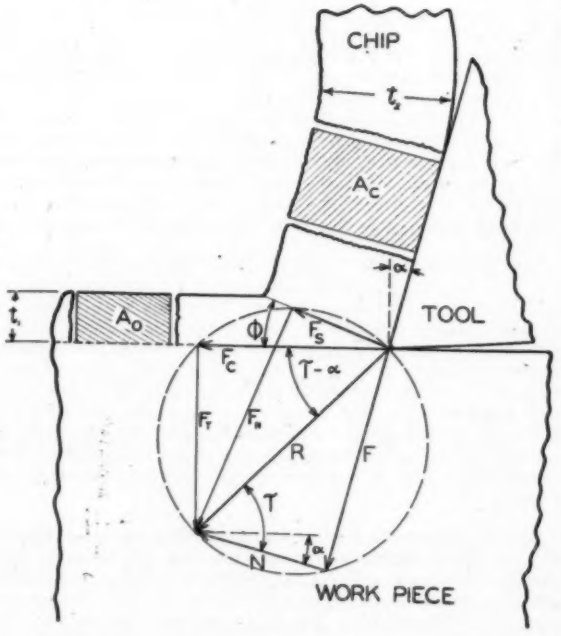

FIG. 1. Condensed force diagram for orthogonal cutting.

* Part I of this series appeared in the Journal of Applied Physics for May 1945.

where μ = coefficient of friction between chip and tool, S_s = mean shear stress on shear plane, A_s = area of shear plane = $A_0/\sin\phi$, S_n = mean compressive or normal stress on shear plane, W_f = work dissipated in friction per unit volume of metal removed, W_s = work dissipated in shear per unit volume of metal removed, ϵ = shearing strain undergone by chip = $\cot\phi+\tan(\phi-\alpha)$ and W_c = total work dissipated in cutting per unit volume of metal removed. The meaning of the other symbols is evident from Fig. 1. All these symbols were defined and more fully discussed in the previous paper.

The physical properties governing the plastic behavior of the work material evidently determine what value the shear angle, ϕ, will assume for any given value of the angle $\tau-\alpha$ in Fig. 1. According to the principle of minimum energy, the angle ϕ will assume such a value as to make the total work done in cutting a minimum. Since the force component F_c, the cutting force, is alone responsible for the total work done in cutting per unit distance traveled by the tool, it follows that, for any given value of angle $\tau-\alpha$, the angle ϕ will assume such a value as to make F_c a minimum. This principle will be employed in determining the plasticity conditions for the cutting process.

From the geometry of Fig. 1 it can be seen that

$$F_c = R\cos(\tau-\alpha) = F_s\cos(\tau-\alpha)/\cos(\phi+\tau-\alpha).$$

But

$$F_s = S_s A_0/\sin\phi.$$

Therefore

$$F_c = S_s A_0\cos(\tau-\alpha)/\sin\phi\cos(\phi+\tau-\alpha). \quad (17)$$

CASE I. CONSTANT SHEAR STRENGTH

A. Theory

The very simplest procedure is to assume first that the shear strength of the material being cut is a true constant,[1] invariant with respect to ϕ, and is thus the only physical property controlling the plasticity of the material. Thus

$$S'_s = b, \quad (18)$$

where b is a constant and S'_s is the shear *strength* of the material being cut, as distinguished from S_s which is the shear *stress* on a plane defined by angle ϕ. During cutting, when shear is occurring,

$$S_s = S'_s \quad (19)$$

on the shear plane itself. Then in this case, in view of Eqs. (18) and (19), Eq. (17) becomes

$$F_c = bA_0\cos(\tau-\alpha)/\sin\phi\cos(\phi+\tau-\alpha). \quad (20)$$

The application of the principle of minimum energy as already outlined, carried out by differentiation of Eq. (20) and equating to zero, then leads to the following result

$$\frac{dF_c}{d\phi} = -bA_0\cos(\tau-\alpha) \times \frac{\cos\phi\cos(\phi+\tau-\alpha)-\sin\phi\sin(\phi+\tau-\alpha)}{\sin^2\phi\cos^2(\phi+\tau-\alpha)} = 0,$$

or

$$\cos(2\phi+\tau-\alpha) = 0;$$

and thus

$$2\phi+\tau-\alpha = 90°. \quad (21)$$

This is a plasticity condition already arrived at by Ernst and Merchant[2] by use of the assumption that the direction of shear coincides with the direction of maximum shearing stress.

Equations (19) and (21), representing the plasticity conditions for Case I, can be substituted into the force equations given in the introductory section to yield equations free of all force components, thus eliminating the necessity for force measurements. Such equations are, of course, valid only in the case of materials which conform to the assumption of constant shear strength so satisfactorily as to make Eq. (21) a good approximation. Making these substitutions, Eq. (9) becomes:

$$\mu = \tan\tau = \cot(2\phi-\alpha). \quad (22)$$

Equation (10) becomes, in terms of the invariants and ϕ

$$F = A_0 S'_s\cos(2\phi-\alpha)/\sin^2\phi. \quad (23)$$

Equation (11) becomes

$$F_s = A_0 S'_s/\sin\phi. \quad (24)$$

Equation (12) can be written

$$S_s = S'_s. \quad (19)$$

[1] Actually, as will be seen later from the discussion of Case II, it is not as important for this analysis that the shear strength be totally invariant as that it be invariant with respect to the normal stress acting on the shear plane. Fulfillment of this latter condition is sufficient to make the equations derived in this section valid to a very good degree of approximation.

[2] H. Ernst and M. E. Merchant, "Chip Formation, Friction and High Quality Machined Surfaces," *Surface Treatment of Metals* (American Society for Metals, 1941), pp. 299–378.

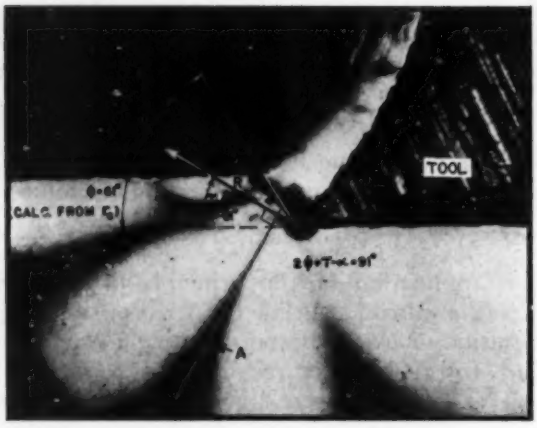

FIG. 2. Photomicrograph illustrating plasticity conditions in cutting celluloid, employing photoelasticity technique. Picture snapped while cutting.
($t_1=0.010''$, $V_c=0.75$ in/min., $\alpha=45°$, $\times 85$.)

Equation (13) becomes

$$S_n = S'_s \cot \phi. \tag{25}$$

Equation (14) transforms to

$$W_f = S'_s[\cot \phi - \tan (\phi - \alpha)]. \tag{26}$$

Equation (15) is virtually unchanged

$$W_s = S'_s \epsilon. \tag{27}$$

Equation (16) becomes

$$W_c = 2S'_s \cot \phi. \tag{28}$$

B. Experiment

It is found from experiment that Eq. (21) is a poor approximation in the case of the cutting of a polycrystalline metal. This is evident from a glance at Figs. 6 and 8, which are to be discussed more fully in connection with Case II.

Equation (18), and consequently also Eq. (21), may offer a good approximation in the case of certain synthetic plastics. Figure 2 is presented by way of example. It is developed from a photomicrograph snapped during the orthogonal cutting of a piece of transparent *celluloid* illuminated with polarized light according to standard photoelastic technique. Under these conditions the "black brush," A, divides a region of tension, on the right, from one of compression, on the left. Thus the resultant force, R, must be perpendicular to this brush, as shown. The angle $\tau-\alpha$ is therefore negative and by measurement from the figure is equal to $-31°$. By measurement of the chip-length ratio or cutting ratio, r_c, and application of Eq. (7)[3] Part I, the illustrated shear angle was found to be 61°. Thus from experiment,

$$2\phi+\tau-\alpha=2(61°)-31°=91°$$

in close agreement with Eq. (21).

CASE II. S'_s A FUNCTION OF NORMAL STRESS[4]

A. Theory

As already pointed out, Eq. (21) is a poor approximation in the case of a polycrystalline metal. However, as is well known, the shear strength of polycrystalline metal is not a constant, but is influenced by a number of different quantities. The most important of these are temperature, rate of shear, shearing strain (plastic), and the stress acting normal to the planes of shear. The last of these has often been overlooked. The question arises as to which, if any, of these quantities are mainly responsible for the poor approximation obtained when the shear strength is assumed constant. Specifically, which of these quantities will influence the direction in which the metal lying ahead of the cutting edge will shear? Of the quantities previously enumerated, the normal or compressive stress existing on the potential shear planes ahead of the cutting edge is the only one which is active in influencing shear strength when the metal is merely stressed and has not yet started to undergo plastic strain.

---

[3] $$\tan \phi = r_c \cos \alpha/(1-r_c \sin \alpha). \tag{7}$$

[4] Since writing this section, the author has been able to obtain a complete English translation of the Finnish article by V. Piispanen (V. Piispanen, Teknillinen Aikakauslehti **27**, 315–322 (1937), cited as reference 5 in the first paper of this series. On studying this translation it was found to the author's surprise that Piispanen has already recognized the importance of the normal stress on the shear plane in influencing the angle of shear, and has worked out a graphical method, based essentially on the principle of minimum energy, for finding this angle of shear when the direction of the resultant force R is known. Piispanen also assumes that the normal stress influences the shear strength in the manner given by Eq. (29) herein. The treatment is entirely graphical and no mathematical results are developed, but this graphical method should yield the same quantitative values for shear angle and forces as does the mathematical method developed herein. Piispanen also has attempted to take into account the effect of strain hardening on the direction of shear in his graphical method, though here the treatment is not as straightforward and is open to question. No experimental data is presented.

It seems likely, therefore, that it is this quantity which will mainly influence the direction which the successive shear planes will take when they begin to form in the metal lying ahead of the cutting edge, as the cutting tool progresses from plane to plane. Temperature, rate of shear, and shearing strain should all be secondary in their influence on the shear angle, compared to the compressive stress on the shear plane. Therefore, to obtain a simple first approximation, the effect of these secondary quantities will be neglected in developing the theory, and only the effect of compressive stress on shear strength will be taken into account.

The effect of compressive or normal stress, S_n, on the shear strength of a polycrystalline metal[5] has been quite extensively investigated by Bridgman[6] by two different methods. The first method indicates the relationships between shear strength and compressive stress to be generally of the form shown in Fig. 3, which has been adapted from a curve given by him in the first of the references cited. The second method which closely duplicates conditions existing in the metal cutting process, confirms the fact that the relationship is virtually linear, as seen from Fig. 4,

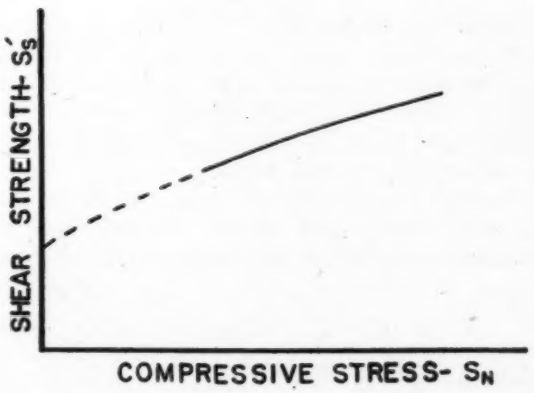

FIG. 3. Typical form of relationship between shear strength and compressive stress for most materials, according to Bridgman.

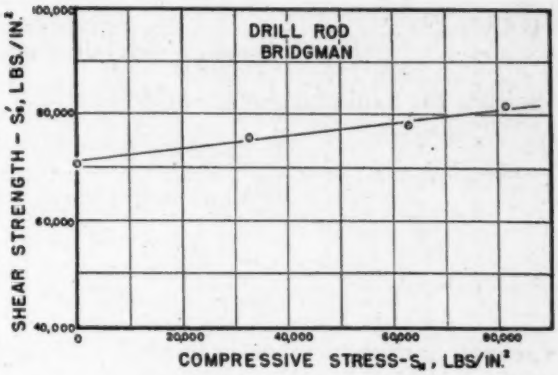

FIG. 4. Shear strength *versus* compressive stress at $\epsilon = 1$ for a sample of drill rod, from Bridgman's data. ($S_0 \approx 70$, 100 p.s.i., $k \approx 0.125$.)

which has been constructed from data presented by Bridgman for a sample of drill rod, in the fourth of the references cited, and represents the relationship between shear strength and compressive stress at a shearing strain of unity.

From Figs. 3 and 4 it is evident that a relationship of the form

$$S'_s = S_0 + kS_n, \tag{29}$$

where S_0 and k are constants of the metal, represents with sufficient accuracy the experimental curves shown there. S_0 is the shear strength of the metal under zero compressive stress, and is roughly equal to one-half the tensile strength, at high values of strain. The constant k of course represents the slope of the shear strength *vs.* compressive stress curve.

In the orthogonal cutting of metal, the expression for the normal stress, S_n, acting on the shear plane is given by Eq. (13), or

$$S_n = S_s \tan(\phi + \tau - \alpha). \tag{13}$$

As before, on the shear plane during cutting

$$S_s = S'_s. \tag{19}$$

Thus when applied to orthogonal cutting Eq. (29) becomes, by substitution of (13) and (19)

$$S'_s = S_0 + kS'_s \tan(\phi + \tau - \alpha),$$

and, solving for S_s

$$S'_s = S_0/[1 - k \tan(\phi + \tau - \alpha)]. \tag{30}$$

Substitution of Eqs. (19) and then (30) in Eq. (17) for the cutting force, in preparation for the application of the principle of minimum energy,

[5] It appears that the normal stress acting on a shear or slip plane in a metallic single crystal has no effect on its shear strength. See, for example, the cases cited by C. S. Barrett, *Structure of Metals* (McGraw-Hill Book Company, Inc., New York, 1943), pp. 295–296. It may be that the effects discussed here are therefore sensitive to grain size, among other things, and arise from interference and discontinuity of slip planes between adjacent grains.

[6] P. W. Bridgman, Phys. Rev. **48**, 825–847 (1935); Proc. Am. Acad. **71**, 386–460 (1937); J. App. Phys. **8**, 328–336 (1937); J. App. Phys. **14**, 273–283 (1943).

leads to

$$F_c = S_0 A_0 \cos(\tau-\alpha)/[\sin\phi\cos(\phi+\tau-\alpha) - k\sin\phi\sin(\phi+\tau-\alpha)]. \quad (31)$$

Applying the minimum energy principle

$$\frac{dF_c}{d\phi} = -S_0 A_0 \cos(\tau-\alpha)\left\{\frac{\cos\phi\cos(\phi+\tau-\alpha)-\sin\phi\sin(\phi+\tau-\alpha)}{[\sin\phi\cos(\phi+\tau-\alpha)-k\sin\phi\sin(\phi+\tau-\alpha)]^2}\right.$$

$$\left. -k\frac{\cos\phi\sin(\phi+\tau-\alpha)+\sin\phi\cos(\phi+\tau-\alpha)}{[\sin\phi\cos(\phi+\tau-\alpha)-k\sin\phi\sin(\phi+\tau-\alpha)]^2}\right\} = 0,$$

or, equating the expression in braces to zero and simplifying trigonometrically

$$\cos(2\phi+\tau-\alpha) = k\sin(2\phi+\tau-\alpha),$$

and thus

$$\cot(2\phi+\tau-\alpha) = k. \quad (32)$$

This plasticity condition can also be written

$$2\phi+\tau-\alpha = C, \quad (33)$$

where $C = arc\cot k$. As is to be expected, Eq. (33) reduces to Eq. (21) if the shear strength of the material is independent of compressive stress.

As pointed out earlier, Eq. (33) still represents an approximation, since it takes no account of the effect of strain, rate of shear, and temperature rise on shear strength and on the constants k and S_0. Nevertheless, as will be seen in the section which presents the results of experiment, the equation affords a surprisingly good approximation, especially over the usual range of strain and rate of shear encountered in practice.

Equations (19) and (33), representing the plasticity conditions for Case II, can be substituted in the force equations given in the introductory section to yield equations free of all force components, as was done for Case I. Making these substitutions, Eq. (9) becomes

$$\mu = \tan\tau = \tan(C-2\phi+\alpha). \quad (34)$$

Equation (10) becomes

$$F = A_0 S'_s \sin(C-2\phi+\alpha)/\sin\phi\cos(C-\phi), \quad (35)$$

and Eq. (11) is again

$$F_s = A_0 S'_s/\sin\phi. \quad (24)$$

Equation (12) becomes, by virtue of Eq. (30)

$$S'_s = S_0/[1-k\tan(C-\phi)]. \quad (36)$$

Equation (13) becomes

$$S_n = S'_s\tan(C-\phi). \quad (37)$$

Equation (14) transforms to

$$W_f = S'_s[\tan(C-\phi)-\tan(\phi-\alpha)]. \quad (38)$$

Equation (15) is again

$$W_s = S'_s\epsilon. \quad (27)$$

Equation (16) becomes

$$W_c = S'_s[\tan(C-\phi)+\cot\phi]. \quad (39)$$

The cutting force is given by

$$F_c = A_0 S'_s[\tan(C-\phi)+\cot\phi], \quad (40)$$

and the thrust force by

$$F_t = A_0 S'_s[\tan(C-\phi)\cot\phi - 1]. \quad (41)$$

B. Experiment

Equation (33) has been tested quite extensively by experiment, under conditions of orthogonal cutting with a straight-edged tool generating a type 2 chip. The experimental methods and equipment used have been described in the previous paper of this series.

Typical results obtained from cutting tests on an N.E. 9445 steel of 187 Brinell hardness number and a Meyer "n" value of 2.32, machined

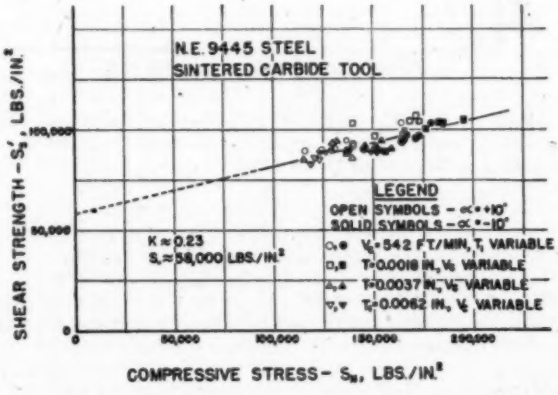

FIG. 5. Relation between shear strength and compressive stress observed when cutting N.E. 9445 steel with sintered carbide tool.

with a sintered carbide tool, are given in Figs. 5 and 6. The data were obtained from a large number of cutting tests covering a range of cutting speed (V_c) from 200 to 1570 ft. per minute, at values of feed per revolution (t_1) from 0.0005 to 0.0079 inch, and with cutting tools having rake angles (α) of $+10°$ and $-10°$. The tools were resharpened after each reading to insure constant, maximum keenness of the edge.

In Fig. 5 values of the shear strength, S'_s, observed in cutting this steel, as calculated from Eqs. (12) and (19), are plotted against the observed compressive stress, S_n, acting on the shear plane, as obtained from Eq. (13). From the slope of this curve the constant k (Eq. (32)) for the 9445 steel is found to be approximately 0.23, and therefore the constant C is approximately 77°. Thus for this steel, according to

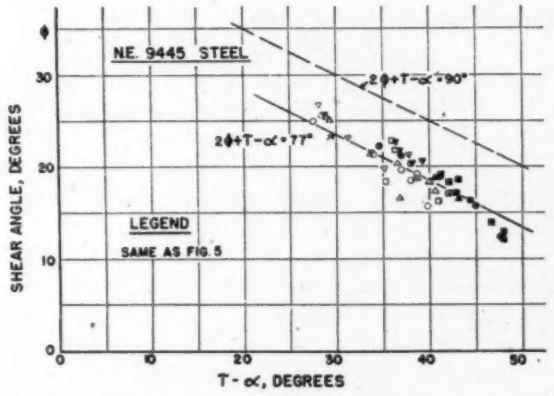

FIG. 6. Comparison between observed values of ϕ *vs.* $\tau-\alpha$ and theoretical curves, for N.E. 9445 steel.

Eq. (33), $2\phi+\tau-\alpha=77°$. In Fig. 6 this equation is represented by the full line so labeled. In this figure the observed values of the shear angle, ϕ, have been plotted against the observed values of angle $\tau-\alpha$, as obtained from the cutting tests on the N.E. 9445 steel. It may be seen that the observed points obey the relationship expressed by Eq. (33) surprisingly well. Further, they are in agreement with the numerical value of 77° for the constant C obtained from Fig. 5. It is also evident from Fig. 6 that Eq. (21), represented by the dashed line, is a much poorer approximation to the observed results than is Eq. (33).

Another set of experimental results, obtained on an SAE 4340 steel of 200 Brinell and a Meyer "n" value of 2.28, is shown in Figs. 7 and 8. The slope of the shear strength *vs.* compressive stress curve for this steel, obtained from Fig. 7, is approximately 0.175, and thus the constant C

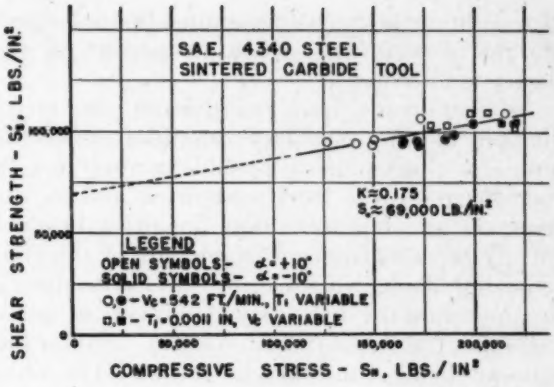

FIG. 7. Same as Fig. 5 except for SAE 4340 steel.

is approximately 80°. In Fig. 8 are plotted the values of ϕ and $\tau-\alpha$ observed for this steel. In this case, too, the values are in good agreement with Eq. (33) and with the value of 80° for the constant C.

CONCLUSIONS

The simple plasticity condition represented by Eq. (33) appears to offer a degree of approximation sufficiently accurate for many practical cases in the cutting of metals, in spite of the fact that in formulating this condition no account has been taken of the effect of plastic strain, rate of shear, and the resulting temperature rise at the shear plane. That these variables do have some effect on the plasticity conditions in the cutting of polycrystalline metal can be seen qualitatively from Figs. 6 and 8. In these figures the direction representing the trend of any group of points obtained by changing only one variable (as characterized by a single common symbol in the figure) is seen to cross the theoretical solid line

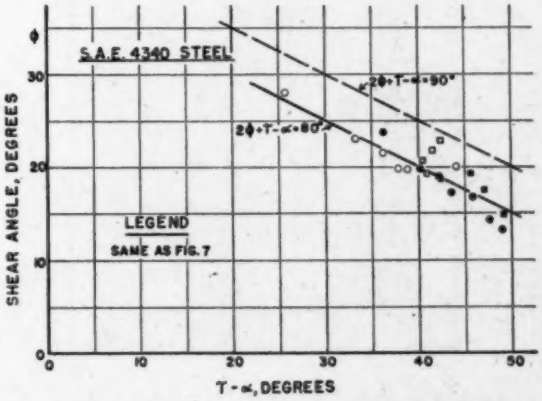

FIG. 8. Same as Fig. 6 except for SAE 4340 steel.

at a slight angle. Such effects must be the subject of later experiments, when refinement of the theory is in order.

As has already been pointed out, the introduction of the plasticity condition into the force equations makes it possible to analyze with good accuracy the force system as well as the geometry of chip formation, in an orthogonal cutting process, from measurements of the chip geometry alone. No force measurements during the operation are necessary. However, in order to do this, the values of S_0 and k (Eq. (29)) for the material being cut must be known. The only method which the present investigation offers for determining these constants is initial cutting tests on the material, with measurement of both forces and chip geometry. It seems likely, however, that means will be developed for determining these constants from much simpler types of mechanical tests, now that these particular mechanical properties have been demonstrated to be of considerable significance in influencing "machinability." Measurement of S_0 and k may become an important control measurement in the selection of steels and other metals which are to be subjected to machining operations. However, this last will depend to a considerable extent on how strongly these constants are found to influence the life of the cutting tool, since tool life is ordinarily the most important of the elements covered by the term "machinability."

The findings presented here, we believe, constitute another step toward the goal of establishing a sound basis for predicting the chip geometry, the forces, and the tool life to be expected from a given work material from measurements of its mechanical properties, and for "designing" new steels and other materials of desired "machinability" qualities, all without being bound to empiricism.

The Frictional Properties of Some White Metal Bearing Alloys: The Role of the Matrix and the Hard Particles

D. TABOR
Council for Scientific and Industrial Research, Melbourne, Australia
(Received December 1, 1944)

A previous paper has described an investigation of the frictional properties of alloys of the copper-lead type which consist of a *hard* matrix (copper) in which are dispersed particles of a soft material (lead). It was shown that these alloys function by the extrusion and smearing of the soft phase over the hard matrix, so providing metallic-film lubrication. This paper describes experiments on a typical lead-base bearing alloy which consists of a *soft* matrix in which are dispersed numerous *hard* crystallites. Measurements of the friction were made at room temperature and at elevated temperatures for clean and for lubricated surfaces. Comparison with a special alloy consisting of the matrix material alone, showed that the hard particles played no appreciable part in the basic frictional and wear properties of the bearing alloy. It is suggested that the *frictional* behaviour of the bearing alloy is determined essentially by the properties of the matrix material itself although in practical running operations there may be other properties which determine the suitability of the alloy for use in bearings. Similar experiments are described on a typical tin-base bearing alloy and a corresponding tin-base "matrix" alloy.

1. INTRODUCTION

THE major amount of wear and seizure in bearings occurs when the journal and bearing alloy are running under conditions of boundary lubrication. It is therefore important that the frictional and wear properties of these alloys should be studied under such conditions, and that we should have a clearer understanding of the physical processes that occur during this type of sliding.

It has been pointed out[1] that one factor of great importance is the temperature of the metal surfaces. When the bearing is running, the frictional heat may cause a local softening or melting at the regions where the moving metals are momentarily in contact.[2,3] For this reason it is desirable that one of the constituents of a bearing metal should have a relatively low melting point, so that if excessive heating occurs the metal may melt and flow to another region and so prevent seizure.

For this reason, alloys of the lead-copper type are well suited for use in bearings. These alloys usually consist of a *hard* matrix of copper with the *soft* lead finely dispersed through it. (See Fig. 1.) The friction of these alloys is very much less than that of either of the main constituents and it was shown[1] that their frictional properties resemble very closely those of a hard surface consisting of the matrix material, over which a thin film of the softer metal has been spread.

It was suggested that bearing alloys of this type act by the extrusion and smearing of a thin film of a soft low melting constituent over the surface of a harder matrix. The hard surface takes the load, while the actual sliding takes place on the thin film of the softer metal, thus causing a great reduction in friction.[1] In cases of excessive loading or heating, the surface film of the softer metal will melt and flow to another portion of the surface, so reducing the chances of seizure and the wear, while the mechanical properties of the matrix material may be little affected. In this way the extruded softer constituent may play a fundamental part in reducing the friction, wear, and seizure between the sliding surfaces.

It is clear, however, that this explanation is not applicable to all types of bearing alloys. A large class of bearing alloys (e.g. "white-metal"

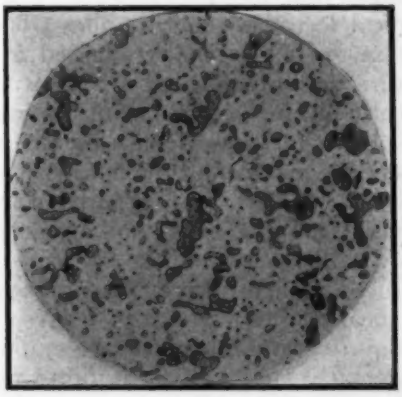

FIG. 1. Non-dendritic copper-lead alloy. The lead particles, shown as the gray constituent, are dispersed throughout the hard copper matrix.

[1] Bowden & Tabor, Council for Scientific & Industrial Research (Australia), Bull. No. 145 Paper II (1942), Bull. No. 155; J. App. Phys. **14**, 141 (1943). See also Heaton, Bristow, Whittingham, and Hughes, Nature **150**, 520 (1942).
[2] Bowden and Ridler, Proc. Roy. Soc. **A154**, 640 (1936).
[3] Matthew, J. Roy. Tech. Coll. Glasgow **4**, 360 (1940).

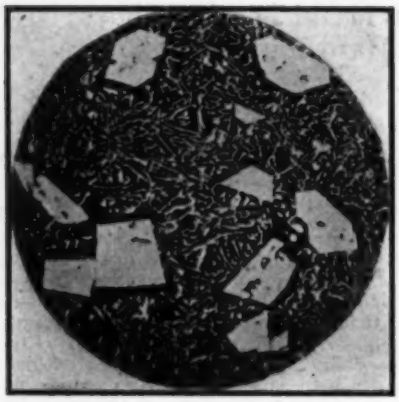

FIG. 2. Lead-base bearing alloy. This consists of a lead-tin-antimony eutectic (the fine duplex structure) in which are dispersed the hard cuboids of tin-antimony compound. The dark areas surrounding the cuboids consist of a lead-rich solid solution. The matrix consists of the eutectic and the solid solution.

bearings) possess a duplex structure consisting of *hard* crystals embedded in a relatively *soft* matrix (see Figs. 2 and 3). In this case the soft matrix forms the continuous phase, and it is clear that the isolated hard crystallites cannot bear the load in the same way as the copper matrix of a copper-lead alloy.

It has indeed been suggested[4] that the function of the hard crystals is to resist wear, and that of the softer constituents to permit a more uniform distribution of the load, by allowing any of the hard crystals that are heavily loaded to sink, so that the load is spread over a greater area. In spite of this and similar theories, the mechanism of these bearing alloys is by no means certain. For a further discussion see, for example, Bassett,[5] Desch.[4]

This paper describes experiments carried out on a typical lead-base bearing alloy. The frictional behavior has been investigated at room temperature and at elevated temperatures, in the presence and in the absence of lubricant. In order to obtain further evidence on the respective roles of the matrix and the hard crystallites, a special matrix alloy was prepared consisting of the matrix material only, and its properties compared with those of the bearing alloy. Similar measurements were also made on a tin-base bearing alloy and a corresponding matrix alloy. It should, however, be emphasized that these matrix alloys are only approximations to the complex phase relationships existing in their respective bearing alloys. Frictional measurements were also made using pure lead and pure tin.

It is emphasized that in this paper the investigation is confined to the basic *frictional* properties of the alloys under clearly defined experimental conditions of load, speed, etc. It is, of course, evident that in practice the suitability of an alloy is not only determined by its frictional and wear properties. Many of its physical properties may play a vital part in determining its performance in a running engine. The present investigation does, however, indicate that the general theory of certain white-metal bearing alloys needs to be reconsidered.

2. EXPERIMENTAL

The apparatus was similar in design to that described in earlier papers.[6] The upper surface was in the form of a hemispherical slider, while the lower surface was in the form of a flat plate which was driven forward at a uniform rate. Since the inertia of the system supporting the upper surface is small it is capable of responding readily to any rapid fluctuations in the frictional force which may occur between the sliding surfaces.

The steel surfaces were finely ground and prepared grease-free in a manner described in earlier papers. The surfaces of the soft metals were cleaned by fine scraping or by turning with a dry clean tool on the lathe without the use of cutting fluid. In some cases these specimens

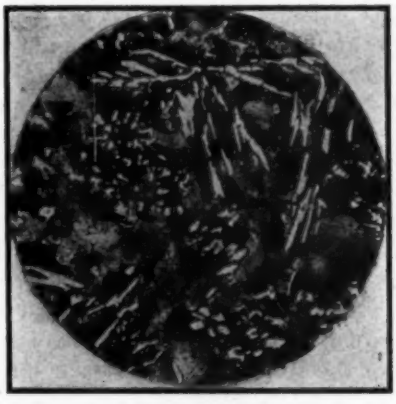

FIG. 3. Tin-base bearing alloy. This consists of a tin-rich solid solution (the matrix) in which are embedded the hard acicular crystallites of copper-tin compounds.

[4] Desch, *Metallography* (Longmans, Green and Company, New York, 1937).

[5] Bassett, *Bearing Metals and Alloys* (Edward Arnold and Company, London, 1937).

[6] Bowden and Leben, Proc. Roy. Soc. **A169**, 371 (1939); Phil. Trans. **A239**, 1 (1940).

were polished and etched as for metallographic examination*; they were then thoroughly washed and allowed to dry before use. A thin film of water would spread evenly over surfaces prepared in this manner showing the absence of gross surface contamination.

Each combination was usually tested in two ways; first with one metal as the upper curved surface and then with the metals interchanged. In all these experiments the speed of sliding was low; it varied from 0.01 to a few centimeters per second, so that the surface temperature of the metals were sensibly the same as their bulk temperature.

3. MATERIALS

The bearing alloy under investigation (designated lead-bearing alloy) had the following composition:—antimony 15.0 percent, copper 0.5 percent, tin 6.0 percent, and lead 78.5 percent.

The microstructure is shown in Fig. 2 and it is seen that the alloy consists of a lead-tin-antimony eutectic (possessing a fine duplex structure) in which are dispersed the hard cuboids of tin-antimony compound. The dark areas surrounding the cuboids consist of a lead-rich solid solution. The matrix consists of the eutectic and the solid solution.

A special microhardness apparatus was constructed for measuring the hardness of the various phases of the alloys investigated. The indentor consisted of a finely polished pyramidal diamond, and the load used was between 0.3 and 1 g. The diamond left a well defined impression in the surface of the metal of diameter between 10^{-3} and 10^{-4} cm. The apparatus was calibrated by making similar impressions in pure metals of known hardness. This method gave results reproducible to a few percent.

With the lead-bearing alloy, microhardness measurements showed that the matrix material had a hardness of approximately 19, while the cuboids had a hardness of over 110 in equivalent Vickers units. The mean (macroscopic) hardness, as measured on the Vickers machine, was 21.

The lead-bearing alloy was compared with a matrix alloy (designated as lead-matrix alloy) possessing the following composition:—antimony 10 percent, lead 87 percent, tin 3 percent, and copper 0.

* Specimens were polished on a rotating cloth disk using fine alundum as abrasive and treated with appropriate etchants.

FIG. 4. Lead-base matrix alloy. The dark areas are dendrites of lead-rich solid solution. The background, possessing the fine duplex structure, is a lead-tin-antimony eutectic. This alloy is similar in composition and structure to the matrix material of the lead-base bearing alloy shown in Fig. 3. There are no hard particles present.

The microstructure is shown in Fig. 4 and it will be seen that it consists of dendrites of lead-rich solid solution set in a duplex matrix of lead-tin-antimony eutectic. There are no hard particles present and the structure approximates to that of the matrix material of the lead-base bearing alloy. Microhardness measurements on the matrix alloy show that the lead-rich dendrites and the lead-tin-antimony eutectic are of equal hardness to within a few percent, the Vickers hardness being *ca.* 18.

The hardness values of the metals used are summarized in Table I, and as a matter of interest the hardness of a typical non-dendritic copper-lead alloy is included.

TABLE I.

Material	Macroscopic hardness, Vickers	Microhardness in equivalent Vickers units
Pure lead	4	
Lead-bearing alloy	21	Matrix 17 Cuboids 110
Lead-matrix alloy	18	Lead-rich solid solution 18 Duplex Pb-Sn-Sb eutectic 18
Steel	166	
Copper-lead alloy	35	Copper matrix 56 Lead phase 8

4. TYPES OF SLIDING

The frictional measurements show that the sliding may proceed in intermittent jerks (stick-slip motion), or it may be smooth. When stick-slip motion occurs, the upper slider welds on to

TABLE II. Friction of steel, lead, and lead alloys, unlubricated.

Surface	$\mu_{max.}$	μ_{mean}	Type of motion
Steel on lead	0.9 –1.0	0.9 –1.0	Fairly smooth
Steel on lead-bearing alloy	0.4 –0.45	0.35	Small stick slips
Steel on lead-matrix alloy	0.35–0.4	0.35–0.4	Smooth
Lead on steel	0.9	0.5	Very large stick slips
Lead-bearing alloy on steel	0.5 –0.55	0.35–0.4	Stick slips
Lead-matrix alloy on steel	0.65–0.7	0.4	Large stick slips

the lower surface and moves with it until the restoring force exceeds the strength of the metallic junctions formed, and slip occurs. The slider seizes again at the next stick, and the behavior is repeated. With surfaces moving extremely slowly, the friction at the stick (referred to as μ_{max}) is the coefficient of static friction and is a measure of the tendency of the surfaces to seize. The amplitude and frequency of the slip depend on many factors such as the natural frequency, the moment of inertia, and the damping of the moving parts, as well as on the load and speed.[7] Recent investigations by Sampson, Morgan, Reed, and Muskat[8] have also shown that the frictional behavior during the slip is very complex. However, with a system that is not heavily damped the mean friction (referred to as μ_{mean}) is approximately equal to the kinetic friction of the surfaces at surface speeds above a few cm/sec. The value of μ_{mean} given in the following tables may, therefore, be considered as a measure of the kinetic friction; it also serves as an additional point of comparison between the respective bearing and matrix alloys.

Stick-slip motion necessarily implies that the static friction is higher than the kinetic friction. For this type of motion the track on the lower surface consists of intermittent smears or gashes corresponding to the seizure of the surfaces at each stick.

Smooth sliding occurs when there is no marked difference between the static and kinetic friction. There is a continuous shearing and seizing of metallic junctions. The corresponding track on the lower surface consists of a continuous smear or groove.

[7] Bowden, Leben, and Tabor, Engineer **168**, 214 (London, 1939).

[8] Sampson, Morgan, Reed, and Muskat, J. App. Phys. **14**, 689 (1943).

5. THE FRICTIONAL BEHAVIOR OF LEAD-BASE ALLOYS

(a) Unlubricated Surfaces

The frictional results are given in Table II. It is seen that the sliding of the softer metals on the steel surface proceeds in stick slips; the sliding of steel on the softer metals is relatively smooth.

The tracks on the steel surface consisted of intermittent smears. The tracks formed on the softer metals consisted of a well defined groove, within which the material was badly torn. In order to show up the nature of the track for the bearing alloy, the surface was polished and etched before the run. Part of the track is shown in Fig. 5, side by side with the unworn portion of the surface. It is clear that the structural arrangement of the crystallites has been obliterated by the passage of the steel slider.

A similar track for the lead-matrix alloy is shown in Fig. 6, and it is clear that the surface has been badly torn by the passage of the steel slider.

It is at once apparent that the frictional behavior of the lead-bearing alloy is very similar to that of the lead-matrix alloy. The type of sliding, the actual values of μ, and the appearance of the tracks are very much alike. The behavior is also similar to that of pure lead except that the friction of the lead-base alloys is appreciably less.

As has been shown in earlier work,[9] the frictional resistance between sliding surfaces is due

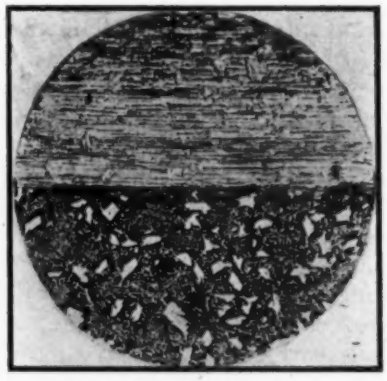

FIG. 5. Portion of track formed in lead-base bearing alloy when clean. It is seen that the structural arrangement of the hard tin-antimony cuboids has been completely obliterated by the passage of the steel slider.

[9] Bowden and Tabor, Council for Scientific and Industrial Research (Australia) Bull. No. 145 Paper I (1942); J. App. Phys. **14**, 80 (1943).

primarily to the shearing of metallic junctions formed at the points of contact S and to the force P required to drag or plough the surface irregularities of the harder surface through the softer one, so that the frictional force may be written as $F=S+P$.

If the ploughing force is small, the frictional resistance may be expressed as

$$F=S=As, \tag{1}$$

where A is the real area of contact between the metals and s is the shear strength of the metallic junctions. In the earlier work it was shown that if there is good adhesion between the sliding surfaces, the shearing occurs within the softer metal itself, and s then corresponds to the shear strength of the softer metal, so that

$$\text{Friction} = (\text{Real area of contact}) \times (\text{Shear strength of softer metal}). \tag{2}$$

With steel sliding on a softer metal therefore, the softer metal flows until the area of real contact is sufficient to support the applied load. If the surfaces are clean, welded metallic junctions will form over the whole of this area. The frictional force (neglecting the ploughing term) is then equal to the force required to shear these metallic junctions and is given by Eq. (2). As the shearing occurs within the softer metal, there will be considerable tearing and smearing of the softer surface.

This theory of metallic friction clearly applies to homogeneous metals such as pure lead, pure tin, etc., where the shearing takes place in the same material that supports the load. In such cases the friction may be expressed as the ratio of the shear strength to the flow pressure of the metal.

With non-homogeneous alloys the frictional behavior may be different. For example, the typical copper-lead alloys shown in Fig. 1 consist of two distinct phases: a hard copper matrix (Vickers hardness 56) and dispersed islands of soft lead (Vickers hardness about 8.) During sliding the lead is squeezed out and smeared over the copper matrix. The copper takes the load giving a relatively small area of contact A and the shearing occurs within the thin film of extruded lead of low shear strength s. As a result, extremely low coefficients of friction may be obtained. The smeared lead is clearly visible in the track, and if it is dissolved with a gentle etchant, the original structure of the copper matrix is still discernible.

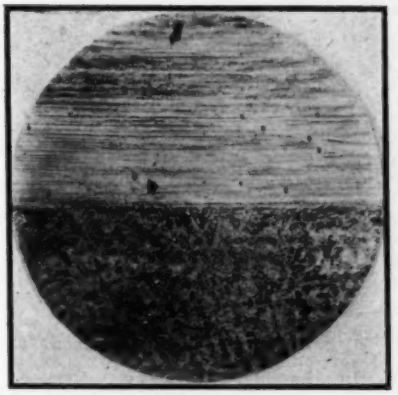

FIG. 6. Portion of track formed in lead-base matrix alloy when clean. It is seen that the crystalline arrangement of the surface has been badly damaged by the passage of the steel slider.

On the other hand the lead-base matrix alloy shown in Fig. 4 also consists of two phases, but microhardness tests show that both these phases are of almost equal hardness. Examination of the track formed during sliding shows that there is no preferential smearing of one phase over the other. The alloy as a whole welds on to the steel and is torn and smeared during the run, while the whole of the structure of the alloy is completely disturbed by the passage of the steel slider. It is evident that shearing takes place in the same material that supports the load, namely, the whole of the alloy. From the frictional point of view, therefore, the lead-base matrix alloy behaves as a homogeneous material.

In the case of the lead-base bearing alloy the track (Fig. 5) shows that the arrangement of the hard crystallites has been obliterated by the passage of the steel slider. It is clear that the matrix material has been smeared over the surface. This observation, and the fact that the value of the friction and the type of sliding are very similar to those of the matrix alloy, suggest that the metallic junctions producing the frictional resistance consist of the matrix material itself.

The microstructures show that the bearing alloy consists of a relatively soft matrix in which are embedded a large number of small hard crystallites. Since the soft matrix is the continuous phase, it is clear that the crystallites cannot contribute appreciably to the hardness of the alloys: the hardness (and flow pressure) must be determined essentially by the hardness of the matrix itself. This view is confirmed by the microhardness tests which show that the

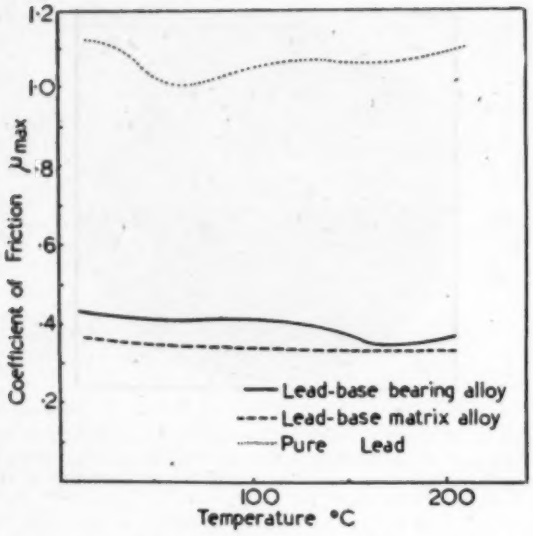

FIG. 7. Variation of friction with temperature for pure lead, and lead-base alloys.

hardness of the matrix material is almost the same as the macroscopic hardness of the alloy as a whole. It should also be noted that the hardness of the matrix alloy is similar to, though somewhat less than, that of the bearing alloy. Another significant property is the variation of hardness with temperature. This was investigated using the steel slider as the upper surface. The temperature of the lower surface was gradually raised to 200° C and a continuous record of the friction and the surface temperature was made. When the run was completed, the track width was measured at various points in the run. As the square of the track width is an approximate measure of the area of contact, which in turn is a measure of the hardness, this provides a method of following the way in which these quantities vary during the course of the run.[1] Figure 7 shows that the hardness and the variation of hardness with temperature are very similar for both the bearing alloy and the matrix alloy. It follows that in the bearing alloy, the load is taken essentially by the matrix.

These observations suggest that the action of the bearing alloy is essentially the same as that applying to pure lead and to the matrix alloy, *viz.*, the shearing takes place in the same material that supports the load. In this case it is the matrix material of the bearing alloy.

(b) Effect of Temperature

This view is confirmed by the fact that when the steel slider is used as the upper surface, the friction is almost independent of the temperature for the lead-base bearing alloy, as well as for the lead-base matrix alloy and for pure lead (see Fig. 8). This is a general result for all homogeneous metals.[1,10] As the temperature is raised, the flow pressure p decreases, so that the area of contact A increases. This is accompanied, however, by a corresponding decrease in the shear strength s of the metallic junctions, so that the resultant frictional force observed ($F=As$) is almost constant.

This result should be compared with that observed for a typical non-dendritic copper-lead alloy, where the friction decreases as the temperature rises.[1] In this case the copper matrix which takes the load, retains its hardness to a large extent, so that the area of contact A remains essentially unchanged. On the other hand the extruded lead-film softens with increasing temperature, so that the shear strength s decreases. As a result the friction given by As decreases with increasing temperature.

(c) The Effect of Repeated Sliding over the Same Track

The slider was run over the same track several times in succession and the friction recorded. In some cases the track was photographed. The frictional results are given in Table III.

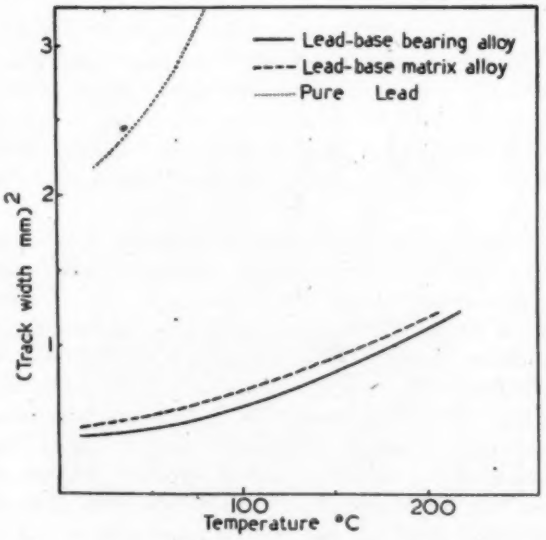

FIG. 8. Variation of square of track width with temperature for pure lead and lead-base alloys. The square of the track width is a measure of the reciprocal of the hardness.

[10] Bowden and Hughes, Proc. Roy. Soc. **A172**, 263 (1939).

For pure metals, when the same track is traversed a number of times, there is, as has been pointed out in earlier papers, no marked change in friction. The area of contact is essentially unaltered, and the metallic junctions formed are of the same nature as in the first run. With steel on pure lead there is an increase in friction at the second run, but the friction does not increase further with subsequent runs. The change in friction of the lead-base alloys with wear is very marked. The friction for the first run is of the order of $\mu = 0.4$–0.5, while for the 20th run the friction increases to about $\mu = 0.8$. The reasons for this increase are not certain. It is probably due to the cumulative pick up of the alloy on the steel surface which gives more intimate contact between the sliding surfaces. This is confirmed by the fact that with further traversals of the same track, the friction approaches the value of the alloy sliding on itself. The results given in Table III show that the frictional behavior of the lead-base bearing alloy and the lead-base matrix alloy are very similar with respect to wear.

TABLE III. Effect of repeated sliding over the same track, unlubricated.

Surfaces	Coefficient of friction μ_{max} 1st	2nd	20th	100th
Steel on lead	1.0	1.4	1.4	
Steel on lead-bearing alloy	0.4	0.4	0.7	
Steel on lead-matrix alloy	0.4	0.45	0.8	
Lead on steel	0.9	1.0	1.0	
Lead-bearing alloy on steel	0.55	0.55	0.75	0.95
Lead-matrix alloy on steel	0.7	0.78	1.1	1.2

(d) The Wear of the Alloys on Steel

The wear properties of the alloys were compared by the following method. The upper surface was made of the alloy, and the lower surface of steel. The upper surface was run over the lower surface repeatedly for 400 runs (corresponding to a total track length traversed of 3000 cm). It was then weighed and the loss in weight determined. The friction was also observed during the runs. The surfaces were unlubricated. The amount of wear and the main friction results are summarized in Table IV.

TABLE IV. Wear of lead-base alloys on steel, unlubricated.

Surface	Coefficient of friction μ_{max} 1st run	100th run	400th run	Wear after traversing 3000 cm of track mg
Lead-bearing alloy	0.55	1.0	1.0	11
Lead-matrix alloy	0.7	1.2	1.2	14

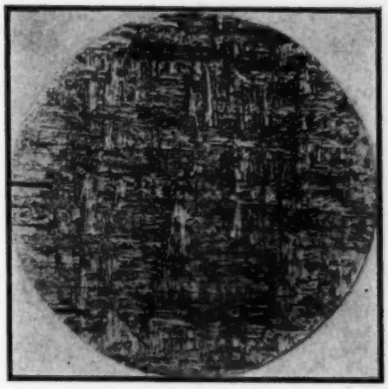

FIG. 9. Track formed by lead-base bearing alloy after traversing the same steel surface 400 times. The smearing of the alloy is very marked and completely obliterates the lapping marks in the steel surface.

During the sliding process the alloy welds on to the steel surface. If the metallic junctions formed are firmly attached to the steel surface, the shearing occurs within the material of the slider, and small fragments of the alloy are left adhering to the steel. With repeated traversals the process is repeated until an appreciable layer of alloy material is smeared on to the steel surface. This is shown clearly in the photomicrographs of the tracks after 400 runs (Figs. 9 and 10). It is seen that at this stage the track almost completely obliterates the lapping marks in the steel surface. It is evident that there is good adhesion between the alloys and the steel and that the shearing does not occur in the junctions at the steel interface but within the bulk of the alloy itself. This is also borne out by the curling up of the worn fragments of alloy and their adhesion to the edge of the slider which occurred during these experiments. The marked wiping of alloy on to the steel surface is probably the reason for the increase in friction observed. After traversing the same track several hundred times, the friction approaches the value for the alloy sliding on itself.

The wear of the lead-base bearing alloy is lower than that of lead-base matrix alloy, but is of the same order. It is evident therefore that the general behavior, the appearance of the track, and the actual values of the wear of the bearing alloy, are very similar to those of the matrix alloy.

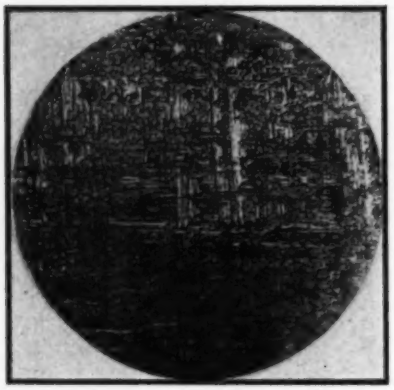

FIG. 10. Track formed by lead-base matrix alloy after traversing the same steel surface 400 times. The smearing of the alloy is very marked and completely obliterates the lapping marks in the steel surface.

(e) Surfaces Lubricated with Mineral Oil

In these experiments the lubricant used was a refined mineral oil and was applied as a thin smear. The friction results are given in Table V.

TABLE V. Friction of lead-base alloys lubricated with mineral oil.

Surfaces	μ_{max}	μ_{mean}	Type of motion
Steel on lead	0.5	0.3	Large stick slips
Steel on lead-bearing alloy	0.12	0.12	Smooth sliding
Steel on lead-matrix alloy	0.14	0.14	Smooth sliding
Lead on steel	0.4	0.22	Large stick slips
Lead-bearing alloy on steel	0.32	0.18	Large stick slips
Lead-matrix alloy on steel	0.35	0.2	Large stick slips

It is seen that the frictional behavior of the bearing alloy is very similar to that of the matrix alloy. The friction of both alloys is lower than that of pure lead. This is particularly marked when the upper surface is of steel.

When the upper surface is of steel the track formed in the alloy consists of a well-defined groove. If the alloys are prepared by polishing and etching, the track may be shown up clearly against the unworn portion of the surface. A typical track for the lead-bearing alloy is shown in Fig. 11, and for the lead-matrix alloy in Fig. 12. It is clear that for both alloys the crystalline structure of the surface has been little disturbed by the passage of the steel slider.

It has been pointed out above that the friction of metal surfaces is determined by the area of real contact A and the shear strength s of the metallic junctions. It is clear, however, that in general the strength of the junctions will depend on the intimacy of contact and strength of adhesion of the metals at the points of real contact. This in turn, will be greatly influenced by the presence of surface films as has been discussed in greater detail in an earlier paper.[1]

Under most experimental conditions, metal surfaces are covered with a thin oxide layer, and other contaminating films. During sliding, these films are torn, many of the surface irregularities penetrate through them, and some metallic contact does occur. We should expect the amount of metallic contact, and the adhesion and shear strength of the junctions, on the whole, to be less than that of the pure metals. Earlier experiments have shown that this is indeed so.**

With soft metals, however, there is considerable distortion of the surfaces and the breakdown of these surface films is very marked. As a result the adhesion is good over most of the area of contact; shearing takes place within the softer metal itself, and the mean shear strength of the junctions becomes approximately equal to the shear strength of the softer metal.

On the other hand, the deliberate addition of suitable lubricant films to the metals, diminishes the intimacy of contact and the strength of adhesion at the junctions. As a result there is a marked reduction in friction and in the amount of metallic seizure and tearing. In the case of the lead-base bearing alloy, for example, lubricated with mineral oil, the original arrangement of the

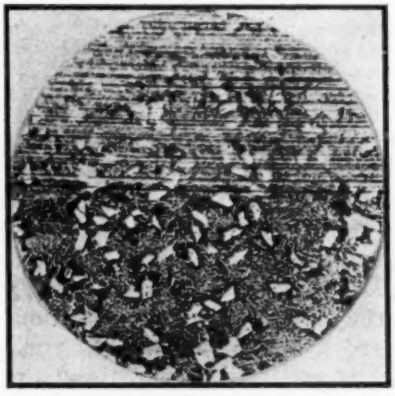

FIG. 11. Portion of track formed on lead-base bearing alloy. First run, lubricated with mineral oil. The arrangement of the hard tin-antimony cuboids had been very little disturbed by the passage of the steel slider. The smearing of the track has been greatly reduced by the presence of the lubricant. Compare with Fig. 5.

** If the surface films are removed by outgassing in high vacuum (see reference 10) the friction increases considerably and values of $\mu = 6$ have been observed, for example, for outgassed nickel or tungsten.

hard crystallites is clearly visible in the track, and it is apparent that although the surface has been deformed by the passage of the steel slider, the tearing and smearing of the matrix material has been very greatly reduced (Fig. 11). However, a certain amount of metallic adhesion has occurred as may be seen from the fine parallel scratches in the track. Similar effects are observed with the lead-base matrix alloy (Fig. 12).

It is clear that the presence of the lubricant film has greatly reduced the extent of metallic seizure. It is true that a certain amount of metallic adhesion and tearing has occurred, where the surface irregularities on the steel slider have torn through the lubricant film. Nevertheless the total area over which this

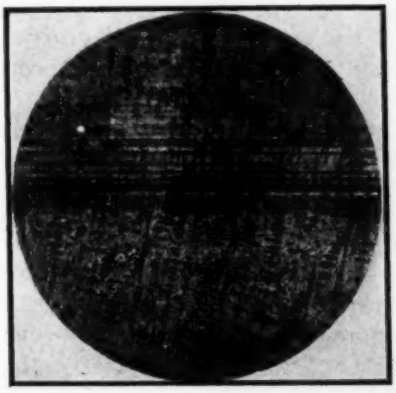

FIG. 12. Portion of track formed on lead-base matrix alloy. First run, lubricated with mineral oil. The crystalline arrangement of the surface has been very little disturbed by the passage of the steel slider, and the smearing has been greatly reduced. Compare with Fig. 6.

metallic seizure has taken place is very much smaller in the presence of the lubricant film than in its absence. It is indeed probable that the main effect of adding a lubricant is to reduce both the area of intimate metallic contact and the shear strength of the junctions.[9,11]

(f) Effect of Repeated Sliding over the Same Track, Lubricated Surfaces.

Continuous traversals of the same track do not produce any marked change in the friction, as is seen in Table VI.

Examination of the tracks shows that as the slider passes repeatedly over the same track, the amount of tearing and smearing increases cumulatively, and the surface structure of the alloys is

[11] Bowden and Tabor, Nature **150**, 197 (1942).

TABLE VI. Repeated sliding over same track, lubricated surfaces.

Surface	Coefficient of friction μ_{max}. 1st run	20th run	100th run
Steel on lead	0.5	0.5+	—
Lead-bearing alloy	0.12	0.12	0.11
Lead-matrix alloy	0.14	0.15	0.17

increasingly disturbed. With the lead matrix alloy, after the 20th run, the arrangement of the surface structure is almost completely obliterated (Fig. 13). With the lead-bearing alloy the tin-antimony crystallites are still clearly visible after the 20th run, but after the 100th run they have been almost entirely obliterated (Figs. 14 and 15). Nevertheless the surface damage of the alloys is greatly reduced by the presence of the lubricant, and there is relatively little tearing of the surface. The amount of pick-up on the steel slider must also be very small. This accounts for the fact that the friction does not increase appreciably with wear, in marked contrast to the observations described for clean surfaces. It is apparent that the area of contact remains essentially unchanged and the junctions formed are still of the same nature as in the first run.

With the bearing alloy, the fact that the friction for the first run, when the crystallites are still clearly visible in the track, is almost the same as for the 100th run, when the crystallites have been almost completely wiped over by the smeared matrix material, is strong evidence for the view that the friction is determined essentially by the properties of the matrix material.

FIG. 13. Central portion of track on lead-base matrix alloy. Twentieth run, lubricated with mineral oil. The structure of the surface has been almost completely obliterated by the passage of the steel slider.

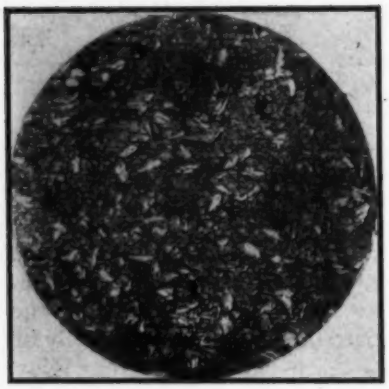

FIG. 14. Central portion of track on lead-base bearing alloy. Twentieth run, lubricated with mineral oil. The tin-antimony cuboids are still clearly visible in the surface of the track.

(g) Effect of Temperature, Lubricated Surfaces

The effect of temperature on the boundary lubricating properties of lubricants has been discussed in previous papers.[12] The break-down of the lubricant is associated with a melting or disorientation of the protective film formed by the lubricant on the metal surfaces. It is markedly dependent on the composition and structure of the sliding surfaces.[13,14]

The effect of temperature on the friction of steel sliding on pure lead and the lead-base alloys lubricated with mineral oil is shown in Fig. 16. The results when the surfaces are lubricated with stearic acid are shown in Fig. 17. In these experiments the metal surfaces were heated to about 70° C; a few crystals of stearic acid were added (M.P. 68°C) and the surfaces allowed to cool to room temperature. There is again a close similarity in behavior of both alloys.

(h) Discussion

These results show repeatedly the similarity between the properties of the lead-base bearing alloy and those of the lead-base matrix alloy. The friction when clean and lubricated, the behavior with respect to temperature and wear, the types of track formed, and the nature of wear are all markedly alike. These properties are also similar to those of pure lead, except that in general the friction of the alloys is less than that of the pure metal. It is evident, therefore, that the behavior of the bearing alloy is similar to that of materials containing no hard crystallites.***

A survey of the main results for the lead-base alloys (summarized in Table VII) indicates that in general, the friction of the lead-base bearing alloy is less by a few percent than that of the corresponding matrix alloy. This difference may be due to the presence of the hard crystallites in the bearing alloy. On the other hand, it is extremely difficult to reproduce in a separate matrix alloy, the complex phase relationships existing in the matrix material of the bearing alloy. This difference in friction may, therefore, be due to differences in the constitution and structure of the matrix alloy and the matrix material of the bearing alloy. The difference in frictional behavior, however, is small and it is apparent that the hard crystallites do not greatly affect the intrinsic frictional or wear properties of the bearing alloy.

It is suggested therefore that the frictional behavior of the lead-base bearing alloy is determined essentially by the properties of the matrix material in it. According to this view, the load is supported mainly by the matrix. The pressure and motion of the steel surface impress the hard crystallites deeper into the matrix and cause an extrusion and smearing of

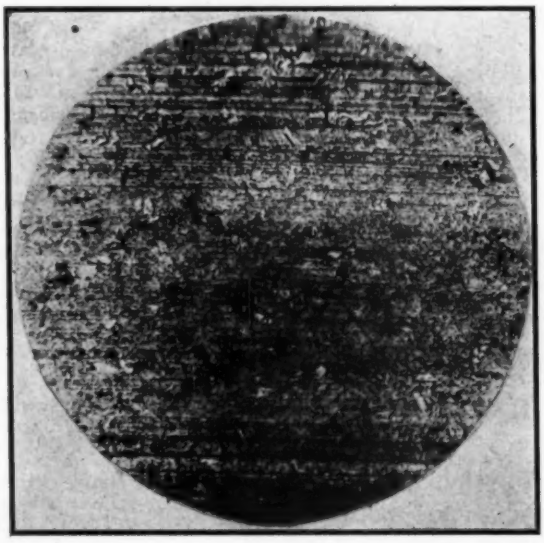

FIG. 15. Central portion of track on lead-base bearing alloy. Hundredth run, lubricated with mineral oil. The hard crystallites have been almost completely obliterated by the repeated passage of the steel slider.

[12] Tabor, Nature **145**, 308 (1940); Nature **147**, 609 (1941).
[13] Hughes and Whittingham, Trans. Faraday Soc. **38**, 9 (1942).
[14] Gregory, Council for Scientific and Industrial Research (Australia), Lubricants and Bearings Section, Report No. A-74 (unpublished).

*** Some earlier workers have made similar suggestions. See for example the discussion in Bassett (see reference 4).

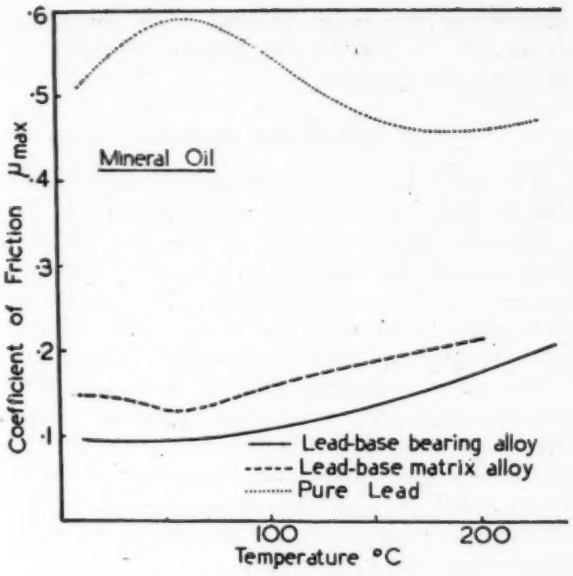

FIG. 16. Variation of friction with temperature for steel sliding on pure lead and lead-base alloys; lubricated with mineral oil.

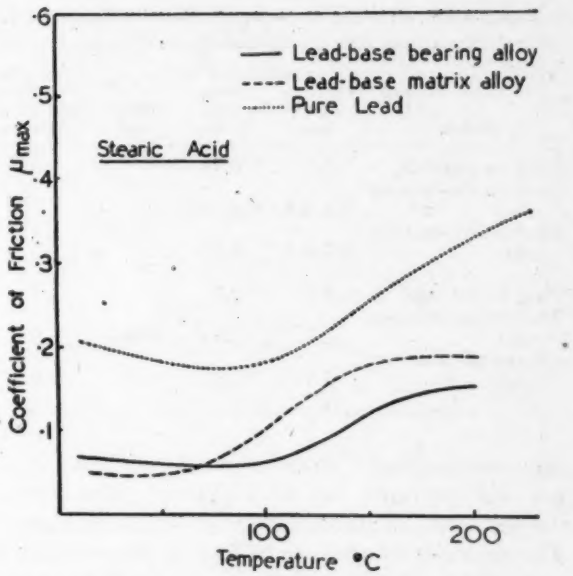

FIG. 17. Variation of friction with temperature for steel sliding on pure lead and lead-base alloys; lubricated with stearic acid.

the matrix material over the surface of the alloy. Welding takes place between the steel surfaces and the matrix material, and the shearing takes place within metallic junctions composed of the matrix material itself. When clean surfaces are used this smearing and tearing of the matrix material over the surface of the track, completely obliterates the arrangement of the hard crystallites. When a lubricant is used, the seizure and smearing is far less and this process is much more gradual. For both clean and lubricated surfaces, the hard crystallites play no appreciable part in the frictional behavior of the bearing alloy.

In practice, however, it is not only the frictional and the wear properties which determine the suitability of an alloy as a bearing metal. It is evident that many of the mechanical properties such as the hardness and its variation with temperature, the compressive strength, and the resistance to mechanical fatigue may all play a vital part in the practical performance. It is true that the hardness of the matrix alloy is of the same order as that of the bearing alloy; but it is about 20 percent lower (measured in Vickers units), and this difference may be of great importance. It is also possible that there may be significant differences in the other mechanical properties, particularly at high temperatures. Such differences between the bearing alloy and the matrix alloy may be, in part, due to the presence of the hard crystallites.

Nevertheless, the evidence supports the view that the hard crystallites make little essential contribution to the *basic frictional* properties of the lead-base bearing alloy. They may, however, play a small but significant role in imparting superior mechanical and physical properties to the alloy under practical running conditions.

6. THE PROPERTIES OF TIN-BASE ALLOYS

A similar series of experiments was carried out on a tin-base bearing alloy with the follow-

TABLE VII. Summary of main results at room temperature for lead-base alloys.

Surface	Coefficient of friction μ_{max} at room temp.						Wear in mg for 3000 cm track clean
	Clean			Mineral Oil		Stearic acid	
	1st run	20th run	100th run	1st run	100th run	1st run	
Steel on—Lead-bearing alloy	0.4–0.45	0.7	—	0.12	0.11–0.12	0.08	11
Lead-matrix alloy	0.4	0.8	—	0.14	0.17	0.06–0.09	14
On steel—Lead-bearing alloy	0.55	0.75	1.0	0.32	—	—	
Lead-matrix alloy	0.7	1.1	1.2	0.35	—	—	

TABLE VIII. Friction of tin-base alloys, unlubricated.

Surface	Coefficient of friction μ_{max} 1st run	20th run	400th run	Wear after traversing 3000 cm of track mg
Steel on pure tin	0.9	0.9		
Steel on tin-bearing alloy	0.7–0.8	0.65–0.8		
Steel on tin-matrix alloy	0.7–0.8	0.85		
Pure tin on steel	0.8	0.9		
Tin-bearing alloy on steel	0.7	0.8	0.6+	0.2
Tin-matrix alloy on steel	0.8	0.85	1.0+	>0.3

ing composition: antimony 6.5 percent, copper 4.2 percent, tin 89.2 percent, and nickel 0.1 per cent. Its mean hardness was 24 (Vickers). The microstructure (see in Fig. 3) shows that it consists of a matrix of a tin rich solid solution, in which are embedded numerous hard needles of copper-tin compound. This alloy was compared with pure tin, and with a tin-base matrix alloy containing 7 per cent antimony, no nickel, and less than 0.4 percent copper. Examination showed that it contained no hard particles and was similar to the matrix material of the tin-base bearing alloy. In hardness and structure, however, it did not appear to be as close an approximation to the matrix of the bearing alloy as was the case with the corresponding lead-base alloys.

(a) Clean Surfaces

All the surfaces tested gave large stick-slip motion when clean. The main friction results are assembled in Table VIII.

It is seen that the friction of the two tin alloys is not very much less than that of pure tin. The results also show that there is no appreciable increase in friction for pure tin and the tin alloys for the first twenty runs. Even after 400 runs the increase in friction is not very marked. This may be due to the fact that the pick-up of the tin alloys on the steel surfaces is relatively small. For example a photomicrograph of the steel surface after the tin-matrix alloy has passed over the same track 400 times shows relatively slight smearing of alloy over the steel. This is confirmed by the wear results. The wear is extremely small: the worn portion of the alloy is brightly burnished and the edges of the worn area are clearly defined.

The effect of temperature on the friction is similar for the pure tin and both tin alloys. From 20° to 200° C the friction remains approximately constant.

(b) Lubricated Surfaces

The main friction results are shown in Table IX for surfaces lubricated with mineral oil.

The frictional behavior of the two alloys is very similar, the friction is low and there is no increase in friction with wear. The tracks are also similar and show the same characteristics as those observed with the lead-base alloys.

The effect of temperature, however, shows a more marked difference in the frictional properties of the two alloys. As may be seen from Fig. 18, the friction of the tin-bearing alloy at 200° C has a value of $\mu_{max}=0.1$ while the tin-matrix alloy has a value of nearer $\mu_{max}=0.4$; its value approaches that of pure tin.

Similar results are observed with stearic acid. At room temperature all three surfaces give smooth sliding with a coefficient of friction of $\mu_{max}=0.21$ for pure tin, 0.07 for tin-bearing alloy, and 0.09 for tin-matrix alloy. At elevated temperatures, however the difference between the two alloys, is more marked. As may indeed be seen from Fig. 19 the frictional behavior of the matrix alloy is intermediate between that of the bearing alloy and of pure tin.

(c) Discussion

It is evident from these results that for unlubricated surfaces the frictional properties of the tin-base bearing alloy are similar to those of the tin-base matrix alloy. The actual values of the friction, the frictional behavior for repeated traversals of the same track, the types of track formed, and the nature of wear are all markedly alike. With lubricated surfaces, at room temperature the friction is also similar, but there is considerable divergence at elevated temperatures. At these temperatures, indeed,

TABLE IX. Friction of tin-base alloys, lubricated with mineral oil.

Surface	Coefficient of friction μ_{max} 1st run	20th run	100th run	Type of motion
Steel on tin	0.6	0.6		Large stick slips
Steel on tin-bearing alloy	0.13	0.13	0.1	Smooth sliding
Steel on tin-matrix alloy	0.13	0.13	0.12	Smooth sliding

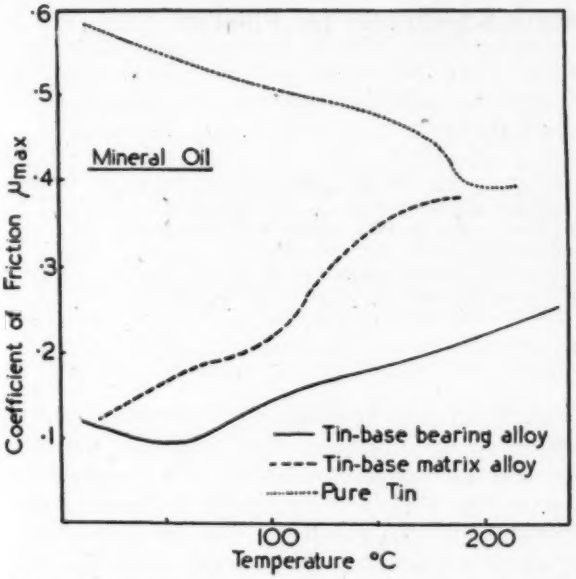

FIG. 18. Variation of friction with temperature for steel sliding on pure tin and tin-base alloys; lubricated with mineral oil.

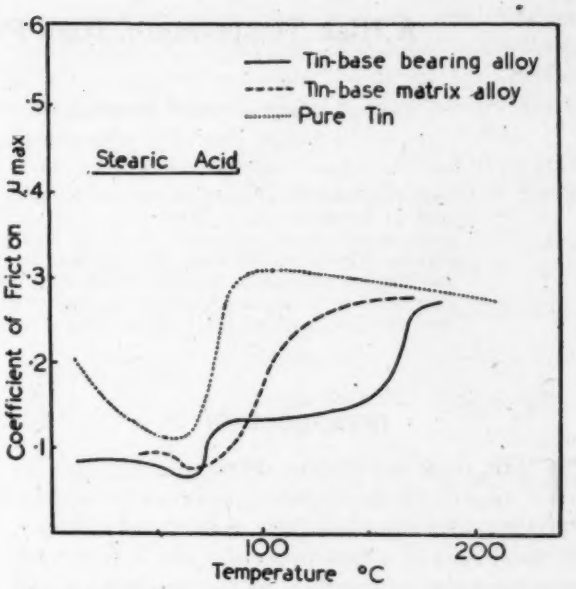

FIG. 19. Variation of friction with temperature for steel sliding on pure tin and tin-base alloys; lubricated with stearic acid.

the frictional behavior of the matrix alloy is intermediate between that of the bearing alloy and of pure tin. It is, of course, possible that slight changes in the composition of the matrix alloy might bring its frictional properties in closer line with those of the bearing alloy. It is, however, possible that with the tin-base bearing alloys the hard acicular crystallites may play a more important part in determining its basic frictional properties.

7. COMPARISON BETWEEN LEAD-BASE AND TIN-BASE ALLOYS

A point of some interest is the comparison between the lead-base and tin-base alloys, particularly in view of the present shortage of tin. The frictional properties of the lead-base bearing alloy when clean and when lubricated, at room temperature and at elevated temperatures are generally slightly better than those of the tin-base bearing alloy. However, its wear on steel surfaces is very much heavier. Its hardness (measured in Vickers units) is also about 15 percent less. Apart therefore, from the question of mechanical properties which may play a vital role in the practical behavior of a bearing, the lead-base bearing alloy should, in practice, be at least as satisfactory as the tin-base alloy, from the point of view of its frictional behavior. Under severe conditions, however, the rate of wear of the lead-base bearing alloy may be very much higher.

8. ACKNOWLEDGMENT

I wish to express my thanks to Dr. F. P. Bowden for his helpful discussion at many points of the investigation and to Mr. R. W. K. Honeycombe for his assistance in the preparation of several alloys and for his general advice on certain metallurgical aspects of this work.

I also wish to thank Mr. J. N. Gregory for making some of the earlier frictional measurements.

A High Temperature, High Pressure Rheometer for Plastics*

H. K. NASON
Monsanto Chemical Company, Plastics Division, Springfield, Massachusetts†

(Received January 3, 1945)

A modified Bingham-type rheometer, designed for operation at temperatures up to 500°F and at pressures up to 2000 p.s.i. is described. Interchangeable orifice plates permit wide variation of shear conditions. With this instrument flow properties may be studied under conditions approximating those encountered in the actual processing of thermoplastics, e.g., by molding or extrusion. Typical results are presented for cellulose acetate, polystyrene, and polyvinyl resin plastics, and correlation with practical experience is pointed out. The instrument is slow, and this limits its usefulness for other than research investigations.

INTRODUCTION

THE most significant distinguishing characteristic of the organic materials commonly known as "plastics" is their ability to be shaped by some sort of a flow process. Flow is involved, at some point or another, in the production and fabrication of all such materials. It is only natural, therefore, that reliable, quantitative methods for studying and measuring the flow properties of plastics are of great technical importance.

A variety of convenient and reliable viscometers are available for use with solutions or with those materials which are relatively fluid at moderate temperatures and pressures. Most of the plastics used for molding and extruding, however, can be processed only at high temperatures and pressures, and do not flow to any appreciable extent under the conditions normally employed in laboratory rheological measurements. Hence, a number of types of apparatus have been developed in an attempt to measure the flow of such plastics under conditions similar to those employed in the actual processing. The experimental difficulties are considerable, however, and no instrument yet developed has proven completely satisfactory from all standpoints. The almost complete omission of such instruments (and of the problem of high temperature, high pressure measurements on plastics) from Scott Blair's excellent review[1] is, perhaps, symptomatic.

Similar problems have been solved rather successfully in glass technology,[2–7] but the methods employed are, unfortunately, not very suitable for use with organic plastics. The asphalt industry has also been rationalized, rheologically speaking, by the excellent work of several rheologists, particularly in America and Britain, but these methods, also have only limited usefulness with the plastics with which we are concerned here.[8–26]

---

* Presented before the 1944 meeting of the Society of Rheology.

† Present address: Monsanto Chemical Company, Central Research Department, Dayton, Ohio.

[1] G. W. Scott-Blair, *A Survey of General and Applied Rheology* (Pitman Publishing Corporation, New York, 1944).

[2] N. W. Taylor and P. S. Dear, "Elastic and Viscous Properties of Several Soda-Silica Glasses in the Annealing Range of Temperature," J. Am. Cer. Soc. [9] **20**, 296–304 (1937).

[3] N. W. Taylor and R. F. Doran, "Elastic and Viscous Properties of Several Potash-Silica Glasses in the Annealing Range of Temperature," J. Am. Cer. Soc. [3] **24**, 103–9 (1941).

[4] N. W. Taylor, E. P. McNamara, and J. Sherman, "A Study of the Elastico-Viscous Properties of a Soda-Lime-Silica Glass at Temperatures near the Transformation Point," Mineral Industries Experiment Station, Tech. Pap. 34, Pennsylvania State College, State College, Pennsylvania, 1937.

[5] J. Boow and W. E. S. Turner, "The Viscosity and Working Characteristics of Glasses. I. The Viscosity of Some Commercial Glasses at Temperatures Between Approximately 500° and 1400°," J. Soc. Glass Tech. **26**, 215–37 (1942).

[6] J. R. Rait, "The Viscosity of Slags and Glasses," Trans. Brit. Cer. Soc. **40**, 157–229 (1941).

[7] R. Hay, "The Viscosity Determination of Blast-Furnace Slags," J. West Scot. Iron Steel Inst. **49**, 89–99 (1942); Chem. Abst. **37**, 1961 (1943).

[8] C. U. Pittman and R. N. Traxler, "Rheological Properties of Asphalts. I. Effect of Temperature," Physics **5**, 221–4 (1934).

[9] R. N. Traxler, C. U. Pittman, and F. B. Burns, "Rheological Properties of Asphalt. II. Discussion of Penetration-Viscosity Relationships," Physics **6**, 58–60 (1935).

[10] R. N. Traxler and H. E. Schweyer, "Rheological Properties of Asphalts. III. A Viscosity Index," Physics **7**, 67–72 (1936).

[11] C. E. Coombs and R. N. Traxler, "Rheological Properties of Asphalts. IV. Observations Concerning the Anomalous Flow Characteristics of Air-Blown Asphalts," J. App. Phys. **8**, 291–6 (1937).

[12] R. N. Traxler and C. U. Pittman, "Penetration-Viscosity Relationship for Asphaltic Bitumens," J. App. Phys. **8**, 70–1 (1937).

[13] R. N. Traxler and H. E. Schweyer, "Measurement of High Viscosity," Proc. A.S.T.M. **36**, II, 518–530 (1936).

Our problems are, in many ways, closely related to those of the rubber industry, and the progress which has been made toward a better understanding of the fundamental rheological properties of rubber, and toward better methods for measuring these properties, has been very useful to plastics technologists. Thus, extrusion,[27–32] parallel-plate,[32–36] shearing-disk,[37–39] and similar types of instruments, originally designed for use with rubber, have been of some value in studying the rheology of plastics. None of the rubber instruments has, however, been wholly satisfactory for use with plastics.

Of all the types of rheometers which have been tried with plastics,[40–62] the parallel-plate,[40–46] and

[14] R. N. Traxler and C. E. Coombs, "The Colloidal Nature of Asphalt as Shown by its Flow Properties," J. Phys. Chem. **40**, 1133–47 (1936).

[15] R. N. Traxler, "Bituminous Plastics-Determination of Flow Properties," Ind. Eng. Chem., Anal. Ed. **8**, 185–8 (1936).

[16] R. N. Traxler, "Flow Properties of Asphalts Measured in Absolute Units," Ind. Eng. Chem. **30**, 322–4 (1938).

[17] R. N. Traxler and L. R. Moffatt, "Flow in Asphalts Shown by the Method of Successive Penetrations," Ind. Eng. Chem., Anal. Ed. **10**, 188–191 (1938).

[18] R. N. Traxler, H. E. Schweyer, and J. W. Romberg, "Rheological Interpretation of Asphalt Tests," Proc. A.S.T.M. **40**, 1182–1200 (1940).

[19] R. N. Traxler, J. W. Romberg, and H. E. Schweyer, "Rotary Viscometer for Determination of High Consistencies," Ind. Eng. Chem., Anal. Ed. **14**, 340–3 (1942).

[20] W. F. Fair, Jr. and E. W. Volkmann, "The Viscosity of Pitches," Ind. Eng. Chem., Anal. Ed. **15**, 235–9 (1943).

[21] W. F. Fair, Jr., and E. W. Volkmann, "Viscosity of Coal Tar Residues," Ind. Eng. Chem., Anal. Ed. **15**, 240–2 (1943).

[22] C. Mack, "The Flow Properties of Asphalts and Their Measurement by the Penetrometer," J. Soc. Chem. Ind. **58**, 306–10 (1939).

[23] D. C. Broome and L. Bilmes, "Some Rheological Problems in Gunned Asphalt," J. Soc. Chem. Ind. **60**, 184–90 (1941).

[24] W. W. Pendleton, "Penetrometer Method for Determining the Flow Properties of High Viscosity Fluids," J. App. Phys. **14**, 170–80 (1943).

[25] R. N. J. Saal and J. W. A. LaBout, "The Relation Between Absolute Viscosity and Penetration of Asphaltic Bitumens," Physics **7**, 408–12 (1936).

[26] R. N. J. Saal and J. W. A. LaBout, "Rheological Properties of Asphaltic Bitumens," J. Phys. Chem. **44**, 149–65 (1940).

[27] J. H. Dillon and N. Johnston, "The Plastic Properties of Several Types of Unvulcanized Rubber Stocks at High Rates of Shear," Physics **4**, 225–35 (1933).

[28] J. H. Dillon, "A Simplified Extrusion Plastometer for Unvulcanized Rubber," Physics **7**, 73–6 (1936).

[29] R. H. Kelsey and J. H. Dillon, "Rheological Properties of Natural and Synthetic Rubbers," J. App. Phys. **15**, 352–9 (1944).

[30] H. A. Schultz and R. C. Bryant, "A New Extrusion Plastometer," J. App. Phys. **15**, 360–3 (1944).

[31] G. P. Bosomworth, "Instrumentation," Ind. Eng. Chem. **33**, 573–4 (1941).

[32] W. M. Widenor, "The Measurement of the Plasticity of Rubber," India Rubber World, 41–6 (November 1, 1939).

[33] I. Williams, "The Plasticity of Rubber and Its Measurements," Ind. Eng. Chem. **16**, 362–4 (1924).

[34] E. Karrer, "A New Plastometer," Ind. Eng. Chem., Anal. Ed. **1**, 158–60 (1929).

[35] E. Karrer, J. M. Davies, and E. O. Dieterich, "A Simplified Goodrich Plastometer," Ind. Eng. Chem., Anal. Ed. **2**, 96–9 (1930).

[36] J. Holkstra, "The Balance Plastometer," Physics **4**, 285–8 (1933).

[37] M. Mooney, "A Shearing-Disc Plastometer for Unvulcanized Rubber," Ind. Eng. Chem., Anal. Ed. **6**, 147–51 (1934).

[38] M. Mooney and R. H. Ewart, "The Conicylindrical Viscometer," Physics **5**, 350–4 (1934).

[39] M. Mooney, "The Rheology of Raw Rubber," Physics **7**, 413–20 (1936).

[40] R. L. Peek, Jr., "A Compression Test for Soft Solids," Bell Lab. Record **11**, 290–5 (1933).

[41] W. G. Wearmouth and J. S. Small, "Flow Properties of Thermoplastics," Brit. Plastics **12**, 377–9 (1941).

[42] W. G. Wearmouth, "Physics and the Plastics Industry," Chem. and Ind. **16**, 1176–82 (1938).

[43] R. Houwink and Ph. N. Heinze, "The Testing of Synthetic Resins with the Plastometer," Kunststoffe **28**, 283–7 (1938)

[44] N. M. Foote, "Thermoplastic Flow of Polystyrene," Ind. Eng. Chem. **36**, 244–8 (1944).

[45] E. G. Couzens and W. G. Wearmouth, "Some Observations on the Mechanical Testing and Flow Properties of Industrial Plastics," J. Soc. Chem. Ind. **61**, 69–74 (1942).

[46] F. J. Bondi and L. T. Work, "Evaluation of Resinous Flow," Mod. Plastics **18**, 57–61, 88, 90 (August, 1941); cf. Bell Lab. Record **21**, 18–19 (September, 1942).

[47] G. L. Peakes, "Measuring Plasticity of Hot Molding Compounds," Plastic Prod. **10**, 53–7 (February, 1934).

[48] G. L. Peakes, "Types of Tests Obtainable with the Flow Tester," Plastic Prod. **10**, 93–8 (March, 1934).

[49] G. L. Peakes, Plastic Prod. **10**, 132–5 (April, 1934).

[50] C. H. Penning and L. W. A. Meyer, "Flow Relations of Thermoplastic Materials," A.S.T.M. Symposium on Plastics, pp. 23–30 (1938).

[51] L. W. A. Meyer, "Measurement of the Flow Temperature of Thermoplastic Molding Materials," A.S.T.M. Bull. No. 105, 23–6 (August, 1940).

[52] C. A. Nash, "Flow Relationship of Thermoplastics," paper presented at 1940 annual meeting of the Society of Rheology.

[53] L. M. Debing and S. H. Silberkraus, "Plasticity of Phenol-Formaldehyde Resins and Molding Powders," Ind. Eng. Chem. **33**, 972–5 (1941).

[54] R. Burns, "Measuring the Plasticity of Molding Compounds," Proc. A.S.T.M. **40**, 1283–8 (1940).

[55] A. Amigo, "Test Apparatus for Molding Materials," Brit. Plastics **12**, 313–6 (1941).

[56] A. N. Luknitzky, Plasticheskye Massey **3**, 43–7 (1934).

[57] F. E. Wiley, "Working-Range Flow Properties of Thermoplastics," Ind. Eng. Chem. **33**, 1377–80 (1941).

[58] H. Stäger, W. Siegfried, and R. Sänger, "Phenolic Resins. II. Mechanical Properties in Relation to Structure," Schweiz. Arch. Angew, Wiss. Tech. **7**, 153–74 (1941).

[59] H. C. Pocklington, "Rough Measurement of High Viscosities," Proc. Camb. Phil. Soc. **36**, 507–8 (1940).

[60] I. F. Kanavetz, "New Method for Determining the Plasticity and Rate of Hardening of Plastic Materials under Molding Conditions," Org. Chem. Ind. (U.S.S.R.) **7**, 368–73 (1940).

[61] A. Schwittman, "A New Method for Determining the Flow Properties and Rate of Hardening of Heat-Convertible Artificial Plastics," Kunststoffe **29**, 190–2 (1939).

[62] M. Speitman, "The Plastographical Measurement of the Polymer-Homolog Conditions of Artificial Resins in Relation to the Method of Formation," Chem.-Ztg. **61**, 415–9 (1937).

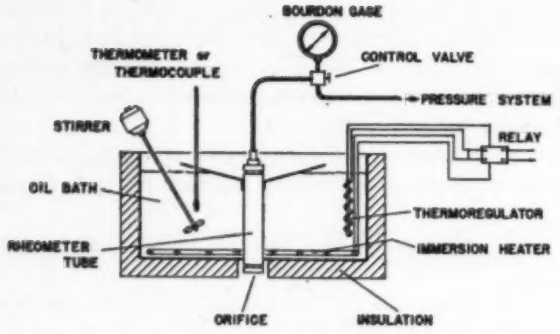

FIG. 1. Schematic diagram of Monsanto rheometer.

extrusion[44,47–56] varieties have been most widely used. The Rossi-Peakes instrument,[47] an extrusion-type, has been rather generally accepted in America, although peculiarly not for the thermosetting plastics, for which it was designed; its use for measuring the flow properties of thermoplastics has been standardized by Committee D-20 on Plastics of the A.S.T.M.[63] For thermosetting plastics, empirical molding tests are still favored.[53,64] None of these methods is entirely satisfactory. Most of them are "hybrid," as Mooney has remarked,[65] and, with thermoplastics at least, most fail to give useful information on rheological behavior at molding temperatures and pressures or to differentiate between materials whose molding characteristics are known to be different.

The instrument described herewith was developed in an effort to obviate some of these disadvantages and to obtain more useful data on the behavior of thermoplastic materials under actual molding and extrusion conditions.

APPARATUS

The apparatus is a gas-actuated viscometer of the Bingham[66] type, and was designed especially for operation at high temperatures and at high pressures. It is shown diagrammatically in Fig. 1, and a photograph of the entire assembly is shown in Fig. 2. The viscometer itself resembles, in some ways, the conventional Saybolt instrument. It comprises a precision-bored steel tube, equipped at the top with pressure fitting, retainer nut and packing ring (a soft lead ring), and at the bottom with orifice plate, retainer nut, and packing ring. This arrangement is shown in Fig. 3. The entire assembly is immersed in an oil bath, suitably equipped for heating, stirring and accurate thermostatic control. Temperatures as high as 500°F may be maintained by using suitable tempering oils as the heat transfer media. Through the top pressure fitting, connection is made to a source of controlled high pressure gas. In our work we have used nitrogen from commercial cylinders (approximately 2000 p.s.i.), and have obtained the desired range of pressures by cascading through a series of pressure bottles (Fig. 2). A carefully calibrated Bourdon gage is used to measure the pressure at the inlet to the viscometer.

The orifice plates can be removed quickly and are interchangeable. Hence, a variety of shear conditions can be obtained by varying the diameter and length of the orifice. The two plates shown in Fig. 4 have proven most useful in our work.

It has been found convenient to preform the test material into a cylinder which just fits into the rheometer tube, and a small mold was built to facilitate this operation. An aluminum ball whose diameter is about $\frac{3}{16}$ inch less than the diameter of the tube is usually placed on top of the material to act as a piston. This prevents channeling and permits a larger number of tests to be made without refilling. Shear between the ball and the walls of the tube is so small relative to the shear at the orifice that it cannot be detected.

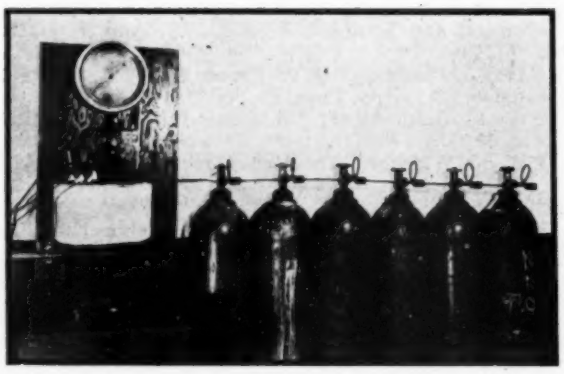

FIG. 2. General view of apparatus.

[63] "Standard Method of Test for Measuring Flow Temperatures of Thermoplastic Molding Materials," A.S.T.M. Designation: D569–43.

[64] "Tentative Method of Testing for Measuring Relative Mobility of Thermosetting Molding Powder," A.S.T.M. Designation: D731–43T.

[65] M. Mooney, "Definition of Consistency and Theoretical Considerations," A.S.T.M. Symposium on Consistency, 1937.

[66] E. C. Bingham, *Fluidity and Plasticity* (McGraw-Hill Book Company, New York, 1922), p. 77.

OPERATION

The orifice plate is secured in place and the oil bath is adjusted to the desired operating temperature. The tube is then filled with the premolded slug of test material and the top pressure fitting is tightened down. Sufficient time is allowed to elapse to insure that the material is at the desired temperature; usually thirty minutes is adequate. The pressure in the first bottle is adjusted to the desired value, and is then allowed to act upon the specimen by adjustment of the control value. The first foot or so of material extruded from the orifice usually contains air bubbles and is discarded.

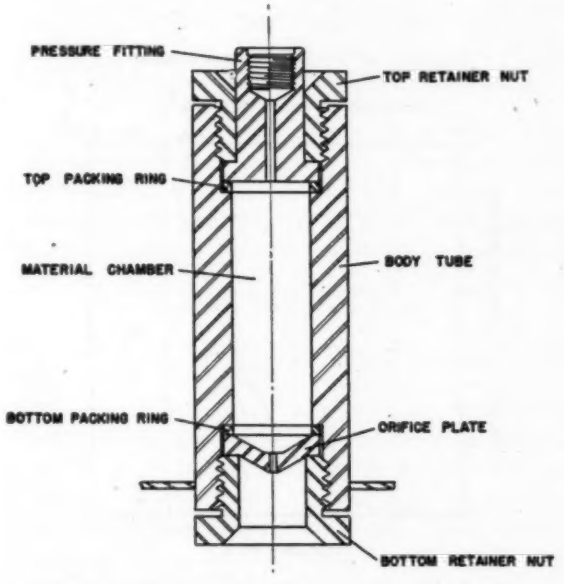

FIG. 3. Rheometer tube with orifice plate in place.

When a steady flow has been obtained, accurately timed samples are collected in weighing bottles, or linear extrusion rate is noted. From these, extrusion rates can be determined. Usually, three to five observations are made, after which extrusion is stopped by closing the valve to the gas cylinder and releasing the pressure from the system. A higher pressure is then built up in the second cylinder, and the above process is repeated to obtain data at a second pressure. In this way, data are obtained for extrusion rates at a series of driving pressures but at constant temperature, and may be plotted. By operating similarly at other temperatures, a family of flow curves can be obtained. A typical set of such curves for polystyrene is shown in Fig. 5. The volume of gas in the pressure cylinders is so

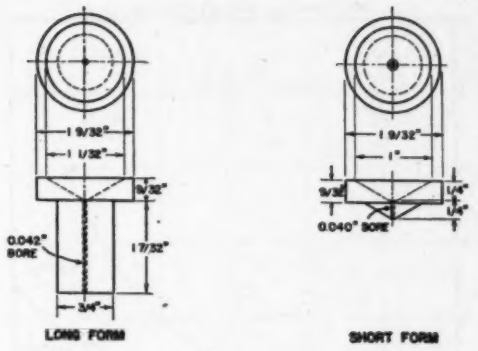

FIG. 4. Orifice plates for Monsanto rheometer.

large relative to the volume of the piping and rheometer tube that no detectable change in pressure occurs during a test run.

At low rates of shear, smooth extruded filaments are obtained. At Reynolds numbers substantially above 800 to 1000, however, the extruded material becomes rough and wavy, and the effect increases as pressure is increased. Advantage may be taken of this effect to study the effect of extrusion conditions on surface smoothness, and special dies have been built to facilitate such studies in special cases.

CALCULATIONS

Shearing stresses and rates of shear are easily calculated from the standard formulae.[67] In our

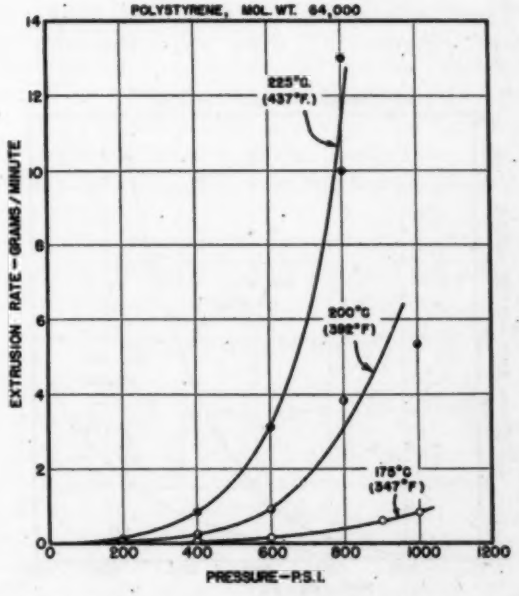

FIG. 5. Flow curves for polystyrene of 64,000 Mol. Wt.

[67] Reference 66, pp. 8–80.

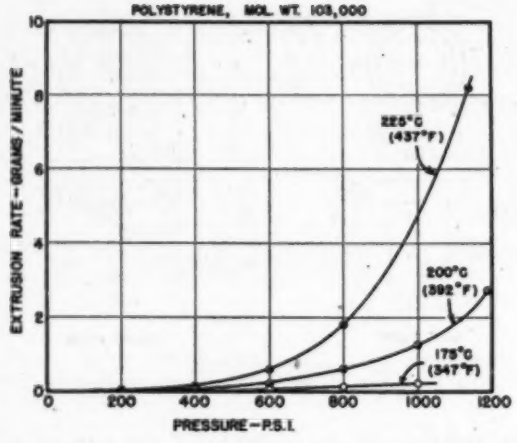

FIG. 6. Flow curves for polystyrene of 103,000 Mol. Wt.

work, however, we usually have not found it worthwhile to express results in these units. The plot of extrusion rate versus pressure conveys sufficient information. Where it is desired to obtain fundamental rheological data, or where basic constants for use in other calculations are needed, the data should be expressed in absolute units. One of the advantages of this instrument is that such calculations can be made and that basic rheological data can be obtained in c.g.s. units.

RESULTS

a. Polystyrene

The standard A.S.T.M. test (Rossi-Peakes flow tester; reference 63) does not adequately distinguish between samples of polystyrene whose behavior under molding and extrusion conditions differ greatly. The Monsanto rheometer gives much more satisfactory results. Figures 5 and 6 show extrusion rate—pressure curves at 175°, 200°, and 225°C for two polystyrene samples of 64,000 and 103,000 molecular weight, respectively. The A.S.T.M. flow temperatures of the materials are 265°F and 275°F, respectively. In Fig. 7, extrusion rate-pressure curves at 200°C for these two materials are plotted together for comparison. (The short orifice was used in all examples shown in this paper.)

It is evident that better differentiation of these materials is obtained with the Monsanto rheometer.

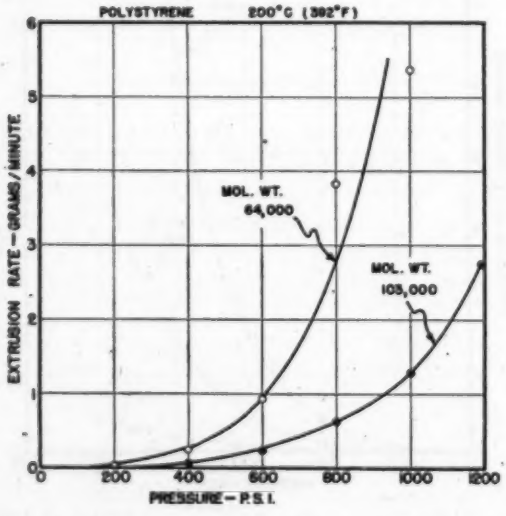

FIG. 7. Comparative flow curves for polystyrenes of 64,000 and 103,000 Mol. Wt.

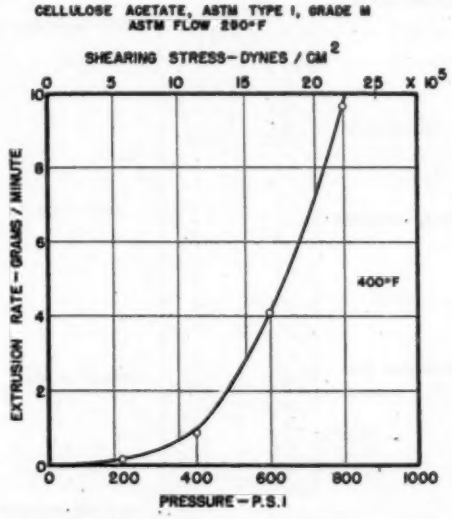
CELLULOSE ACETATE, ASTM TYPE I, GRADE M
ASTM FLOW 290°F
SHEARING STRESS – DYNES / CM²
EXTRUSION RATE – GRAMS / MINUTE
400°F
PRESSURE – P.S.I.

FIG. 8. Typical flow curve for cellulose acetate.

b. Cellulose Acetate

Data for a typical cellulose acetate molding composition are shown in Fig. 8. The material conforms to Type I, Grade M, of A.S.T.M. Specification D706-43*T*,[68] and has an A.S.T.M. flow temperature of 290°F. Flow in grams per minute is plotted against both pressure in psi and shearing stress in dynes per sq. cm at a temperature of 400°F.

A comparison of Figs. 7 and 8 shows that the cellulose acetate possesses better flow than either of the polystyrenes, under comparable conditions of temperature and pressure, although the A.S.T.M. test would seem to indicate the opposite. This is one of the well-known inconsistencies

[68] "Tentative Specifications for Cellulose Acetate Molding Compounds," A.S.T.M. Designation: D706-43T.

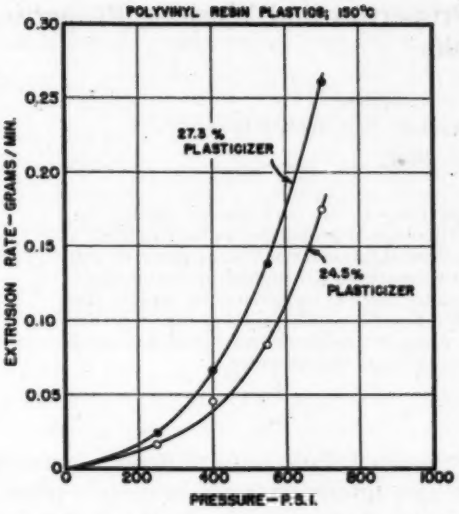

FIG. 9. Effect of plasticizer content on flow curves for polyvinyl resin plastics.

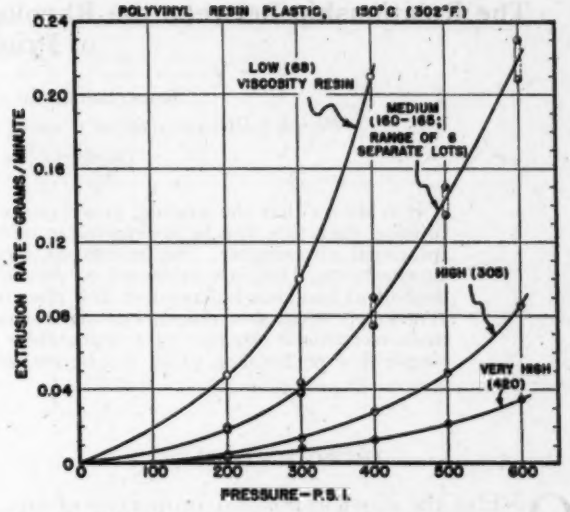

FIG. 10. Effect of resin viscosity (Mol. Wt.) on flow curves of plasticized polyvinyl resin plastics.

of the Rossi-Peakes instrument. The data from the Monsanto rheometer are in agreement with molding experience, which has found that higher temperatures must be used to mold polystyrene.

c. Vinyl Resin Plastics

Figures 9 and 10 are typical of the flow curves which can be obtained with plasticized polyvinyl acetal plastics. Figure 9 shows the effect of plasticizer content on flow at 150°C of compositions based on a medium viscosity resin. Figure 10 shows the effect of resin viscosity on flow at 150°C of compositions containing 27.3 percent plasticizer. Data of this type have been found invaluable in studies of the effect of plastic composition and of processing variables on flow.

It might be well at this point to reemphasize the non-Newtonian nature of most commercial plastic materials. This makes it impossible to obtain a reliable conception of their rheologic behavior by testing at a single fixed temperature, shearing force, or rate of shear, and renders comparisons based on such arbitrarily defined conditions extremely hazardous. Each material must be studied over a range of test conditions, and the entire flow curve must be evaluated, before reliable conclusions can be drawn. This is especially true since some materials show rapid changes in consistency in certain narrow but critical temperature ranges, while other materials change only gradually and show no such critical regions. The present instrument is especially useful for detecting and evaluating such effects.

LIMITATIONS

The principal disadvantage of this instrument is its slowness. Considerable time is required to load the instrument and bring it up to thermal equilibrium. The orifice plate must be removed between each run and the tube cleaned (a soft brass scraper, shaped to fit the tube, has been used to facilitate the cleaning operation). This makes it rather impractical to use the instrument for routine control testing. For special investigations of a research nature, however, this disadvantage is more than offset by the fact that data can be obtained, as outlined above, which can be obtained with no other instrument currently available.

A second important limitation is that the instrument probably cannot be used for plastics which thermoset rapidly.

ACKNOWLEDGMENT

Mr. N. A. Koop cooperated in the design and construction of the instrument. Mr. Russell Omdahl, Dr. C. K. Bump, and Mr. R. D. Dunlop contributed to the results reported herein. To Mr. T. S. Carswell we are indebted for encouragement, criticism, and support of the work.

The Relationship Between the Rheological Properties and Working Properties of Printing Inks

ROLF BUCHDAHL AND JOAN E. THIMM
Research Division General Printing Ink Corporation New York, New York

(Received December 22, 1944)

It is shown that the working properties of a printing ink, i.e., its performance during the printing operation, can be interpreted in terms of the rheological properties as measured in a rotational viscosimeter. The instrument used in this investigation is a viscosimeter of the Stormer type. Data are presented to show that it is necessary to distinguish between time-dependent and time-independent flow phenomena. Various theories suggested to explain the time-independent flow phenomena are discussed briefly. The flow of a printing ink over the main mechanical elements of a typographic printing press is analyzed and correlated with simple flow phenomena which can be measured in a rotational viscosimeter.

INTRODUCTION

ONE of the most important properties of any printing ink is its performance during the printing operation. To be satisfactory, the ink material must travel from the reservoir or ink fountain to the printing plate and be distributed in such manner that the film of ink, on printing, gives a satisfactory reproduction of the printing plate. On presses where a plurality of rollers is employed to transfer ink from the fountain and distribute it upon the printing plate, the flow properties of the ink determine whether or not satisfactory transfer through such roller system is secured.

Printing inks are colloidal dispersions of pigments in various organic liquids in which the pigment concentration is 10–70 percent by weight. The rheological properties of such systems are complex and can best be evaluated in a rotational viscosimeter, measuring the rate of shear as a function of the shearing force. Wolarwitsch and Borinewitsch,[1] Arnold and Goodeve,[2] and Green and Weltmann[3–5] to name a few, have reported flow measurements on printing inks or similar materials. The significance of the flow properties in the printing process, however, is not discussed in these papers. On the other hand, Bekk,[6] Green,[7] and Reed[8] among others, have reported data using different instruments which give information about certain properties of printing inks considered important in the printing process, such as "tack," and "length." In this prior work attempts have been made to reproduce fairly accurately some mechanical phase of the printing process. This approach has, however, a number of serious drawbacks: (1) The results usually cannot be expressed in terms of fundamental rheological quantities. This makes it impossible to relate those data, if they are technically significant, to the actual flow properties of colloidal dispersions as measured in a rotational viscosimeter. (2) By these methods only one of a number of flow properties is determined leaving the description of the rheological properties of a printing ink incomplete. (3) Since it is never possible to reproduce exactly the mechanism of a printing press except by building another one, the results obtained with these different instruments cannot be relied on to give complete information about the performance of a printing ink on a printing press.

This paper describes a somewhat different approach to the subject to overcome the above-mentioned difficulties. It will be shown that it is possible to analyze the flow of an ink on a printing press in terms of simple flow phenomena which in turn can be directly related to results obtained from measurements with a rotational viscosimeter. Such a correlation between the rheological properties and the working properties of printing inks is of particular interest to the Graphic Arts industry. The proper formulation of printing inks is essentially still an "art" because of the lack of objective methods to evaluate the working properties, the color properties, and the final print in terms of scientific quantities. The evaluation of the working properties of printing

[1] M. P. Wolarwitsch and V. S. Borinewitsch, Kolloid Zeits. **77**, 93 (1936).
[2] J. E. Arnold and C. F. Goodeve, Trans. Faraday Soc. **35**, 652 (1939).
[3] H. Green and R. N. Weltmann, Ind. Eng. Chem. Anal. Ed. **15**, 201 (1943).
[4] R. N. Weltmann, J. App. Phys. **14**, 343 (1943).
[5] R. N. Weltmann and H. Green, J. App. Phys. **14**, 569 (1943).
[6] J. Bekk, Deutsch. Drucker **44**, 450 (1938).
[7] H. Green, Ind. Eng. Chem., Anal. Ed. **13**, 632 (1941).
[8] R. F. Reed, Lithograph. Tech. Found. Tech. Bull. No. 2, Research Series No. 4 (1939).

inks in terms of rheological quantities is a first step to establish a science of Graphic Arts.

THE RHEOLOGICAL PROPERTIES OF PRINTING INKS

The instrument used in most of the measurements reported below is a rotational viscosimeter of the Stormer type. It is constructed in such a way that the viscosity coefficient of a Newtonian liquid can be obtained with an accuracy of about ±15 percent without using calibrating liquids or correction factors. The main parts of the instrument are shown in Fig. 1. The part of the viscosimeter containing the liquid is immersed in a constant temperature bath regulated to ±0.1°C. The following equations are used to calculate the rate of shear (D) and the shearing force (F):

$$D=\frac{w_0\times r_1}{r^2\times 1/r_1-1/r_2}, \qquad \begin{matrix} w_0=\text{angular velocity.} \\ r=(r_1+r_2)/2. \end{matrix} \tag{1}$$

$$F=(m\times g\times r_D)/(r_1\times r_2\times h). \tag{2}$$

For a Newtonian liquid a linear relationship exists between the shearing force and the rate of shear at a given temperature (see Fig. 2, curve No. 1), until laminar flow ceases at a given

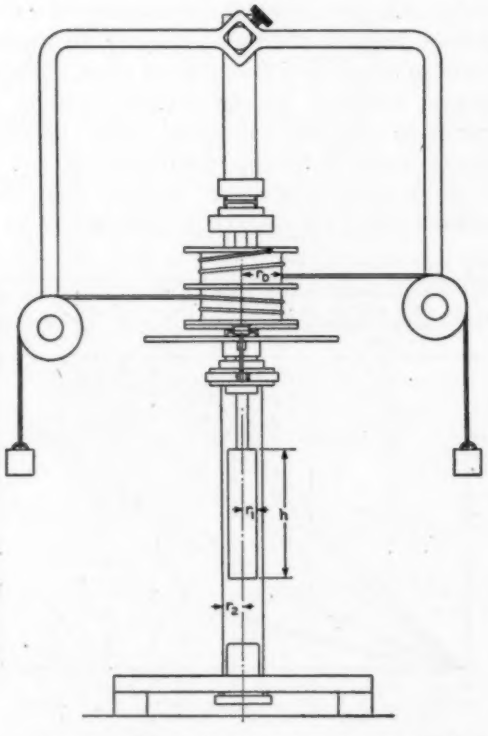

FIG. 1. Diagrammatic sketch of rotational viscosimeter.

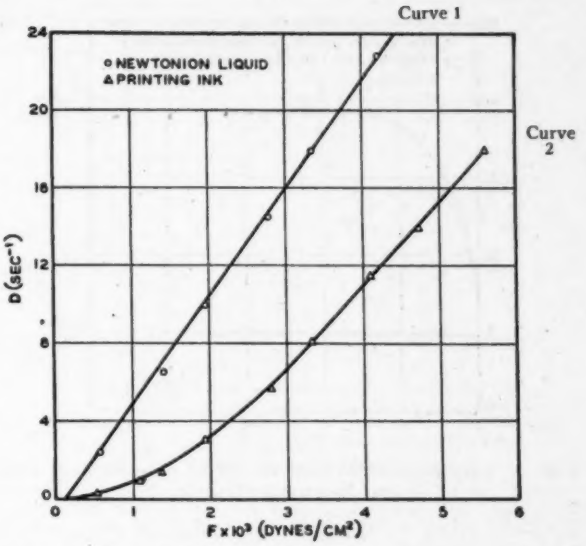

FIG. 2. Time-independent flow curves of a Newtonian and non-Newtonian liquid.

critical rate of shear. The rate of shear for a given shearing force, is independent of time (see Fig. 3, curve No. 1) if the time element is not shorter than a few seconds.*

The flow properties of colloidal systems such as printing inks are somewhat more complicated. For a given shearing force the rate of shear is usually a function of time as shown, for example, in curve No. 2 of Fig. 3. The rate of shear always approaches a constant or equilibrium value which is independent of time, irrespective of the changes in the rate of shear previous to the establishment of a constant value. Plotting the equilibrium values as a function of the shearing force generally gives a relationship such as that shown in curve No. 2 of Fig. 2. The slope of this curve, which has the dimensions of viscosity, is now a function of the shearing force. For dispersions such as printing inks, the viscosity usually decreases with increasing shearing force (or rate of shear) until it reaches a constant value. It is generally believed that this type of flow is due to the existence of "structure" which breaks down when the material is sheared. Attempts to obtain a quantitative relationship between the shearing force and the rate of shear on the basis of the concept of "structure" have not, so far, been too successful. Goodeve[9] attempted to develop a theory

* Weltmann, Ind. Eng. Chem., Anal. Ed. 15, 424 (1943), reported data which would indicate the presence of such a time effect for Newtonian liquids. Attempts to duplicate these results, using the instrument described above, were unsuccessful.

[9] C. F. Goodeve, Trans. Faraday Soc. 35, 342 (1938).

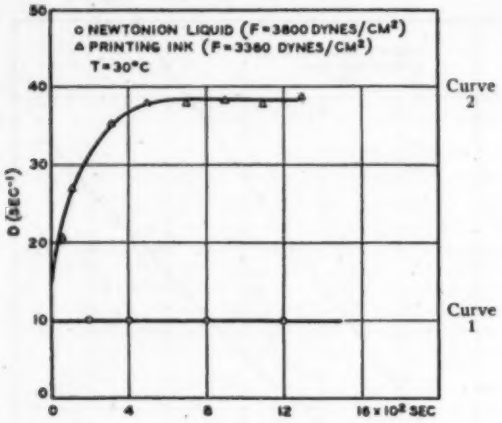

FIG. 3. Time-dependent flow curves of a Newtonian and non-Newtonian liquid.

based on the concept that weak linkages exist between certain units in the system which are broken under the influence of shear; however, the conclusions which can be drawn from his calculations are of a qualitative rather than quantitative nature. Reiner[10] has developed equations for the flow of dispersions in a rotational viscosimeter using the Bingham concept of a "yield value." A comparison between calculated and measured data is only possible for the non-linear part of the equilibrium flow curves, since the slope of the linear part enters into the calculations. Such a comparison shows that Reiner's theory does not satisfactorily account for the non-linear flow properties of printing inks and similar colloidal dispersions. The concept of a yield value is at best a zero approximation.

The fact that the viscosity of certain pigment dispersions is essentially independent of the rate of shear (or shearing force) at higher rates of shear must mean either, that the structure has disappeared entirely, or that it cannot be further reduced by increasing the shearing force. At very low volume concentrations of the dispersed phase the shear-independent viscosity can be calculated, using an equation given by Simha and Guth[11] assuming spherical shape of the colloidal particles. Figure 4 shows the equilibrium flow curves of some carbon black dispersions in the same liquid. Table I gives the viscosity values determined from the shear-independent part of the flow curves. In the table are also shown the calculated viscosities using the equation $\eta=\eta_0(1+2.5V+14.2V^2)$ where η_0 is the viscosity of the liquid at 30°C and V is the volume concentration of the carbon black pigment. (A density value of 1.9 was used for all these carbon blacks.) It is obvious from a comparison of the data shown in Table I that the above equation is not sufficient to calculate correctly the shear-independent viscosities of pigment dispersions, except that it predicts properly the general trend of increase in viscosity with pigment concentration. The agreement is better at lower concentrations as one would expect. At higher concentrations the interference between the dispersed particles is certainly very considerable. Furthermore, it is quite possible that the shape of the carbon black units in the dispersion is not spherical as it has been assumed in the derivation of the equation. More experimental work is in progress to clarify these and other problems related to the equilibrium flow curves of simple pigment dispersions.

The time-dependent flow properties are a further indication of the existence of a structure in these systems. The change of the rate of shear with time is a measure of the rate of (*a*) the breaking of linkages, and (*b*) the recombination of linkages. When the two rate processes are equal, the rate of shear becomes independent of time. The relationship between rate of shear and time depends greatly on the treatment of a given dispersion prior to the measurement. In Figure 5 the rate of shear as a function of time is shown, following different pre-treatment keeping the temperature and the shearing force constant. However, even if the pre-treatment of the dispersions is about the same, various dispersions sometimes show characteristic differences in the

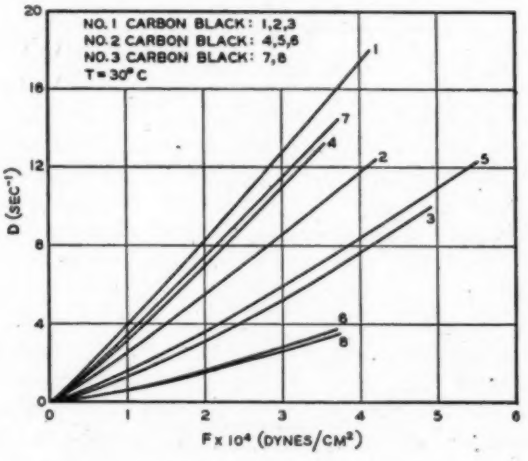

FIG. 4. Time-independent flow curves of various carbon black pigment dispersion in linseed oil.

[10] M. Reiner and R. Riwlin, Kolloid Zeits. **43**, 1 (1927).
[11] R. Simha and E. Guth, Kolloid Zeits. **74**, 266 (1936).

manner in which the equilibrium rate of shear is attained. One typical example is shown in Fig. 6. Both dispersions were left undisturbed (no shearing force applied) for several days after being filled into the viscosimeter. Similar differences can be observed when the dispersions are first sheared at a high shearing force (where the effect of structure on the viscosity has disappeared) followed by measurements at considerably lower shearing forces. Dispersions which exhibit a marked change of the equilibrium viscosity with shear usually show a marked time effect in the non-linear part of the flow curves, indicating that the two phenomena in these systems are definitely related to each other.

Before discussing the relationship of the rheological properties of printing inks to the printing process, some quantitative data for a few typical printing inks are given. Table II gives the values

TABLE I. Measured and calculated shear-independent viscosities of carbon black pigment dispersions in linseed varnish.

Volume concentration of carbon black pigment		Measured viscosity	Calculated viscosity (poises)
Black No. 1	5.7%	2300	1530
Black No. 1	8.8	3200	1870
Black No. 1	12.0	4700	2320
Black No. 2	5.7	2300	1530
Black No. 2	8.8	4000	1870
Black No. 2	12.0	8200	2320
Black No. 3	5.7	2400	1530
Black No. 3	12.0	8000	2320

of shear-independent viscosities for some typical inks and indicates at approximately what speed each ink is used. The relationship between the speed of the press and the shear independent

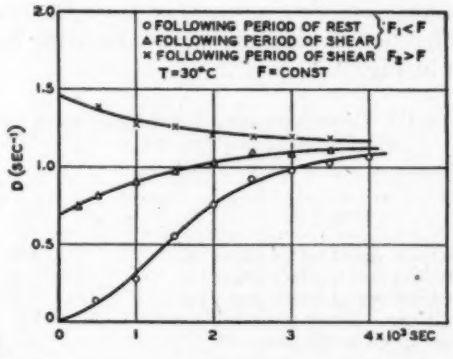

FIG. 5. Time-dependent flow curves as a function of pretreatment of the dispersion.

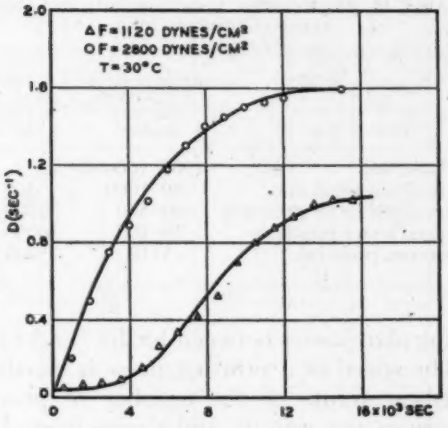

FIG. 6. Time-dependent flow curves for two different dispersions.

viscosity is quite apparent and will be discussed later. Figure 7 shows the viscosity coefficient of some typical printing inks as a function of the shearing force. It should be noticed that in all cases the equilibrium viscosity decreases with increasing shear until it reaches a constant value.

The time-dependent flow properties vary considerably for different types of inks. The following procedure is used to obtain the data shown in Table III: the ink is sheared for a given period of time, using a shearing force in the range where the viscosity is shear-independent. This is followed immediately by measuring the change in the rate of shear during a one-minute interval, using a shearing force such that the equilibrium viscosity is higher (by a constant factor) than the shear-independent viscosity. The reasons for using this particular procedure to obtain comparative data on the time-dependent flow properties are described in the next section.

THE FLOW OF PRINTING INKS ON A PRINTING PRESS

The proper transfer of the ink from the printing plate to the paper (or any other surface which might be chosen) is the main function of a printing press. This is achieved by distributing a constant amount of ink per unit time from a reservoir (or "fountain") over a distributing system of rollers onto a printing plate. Many printing presses consist, therefore, of three distinct elements which are shown schematically in Fig. 8.* The thickness of the ink film on the

* There exists a large number of different printing presses depending on the type surface of the printing plate used (typographic, lithographic or intaglio); in any one of

TABLE II. Shear-independent viscosity of various types of printing inks.

Type of ink	Range of shear-independent viscosity (poises)	Range of press speed (number of impressions per hour)
Offset base ink	1000–100000	——
Offset or proof press ink	150–1000	300–1000
Medium speed letter press ink	100–500	2000–5000
High speed letter press ink	10–100	10000–20000
Rotogravure press ink	1–10	5000–20000

printing plate varies between 1×10^{-4} and 5×10^{-4} cm. The speed of a printing press is usually expressed in terms of the number of prints or impressions per minute and varies from 2 to 3 impressions per minute for a hand operated press to 500 impressions per minute for high speed newspaper presses. The geometry of the various elements, shown in Fig. 8, is too complicated to permit the solution of the hydrodynamic viscosity equation relating the rate of shear to the shearing force. However, it will now be shown that an approximation of this complicated flow process is sufficient to correlate the "flow" of an ink on the printing press with the rheological properties discussed in the previous section.

In the first element of a printing press, the fountain, one is dealing essentially with the flow of a liquid through an orifice. Because of the large distance between the shearing surfaces (except at the orifice itself) the average rate of shear (or shearing force) acting on the ink is small, even though the speed of the first roller might be fairly high. At low shearing forces the viscosity coefficient of most printing inks increases, as was shown in Fig. 7. Depending on the speed of a given printing press the fountain has to deliver a certain volume of ink per unit time to the first roller of the distributing system. The viscosity is one of the factors determining the volume of liquid flowing out of an orifice. The two inks shown in Fig. 9 have about the same equilibrium viscosity at high shearing forces, whereas, at shearing forces below 8000 dynes/cm² ink No. 1 has a considerably higher viscosity than ink No. 2. Under a given set of press conditions—speed, opening of orifice—the fountain might deliver the correct amount of ink No. 2; under the same conditions ink No. 1 would be unsatisfactory.

these three cases the paper can be fed into the press in form of a roll (web) or in single sheets. The discussion of these modifications, however, is outside the scope of this article; intaglio presses do not have distributors as shown in Fig. 8.

It has been assumed, so far, that the ink is in an equilibrium condition when it reaches the first roller. This is certainly not correct in many cases. In filling the fountain, the ink receives a certain amount of agitation, and the effect of the shearing force acting on the liquid in the fountain lasts for a certain period of time. The ink, therefore, might or might not be in an equilibrium

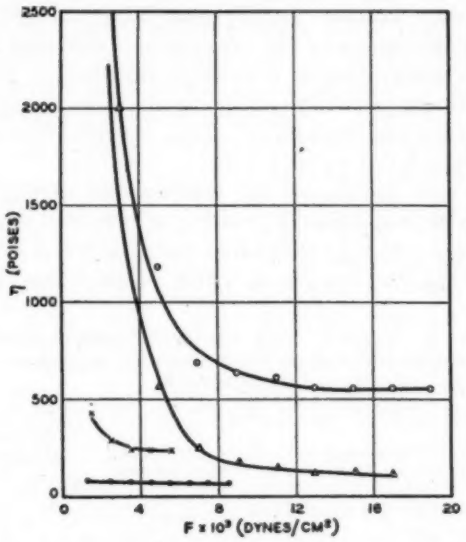

FIG. 7. Viscosity as a function of shearing force of various printing inks.

condition, depending on the time-dependent flow properties of the particular material. However, the shearing forces acting on the ink in the fountain are always small, and in most cases the total amount of shear received by the ink in the fountain is also small. The establishment of an equilibrium value, therefore, will follow a curve as shown in Fig. 5 (△ symbol). An ink which has not reached equilibrium condition will have a higher viscosity than one which has. Hence, time-dependent flow properties tend to increase the difference in viscosity at low shearing forces, shown in Fig. 9.

TABLE III. Time-dependent flow properties of some typical printing ink.

Type of ink	t_1-t_0* (sec.)
Medium speed letter press ink	400
Medium speed letter press ink	6
Medium speed letter press ink	0.4
High speed letter press ink	131
High speed letter press ink	17

* $t_1-t_0\sim1/D_1-1/D_2$.

The second element of a printing press—the distributing system—consists of a number of rollers. Through the shearing action produced between the two surfaces of roller, the ink is spread out into a thin and uniform film. The shearing force acting on the ink is determined by the pressure existing between the rotating surfaces, whereas the speed or the angular velocity of the surface of the various rollers and the number of rollers determine the total shear the ink receives before it reaches the printing plate. It is important to point out that the speed of rotation of the roller system is determined by the number of impressions to be printed per minute. The flow of an ink in this element can be related to the flow of a liquid in a rotational viscosimeter operated intermittently, where the frequency of the shearing motion depends on the speed and the number of rollers touching. The torque acting on a thin layer of the ink as it is pulled apart by the separation of the roller surfaces rotating at a considerable velocity is always rather high. At this stage, then, it is the shear-independent viscosity which is of importance. Too high a viscosity will produce insufficient spreading, whereas, too low a viscosity leads to streaking and non-uniform distribution of the ink on the rollers and the printing plate. Because of the intermittent nature of the distributing system, the time-dependent flow properties must be taken into consideration. During the time the ink is not sheared, the viscosity can remain constant or can

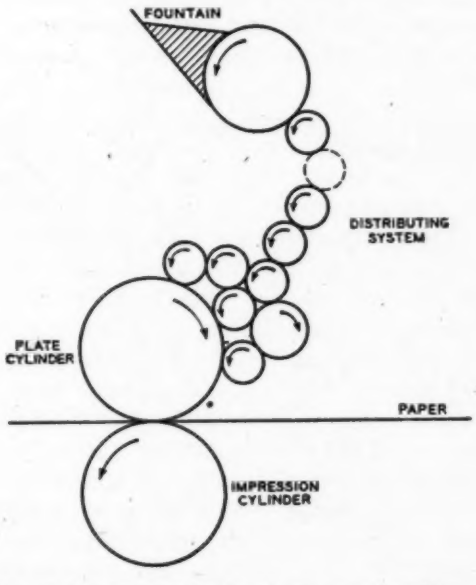

FIG. 8. Diagrammatic sketch of a typographic inking system.

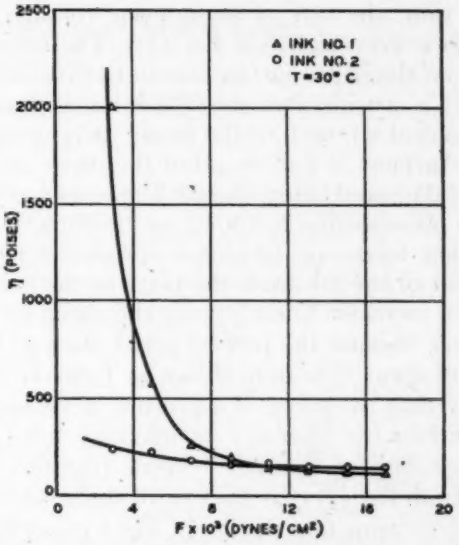

FIG 9. Viscosity as a function of shearing force of two printing inks.

increase. The increase of viscosity as a function of time for infinitely small shearing forces—thixotropy—is a well-known phenomenon in many colloidal systems. (The third possibility—decrease in viscosity after shear at high shearing forces—has not been observed in any commercial printing ink.) This leads to an increase in the "effective" viscosity of the ink during the period of distribution. The time-dependent flow properties do assume much greater importance in the transfer of the ink from the last distributing roller to the printing plate, particularly in the typographic process. When the ink is transferred to the raised part of the printing plate, the ink has a tendency to flow into the lower parts of the plate which should remain entirely free from ink. If immediately after depositing the ink the viscosity increases, this tendency of the ink to flow is considerably reduced. This important working property of a printing ink—usually referred to as "shortness" and "length"—is directly related to the speed of building up the structure after it has been broken down at high shearing forces. In order to evaluate this working property the procedure described above was followed. Results obtained in this manner agree very well with subjective evaluations carried out by various observers and also with actual printing tests.

In the final step the ink is transferred from the printing plate to the paper by contact between the two elements. Upon separation the ink film is sheared and finally broken. Since this film is

very thin, the rate of shear even at fairly low speeds is very high (see Eq. (2)). The force exerted on the paper surface due to the viscosity of the ink is considerable; and if it is larger than the mechanical strength of the paper (perpendicular to its surface), a part or all of the paper surface will be damaged before the ink film has separated. (This phenomenon is known as "picking"). The shearing force—or tackiness—produced in the transfer of the ink from the plate to the printed surface increases linearly with the speed or rate of shear because the process takes place at high rates of shear. The data shown in Table II show clearly that the speed of a printing press largely determines the viscosity an ink may have and still not damage the paper during transfer. It is clear from Eq. (2) that the rate of shear increases with decreasing film thickness. For a given linear (or rotational) speed the shearing force produced during separation of an ink film increases therefore, with decreasing film thickness. The shearing force acting during the transfer process can be influenced by the time-dependent flow properties. A "short" ink usually is somewhat "tackier" than a "long" ink if both inks have about the same equilibrium viscosity at high rates of shear. The structure builds up more markedly in a "short" ink after transferring the ink from the rollers to the printing plate, requiring a higher shearing force to separate the ink film at a given speed. The differences in the time-dependent flow properties, however, must be rather large to contribute to an increase in tack. Tack is also of great importance in wet-multicolor printing, where several inks are printed in quick succession. In four-color printing, the order is usually yellow, red, blue, and black, and data given in Table IV show that

TABLE IV. Shear-independent viscosity and order of printing in wet-multicolor printing.

Type of ink	Shear independent viscosity (poises)	Order of printing
Yellow medium speed letter press ink	550	first
Red medium speed letter press ink	250	second
Blue medium speed letter press ink	125	third
Black medium speed letter press ink	110	fourth

the shear independent viscosity of a commercial set of inks decreases in this order.

It has been shown how the working properties of a printing ink can be interpreted in terms of the rheological properties, as measured in a rotational viscosimeter. The viscosity at high rates of shear is of primary importance in the transfer of the ink from the roller to the printing plate, and from the printing plate to the paper surface. The viscosity at low rates of shear determines the transfer from the fountain to the roller system. Because the viscosity of printing inks is not only a function of the shearing force, but also of time, the change of viscosity with time plays an important part in the flow of the ink on each element of a printing press.

ACKNOWLEDGMENT

The authors are indebted to members of the Research Division of the General Printing Ink Corporation for help and advice in this work. The instrument was designed by Dr. Carsten C. Steffens.*

* Present address: The Solvay Process Company, Syracuse, New York.

Electromagnetic Field Inside a Cylinder with a Gap

C. C. WANG
Westinghouse Electric and Manufacturing Company, Bloomfield, New Jersey
(Received October 25, 1944)

Complete equations below the lowest cut-off frequency of transverse magnetic type relating the high frequency electric field and magnetic field inside a metallic cylinder excited through a gap and an assumed field at the gap are developed. Curves are calculated based on the equations which can be used to estimate the relative field strength at different points inside the cylinder. Equivalent capacitance due to the energy storage in the cylinder can be calculated and used for estimating the resonant frequency of the associated cavity. The equations can be degenerated to an electrostatic form and used for electron optical calculations.

ELECTROMAGNETIC FIELD INSIDE A CYLINDER WITH A GAP

General Introduction

IN the development of high power klystrons, it is the general tendency to dispense with the grid structure completely because too large a heat dissipation, due to electron bombardment, makes difficult the design of a suitable grid. The electron beam is under the action of the electromagnetic field established in a hollow cylinder by a resonator through a gap opening. Naturally, the electric field will not be uniform all the way across the cylinder as in the case of the klystron with grid structure and the field is not limited longitudinally, to the distance of the gap spacing.

Then we have the following questions:

(1) What effect would the removal of the grid structure have upon the velocity modulation and the energy interchange between the electron beam and the resonator as each part of the beam reacts differently from the other?

(2) Does it pay to use a hollow cylindrical electron beam where more electrons are concentrated in a narrow belt of relatively small variation of electric field and perhaps with better electric efficiency, and if so, to what extent?

(3) The electric field across the gap is higher than that in the beam. To perform the same degree of modulation and energy interchange, by what factor must the a.c. voltage at the gap be changed in the calculation of the bunching formula? If the resonator possesses the same unloaded shunt resistance as in the case with a klystron with grid structure, then this increase of gap voltage means square proportion increase of electric cavity loss and hence the resonator electric efficiency decreases.

(4) How can one estimate the resonating frequency of the resonator as a result of the removal of the grid structure? How is this related to the gap width, the cylinder diameter, etc.?

(5) Is there any possibility of energy interchange or coupling between two resonators through the extension of the electromagnetic field in the longitudinal direction?

The following analysis does not give direct answers to all the above questions. To answer all the above questions, one has to know more about the properties of high density electron beams. However, the following is the solution of the field distribution without space charge presented in normalized dimensions, so that one can use it as a starting point for further discussion.

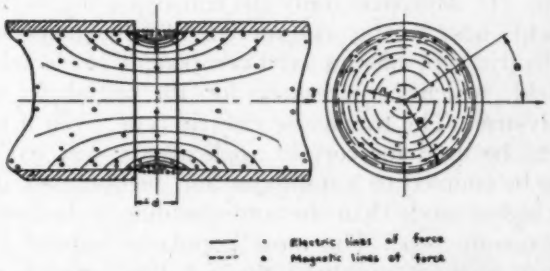

FIG. 1. Sketch of the electric and magnetic fields inside a cylinder excited through a gap.

The General Electromagnetic Field Equations

Let us consider the case of two metallic circular cylinders separated at a distance d and with inner radius a. The coordinates are chosen as indicated in Fig. 1. The field is excited through the gap opening by the resonator, which is at the outside of the cylinder. It is well-known that such a field in cylindrical coordinates can be expressed in terms of an arbitrary combination of the scalar wave functions[1] of the form

$$\psi_n = e^{in\theta} Z_n[(k^2-h^2)^{\frac{1}{2}}r] e^{\pm i(hz+\omega t)}, \qquad (1)$$

[1] J. A. Stratton, *Electro-magnetic Theory* (McGraw-Hill Book Company, Inc., New York, 1941), p. 360, section 6.6.

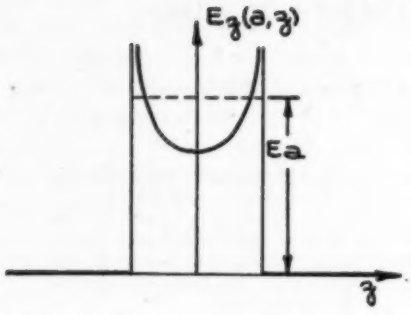

FIG. 2. The actual and assumed axial electric field along the cylinder surface and the gap surface of the same radius.

where $k=2\pi/\lambda$ and λ is the wave-length, ω=angular frequency, Z_n=linear combination of Bessel and Neumann functions, $n=0, 1, 2, 3, \cdots$, and h=an arbitrary constant. The way of combining these functions depends upon the boundary conditions that have to be satisfied. In our special case, there is no reason why any physical quantity should be a function of angular dimension θ if we content ourselves with solutions that have no preferential directions circumferentially, which is generally true in klystrons. Thus, the value of n will be 0 in Eq. (1). Moreover, only the transverse magnetic field has to be considered. The transverse electric type has no axial component of electric field, which is necessary for the action in a klystron. The transverse electric type, even if it can be used for certain applications, will have to be coupled to a resonator and be operated at a higher mode than the corresponding transverse magnetic type. The most popular resonator is just a short circuited coaxial line around a quarter wave-length long. The resonating wave-length calculated by matching the transverse-magnetic type field to the gap field of the resonator will then be the fundamental wave-length of the resonator. In the transverse magnetic field type, the radial magnetic field H_r and the circumferential electric field E_θ are proportional to the first derivative of ψ_n with respect to θ and must be identically zero in Eq. (1) by the above symmetry argument. This, together with the vanishing of the axial-magnetic field H_z in the transverse magnetic field type, leaves us only with the radial electric field E_r, the axial electric field E_z, and the circumferential magnetic field H_θ to be considered, each of which bears a relation to the above function ψ_n as follows:[1]

$$E_r=\pm ih\partial\psi_n/\partial r,$$
$$E_z=(k^2-h^2)\psi_n, \qquad (2)$$
$$H_\theta=(ik^2/\mu\omega)(\partial\psi_n/\partial r).$$

The electric and magnetic lines of forces will take the form as shown in Fig. 1. Other restrictions to the above function are that the Neumann functions have to be zero as they become infinity at $r=0$, which has to be included in the solution, and the e^{jhz} and e^{-jhz} terms must be combined in such a manner as to form $\cos hz$ because ψ must be an even function of z if the field is to be symmetrical about the $z=0$ axis.

With all the above considerations, the magnitude of the axial electric field will have the form

$$E_z(r, z)=\int_0^\infty A(h)J_0[(k^2-h^2)^{\frac{1}{2}}r]\cos hz dh, \qquad (3)$$

where $A(h)$ is an arbitrary function of h. Equation (3) is merely the statement that the electric field, E_z, is an arbitrary superimposition of the elementary functions as represented in (1) and (2) subjected to the stated restrictions. The function $A(h)$ remains to be determined by the boundary conditions.

For infinite conductivity on the wall, the axial electric field must vanish from $Z=d/2$ to ∞, and from $-\infty$ to $z=-d/2$, at $r=a$. With a sharp corner at the gap edges, the axial electric field takes the distribution form as shown in Fig. 2 at $r=a$ as it goes to infinity at the edges. The exact distribution of the axial field within the gap is hard to assume as it perhaps depends more or less, upon the thickness of the cylinder wall, the characteristic of the resonator. Singularity to the degree of $1/[(d/2)^2-z^2]^{\frac{1}{2}}$ has often been assumed in most calculations simply because of the capability of evaluating the transform of the infinite integral. Since we are more or less interested only in the relative values of the field and the average matching of the field inside and

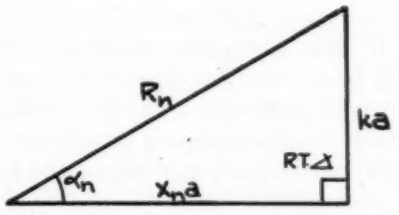

FIG. 3. The right triangle relating the quantities of R_n, ka, x_na and α_n.

outside the cylinder, we will be satisfied by assuming an average value of the electric field E_a as shown in a dotted line in Fig. 2. Thus our simplified boundary condition becomes:

$$\begin{aligned} -\infty < z < -d/2, &\quad E_z(a, z) = 0, \\ -d/2 < z < d/2, &\quad E_z(a, z) = E_a, \\ d/2 < z < \infty, &\quad E_z(a, z) = 0. \end{aligned} \tag{4}$$

Using the standard method of Fourier transformation applied to Eq. (3) with $r=a$, and using the condition (4), we have

$$\begin{aligned} J_0[(k^2-h^2)^{\frac{1}{2}}a]A(h) &= (1/\pi)\int_{-\infty}^{\infty} E_z(a, z)\cos hz dz \\ &= (1/\pi)E_a\int_{-d/2}^{d/2}\cos hz dz \\ &= (2/\pi)(E_a/h)\sin(hd/2), \\ A(h) &= (2E_a/\pi h)\cdot(\sin hd/2)/J_0[(k^2-h^2)^{\frac{1}{2}}a]. \end{aligned} \tag{5}$$

This infinite integral can be evaluated by the familiar contour integrations which are carried out in the Appendix. The result of this is, for $ka<2.405$,

for $-d/2<z<d/2$

$$\frac{E_z(r, z)}{E_a} = \frac{J_0(kr)}{J_0(ka)} - \sum_{n=1}^{\infty}\frac{J_0(R_n r/a)}{R_n J_1(R_n)}\cdot\frac{1}{\cos^2\alpha_n} 2\exp\left(-\frac{d}{2a}R_n\cos\alpha_n\right)\cosh\left(\frac{z}{a}R_n\cos\alpha_n\right); \tag{6}$$

for $d/2<z<\infty$

$$\frac{E_z(r, z)}{E_a} = \sum_{n=1}^{\infty}\frac{J_0(R_n r/a)}{R_n J_1(R_n)}\cdot\frac{1}{\cos^2\alpha_n} 2\exp\left(-\frac{z}{a}R_n\cos\alpha_n\right)\sinh\left(\frac{d}{2a}R_n\cos\alpha_n\right); \tag{7}$$

for $-\infty<z<-d/2$

$$\frac{E_z(r, z)}{E_a} = \sum_{n=1}^{\infty}\frac{J_0(R_n r/a)}{R_n J_1(R_n)}\cdot\frac{1}{\cos^2\alpha_n} 2\exp\left(\frac{z}{a}R_n\cos\alpha_n\right)\sinh\left(\frac{d}{2a}R_n\cos\alpha_n\right), \tag{8}$$

where R_n are the roots of the successive zeros of the Bessel function of the zeroth order, and they bear the relation to α_n and ka as in Fig. 3.

The restriction for $ka<2.405$ or $ka<R_1$, means that we are only able to use the formula with a frequency below the cut-off frequency of the E_{01} mode. This is not a severe restriction, because we are not interested in letting the energy get away through the wave propagation inside the hollow pipe; the tube dimension must be limited to such a value that the relation is correct. In fact, to be safe, ka should be less than 1.84 which is the cut-off value of the H_{11} mode which might be excited if dissymmetry exists, and energy will be lost if ways are provided for coupling the resonator to this mode.

We see that Eq. (8) can be obtained by setting z equal to $-z$ in Eq. (7). This is true because we have already stated that E_z is an even function of z. Similarly, by examining Fig. 1, E_r must be an odd function of z and H_θ be an even function of z as the fields are symmetrical about $z=0$ axis, thus, we have

$$E_z(r, z) = E_z(r, -z), \quad E_r(r, z) = -E_r(r, -z), \quad H_\theta(r, z) = H_\theta(r, -z). \tag{9}$$

Hereafter, we only have to write down equations for $-d/2<z<d/2$ and $d/2<z<\infty$ since for $-\infty<z<-d/2$, solutions can be obtained by Eq. (9).

To get E_r use is made of the divergence equation

$$\nabla \cdot E = 0, \quad \text{or} \quad \partial E_z/\partial z + \partial r E_r/r\partial r = 0, \tag{10}$$

and

$$E_r = -(1/r)\int_0^r r(\partial E_z/\partial z)dr. \tag{11}$$

The lower integration limit is set with the contention that E_r must be zero at $r=0$ by reason of symmetry and one can easily be satisfied by looking into Fig. 1. By substituting (6) and (7) into (11), and carrying out the integration, we have:

for $-d/2<z<d/2$

$$\frac{E_r(r,z)}{E_a} = \sum_{n=1}^{\infty} \frac{J_1(R_n r/a)}{R_n J_1(R_n)} \frac{1}{\cos \alpha_n} 2 \exp\left(-\frac{d}{2a} R_n \cos \alpha_n\right) \sinh\left(\frac{z}{a} R_n \cos \alpha_n\right); \tag{12}$$

for $d/2<z<\infty$

$$\frac{E_r(r,z)}{E_a} = \sum_{n=1}^{\infty} \frac{J_1(R_n r/a)}{R_n J_1(R_n)} \frac{1}{\cos \alpha_n} 2 \exp\left(-\frac{z}{2a} R_n \cos \alpha_n\right) \sinh\left(\frac{d}{2a} R_n \cos \alpha_n\right). \tag{13}$$

To find the magnetic field, we can use the curl equation, i.e.,

$$\nabla \times E = -j\omega\mu H \tag{14}$$

or

$$H_\theta = -(1/j\omega)[\partial E_z/\partial r - \partial E_r/\partial z].$$

Substituting (6) and (12) into (14), and (7) and (13) into (14) respectively, we have

for $-d/2<z<d/2$

$$\frac{j\omega\mu H_\theta}{kE_a} = -\frac{J_1(kr)}{J_0(ka)} - \sum_{n=1}^{\infty} \frac{J_1(R_n r/a)}{R_n J_0(R_n)} \frac{\sin \alpha_n}{\cos^2 \alpha_n} \left\{2 \exp\left(-\frac{d}{2a} R_n \cos \alpha_n\right) \cosh\left(\frac{z}{a} R_n \cos \alpha_n\right)\right\}; \tag{15}$$

for $d/2<z<\infty$

$$\frac{j\omega\mu H_\theta}{kE_a} = \sum_{n=1}^{\infty} \frac{J_1(R_n r/a)}{R_n J_1(R_n)} \frac{\sin \alpha_n}{\cos^2 \alpha_n} 2 \exp\left(-\frac{z}{a} R_n \cos \alpha_n\right) \sinh\left(\frac{d}{2a} R_n \cos \alpha_n\right). \tag{16}$$

The reader can satisfy himself by checking the equation curl $H = j\omega\epsilon E$.

Equations (6), (7), (8), (9), (12), (13), (15), (16) specify completely the electric and magnetic field strength in the cylindrical space in terms of the average axial electric field at the gap.

To examine the convergence of the above series, we see

$$\lim_{n\to\infty} R_n = (n-\tfrac{1}{4})\pi, \quad \lim_{n\to\infty} \sin \alpha_n = ka/R_n = ka/(n-\tfrac{1}{4})\pi, \quad \lim_{n\to\infty} \cos \alpha_n = 1,$$

$$\lim_{n\to\infty} \frac{J_0(R_n r/a)}{R_n J_1(R_n)} = \frac{\left(\frac{a}{r}\right)^{\frac{1}{2}} \frac{\cos\left[(n-\frac{1}{4})\pi r/a - \pi/4\right]}{(R_n)^{\frac{1}{2}}}}{\frac{R_n \sin (n-\frac{1}{2})\pi}{(R_n)^{\frac{1}{2}}}} = (-1)^{n-1} \frac{\left(\frac{a}{r}\right)^{\frac{1}{2}} \cos\left[(n-\frac{1}{4})\pi \frac{r}{a} - \frac{\pi}{4}\right]}{(n-\frac{1}{4})\pi}, \quad \text{for } r/a>0;$$

$$\lim_{n\to\infty} \frac{J_0(R_n r/a)}{R_n J_1(R_n)} = \frac{1}{(R_n)^{\frac{1}{2}}} = \frac{1}{[(n-\frac{1}{4})\pi]^{\frac{1}{2}}}, \quad \text{for } r/a=0; \tag{17}$$

$$\lim_{n\to\infty}\frac{J_1(R_n r/a)}{R_n J_1(R_n)}=(-1)^{n-1}\frac{(a/r)^{\frac{1}{2}}\sin\left[(n-\frac{1}{4})\pi r/a-\pi/4\right]}{(n-\frac{1}{4})\pi},\quad \text{for } r/a>0.$$

Thus, the series of the field E_z and E_r will consist of terms with the limit as n increases indefinitely as:

$$(1/n)\exp(-|d/2a\pm z/a|n)\quad \text{when } r/a>0,$$

and that of E_z will become

$$1/(n)^{\frac{1}{2}}\exp(-|d/2a\pm z/a|n)\quad \text{when } r/a=0.$$

However, H_θ will approach

$$(1/n^2)\exp(-|d/2a\pm z/a|n).$$

All the series are theoretically convergent if $z\neq\pm d/2$, due to the exponential term, but the decrement of the magnitude of the successive terms due to the exponential factor is too small, when $|d/2a\pm z|$ is small, for practical calculation. Thus the series for H_θ converges fairly well and E_r and E_z converge rather slowly when $r/a\neq 0$ and E_z converges very slowly when $r/a=0$, while E_r is identically zero when $r/a=0$.

To make calculation easier, E_r and E_z should be changed by subtracting a known series from the given series such that the resulting series converges much more rapidly. Fortunately such series exist for E_r and E_z when $r/a>0$. Since E_z must be a slowly varying function of r when r/a is near zero, i.e.,

$$\left.\frac{\partial E_z(r,z)}{\partial r}\right|_{r=0}=0, \tag{18}$$

the value of E_z when $r/a=0$ can be estimated easily if we know E_z for small values of r/a. We will then rewrite the equations of E_z and E_r for $r/a>0$. The series we are going to use are the following ones[2]

$$\tfrac{1}{2}\tan^{-1}\frac{\cos x}{\sinh y}=\sum_{n=1}^{\infty}(-1)^{n-1}\frac{\cos(2n-1)x}{2n-1}e^{-(2n-1)y}, \tag{19}$$

$$\tfrac{1}{2}\tanh^{-1}\frac{\sin x}{\cosh y}=\sum_{n=1}^{\infty}(-1)^{n-1}\frac{\sin(2n-1)x}{2n-1}e^{-(2n-1)y} \tag{20}$$

where $y>0$.

We will proceed to show how closely these series approach the above ones. Take the nth term of the series of Eq. (6) and by Eq. (17), we have, with $-d/2<z<d/2$, $r/a>0$,

$$\lim_{n\to\infty}\frac{J_0(R_n r/a)}{R_n J_1(R_n)}\cdot\frac{1}{\cos^2\alpha_n}\left[\exp\left(-\frac{1}{a}(d/2-z)R_n\cos\alpha_n\right)+\exp\left(-\frac{1}{a}\left(\frac{d}{2}+z\right)R_n\cos\alpha_n\right)\right]$$

$$=(-1)^{n-1}\left(\frac{a}{r}\right)^{\frac{1}{2}}\frac{\cos\left[(2n-1)\frac{r}{a}\cdot\frac{\pi}{2}-\left(1-\frac{r}{a}\right)\frac{\pi}{4}\right]}{(2n-\frac{1}{2})\pi/2}\left[\exp\left(-\frac{1}{a}\left(\frac{d}{2}-z\right)\frac{\pi}{4}\right)\right.$$

$$\left.\cdot\exp\left(-\frac{1}{a}\left(\frac{d}{2}-z\right)\frac{\pi}{2}(2n-1)\right)+\exp\left(-\frac{1}{a}\left(\frac{d}{2}+z\right)\frac{\pi}{4}\right)\cdot\exp\left(-\frac{1}{a}\left(\frac{d}{2}+z\right)\frac{\pi}{2}(2n-1)\right)\right] \tag{21}$$

[2] Edwin P. Adams, *Smithsonian Mathematical Formulae and Tables of Elliptic Functions* (Smithsonian Institute, Washington, D. C., First reprint 1938), pp. 139–140, Formula number 6.832 and 6.835.

$$=\left(\frac{a}{r}\right)^{\frac{1}{2}}\frac{\exp\left(-\frac{1}{a}\left(\frac{d}{2}-z\right)\frac{\pi}{4}\right)}{\pi/2}\left[(-1)^{n-1}\cos\left(1-\frac{r}{a}\right)\frac{\pi}{4}\cdot\frac{\cos(2n-1)\frac{r}{a}\frac{\pi}{2}}{2n-\frac{1}{2}}\exp\left(-\frac{1}{a}\left(\frac{d}{2}-z\right)\frac{\pi}{2}(2n-1)\right)\right.$$

$$\left.+(-1)^{n-1}\sin\left(1-\frac{r}{a}\right)\frac{\pi}{4}\cdot\frac{\sin(2n-1)\frac{r}{a}\frac{\pi}{2}}{2n-\frac{1}{2}}\exp\left(-\frac{1}{a}\left(\frac{d}{2}-z\right)\frac{\pi}{2}(2n-1)\right)\right]$$

$$+\left(\frac{a}{r}\right)^{\frac{1}{2}}\frac{\exp\left(-\frac{1}{a}\left(\frac{d}{2}+z\right)\frac{\pi}{4}\right)}{\pi/2}\left[(-1)^{n-1}\cos\left(1-\frac{r}{a}\right)\frac{\pi}{4}\cdot\frac{\cos(2n-1)\frac{r}{a}\frac{\pi}{2}}{2n-\frac{1}{2}}\right.$$

$$\cdot\exp\left(-\frac{1}{a}\left(\frac{d}{2}+z\right)\frac{\pi}{2}(2n-1)\right)+(-1)^{n-1}\sin\left(1-\frac{r}{a}\right)\frac{\pi}{4}$$

$$\left.\cdot\frac{\sin(2n-1)\frac{r}{a}\frac{\pi}{2}}{2n-\frac{1}{2}}\exp\left(-\frac{1}{a}\left(\frac{d}{2}+z\right)\frac{\pi}{2}(2n-1)\right)\right].$$

To do this let us define for abbreviations the following functions, with the help of (19) and (20),

$$F_1(\beta,x)=2e^{-x}\cosh\beta x=e^{-(1-\beta)x}+e^{-(1+\beta)x}, \tag{22}$$

$$F_2(\beta,x)=2e^{-x}\sinh\beta x=e^{-(1-\beta)x}-e^{-(1+\beta)x} \tag{22a}$$

where $\beta<1$,

$$G_1\left(\frac{r}{a},x\right)=\frac{1}{\pi}\left(\frac{a}{r}\right)^{\frac{1}{2}}e^{-x}\left[\cos\left(1-\frac{r}{a}\right)\frac{\pi}{4}\cdot\tan^{-1}\frac{\cos\frac{r}{a}\frac{\pi}{2}}{\sinh 2x}+\sin\left(1-\frac{r}{a}\right)\frac{\pi}{4}\cdot\tanh^{-1}\frac{\sin\frac{r}{a}\frac{\pi}{2}}{\cosh 2x}\right]$$

$$=\sum_{n=1}^{\infty}\frac{2}{\pi}\left(\frac{a}{r}\right)^{\frac{1}{2}}e^{-x}\left[(-1)^{n-1}\cos\left(1-\frac{r}{a}\right)\frac{\pi}{4}\cdot\frac{\cos(2n-1)\frac{r}{a}\frac{\pi}{2}}{2n-1}e^{-2x(2n-1)}\right.$$

$$\left.+(-1)^{n-1}\sin\left(1-\frac{r}{a}\right)\frac{\pi}{4}\cdot\frac{\sin(2n-1)\frac{r}{a}\frac{\pi}{2}}{2n-1}e^{-2x(2n-1)}\right]$$

$$=\sum_{n=1}^{\infty}\frac{2}{\pi}\left(\frac{a}{r}\right)^{\frac{1}{2}}e^{-x}\frac{\cos\left[(2n-\frac{1}{2})\frac{r}{a}\frac{\pi}{2}-\frac{\pi}{4}\right]}{2n-1}(-1)^{n-1}e^{-2x(2n-1)}. \tag{23}$$

$$G_2\left(\frac{r}{a}, x\right)=\frac{1}{\pi}\left(\frac{a}{r}\right)^{\frac{1}{2}}e^{-x}\left[\sin\left(\tfrac{1}{2}-\frac{r}{a}\right)\frac{\pi}{4}\cdot\tan^{-1}\frac{\cos\frac{r}{a}\frac{\pi}{2}}{\sinh 2x}-\cos\left(1-\frac{r}{a}\right)\frac{\pi}{4}\cdot\tanh^{-1}\frac{\sin\frac{r}{a}\frac{\pi}{2}}{\cosh 2x}\right]$$

$$=\sum_{n=1}^{\infty}\frac{2}{\pi}\left(\frac{a}{r}\right)^{\frac{1}{2}}e^{-x}\left[(-1)^{n-1}\sin\left(1-\frac{r}{a}\right)\frac{\pi}{4}\frac{\cos(2n-1)\frac{r}{a}\frac{\pi}{2}}{2n-1}e^{-2x(2n-1)}\right.$$

$$\left.-(-1)^{n-1}\cos\left(1-\frac{r}{a}\right)\frac{\pi}{4}\frac{\sin(2n-1)\frac{r}{a}\frac{\pi}{2}}{2n-1}e^{-2x(2n-1)}\right]$$

$$=-\sum_{n=1}^{\infty}\frac{2}{\pi}\left(\frac{a}{r}\right)^{\frac{1}{2}}e^{-x}\frac{\sin\left[(2n-\frac{1}{2})\frac{r}{a}\frac{\pi}{2}-\frac{\pi}{4}\right]}{2n-1}(-1)^{n-1}e^{-2x(2n-1)}. \tag{24}$$

With a little algebraic manipulation, we can write the Eqs. (6), (7), (12), and (13) as follows, for $-d/2<z<d/2$, $r/a>0$.

$$\frac{E_z(r,z)}{E_a}=\frac{J_0(kr)}{J_0(ka)}-G_1\left[\frac{r}{a},\frac{1}{a}\left(\frac{d}{2}-z\right)\frac{\pi}{4}\right]-G_1\left[\frac{r}{a},\frac{1}{a}\left(\frac{d}{2}+z\right)\frac{\pi}{4}\right]$$

$$-\sum_{n=1}^{\infty}\frac{J_0\left(R_n\frac{r}{a}\right)}{R_nJ_1(R_n)}\cdot\frac{1}{\cos^2\alpha_n}F_1\left(\frac{2z}{d},\frac{d}{2a}R_n\cos\alpha_n\right)$$

$$-(-1)^{n-1}\frac{2}{\pi}\left(\frac{a}{r}\right)^{\frac{1}{2}}\frac{\cos\left[(n-\frac{1}{4})\pi\frac{r}{a}-\frac{\pi}{4}\right]}{2n-1}\cdot F_1\left[\frac{2z}{d},\frac{d}{2a}(n-\tfrac{1}{4})\pi\right], \tag{25}$$

$$\frac{E_r(r,z)}{E_a}=G_2\left[\frac{r}{a},\frac{1}{a}\left(\frac{d}{2}+z\right)\frac{\pi}{4}\right]-G_2\left[\frac{r}{a},\frac{1}{a}\left(\frac{d}{2}-z\right)\frac{\pi}{4}\right]$$

$$+\sum_{n=1}^{\infty}\frac{J_1\left(R_n\frac{r}{a}\right)}{R_nJ_1(R_n)}\cdot\frac{1}{\cos\alpha_n}F_2\left[\frac{2z}{d},\frac{d}{2a}R_n\cos\alpha_n\right]$$

$$-(-1)^{n-1}\frac{2}{\pi}\left(\frac{a}{r}\right)^{\frac{1}{2}}\frac{\sin\left[(n-\frac{1}{4})\pi\frac{r}{a}-\frac{\pi}{4}\right]}{2n-1}F_2\left[\frac{2z}{d},\frac{d}{2a}(n-\tfrac{1}{4})\pi\right]$$

for $d/2<z<\infty$, $r/a>0$. (26)

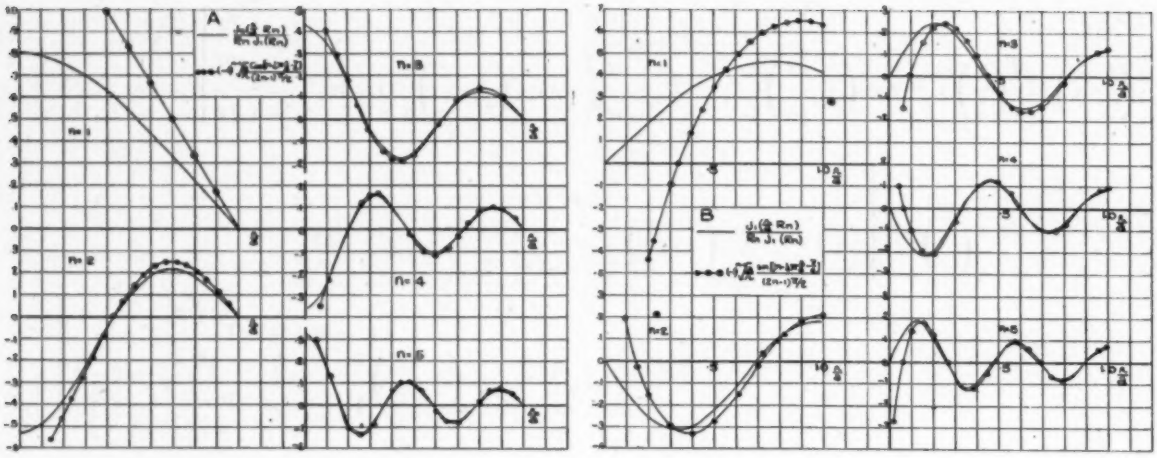

FIG. 4. Curves showing the relative magnitudes of the terms in the series used for calculation.

$$\frac{E_z(r,z)}{E_a}=G_1\left[\frac{r}{a},\frac{1}{a}\left(z-\frac{d}{2}\right)\frac{\pi}{4}\right]-G_1\left[\frac{r}{a},\frac{1}{a}\left(z+\frac{d}{2}\right)\frac{\pi}{4}\right]$$

$$+\sum_{n=1}^{\infty}\frac{J_0\left(R_n\frac{r}{a}\right)}{R_nJ_1(R_n)}\cdot\frac{1}{\cos^2\alpha_n}F_2\left[\frac{d}{2z},\frac{z}{a}R_n\cos\alpha_n\right]$$

$$-(-1)^{n-1}\frac{2}{\pi}\left(\frac{a}{r}\right)^{\frac{1}{2}}\frac{\cos\left(n-\frac{1}{4}\right)\pi\frac{r}{a}-\frac{\pi}{4}}{2n-1}F_2\left[\frac{d}{2z},\frac{z}{a}(n-\tfrac{1}{4})\pi\right]. \quad (27)$$

$$\frac{E_r(r,z)}{E_a}=G_2\left[\frac{e}{a},\frac{1}{a}(z+d/2)\pi/4\right]-G_2\left[\frac{r}{a},\frac{1}{a}(z-d/2)\pi/4\right]$$

$$+\sum_{n=1}^{\infty}\frac{J_1(R_nr/a)}{R_nJ_1(R_n)}\frac{1}{\cos\alpha_n}F_2\left[\frac{d}{2z},\frac{z}{a}R_n\cos\alpha_n\right]$$

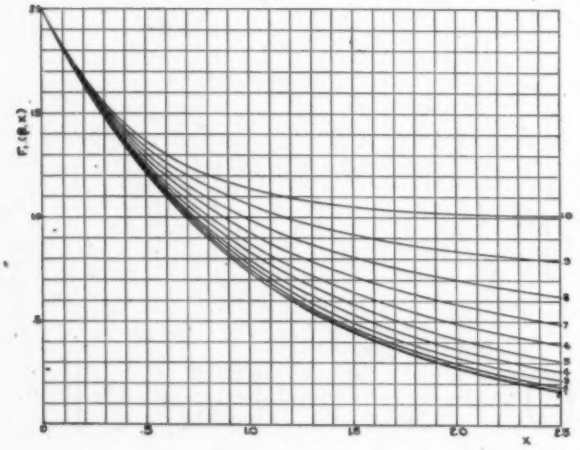

FIG. 5. The function $F_1(\beta, x)$ plotted against x with β as parameter.

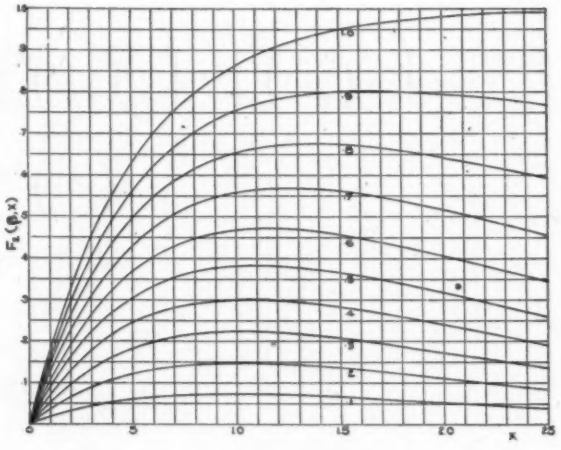

FIG. 6. The function $F_2(\beta, x)$ plotted against x with β as parameter.

$$-(-1)^{n-1}\frac{2}{\pi}\left(\frac{a}{r}\right)^{\frac{1}{2}}\frac{\sin\left[(n-\frac{1}{4})\pi\frac{r}{a}-\frac{\pi}{4}\right]}{2n-1}F_2\left[\frac{d}{2z},\frac{z}{a}(n-\tfrac{1}{4})\pi\right]. \quad (28)$$

In Fig. 4, a series of curves of the terms that compose the principal factors of the two terms contained in the series of the above equations are plotted against r/a for successive values of n. We see how fast they approach each other for all values except in the immediate neighborhood of $r/a=0$. The factors involving F_1, F_2, $1/\cos\alpha_n$ or $1/\cos^2\alpha_n$ approach each other very rapidly. For practical calculation, with $r/a<0.1$, five terms are all that will be necessary. The functions of F_1, F_2, G_1, and G_2 are plotted in Figs. 5 to 8, and are convenient to use. The following are several properties of G_1 and G_2 functions for large and small values of x.

$$G_1\left(\frac{r}{a},0\right)=\frac{1}{2}\left(\frac{a}{r}\right)^{\frac{1}{2}}\left\{\cos\left(1-\frac{r}{a}\right)\frac{\pi}{4}+\sin\left(1-\frac{r}{a}\right)\frac{\pi}{4}\frac{\tanh^{-1}\sin\frac{r}{a}\frac{\pi}{2}}{\pi/2}\right\}. \quad (29)$$

$$G_2\left(\frac{r}{a},0\right)=\frac{1}{2}\left(\frac{a}{r}\right)^{\frac{1}{2}}\left\{\sin\left(1-\frac{r}{a}\right)\frac{\pi}{4}-\cos\left(1-\frac{r}{a}\right)\frac{\pi}{4}\frac{\tanh^{-1}\sin\frac{r}{a}\frac{\pi}{2}}{\pi/2}\right\}. \quad (30)$$

$$\lim_{x\to 0}G_1\left(\frac{r}{a},x\right)=G_1\left(\frac{r}{a},0\right)-\left[G_1\left(\frac{r}{a},0\right)+\frac{2}{\pi}\left(\frac{a}{r}\right)^{\frac{1}{2}}\frac{\cos\left(1-\frac{r}{a}\right)\frac{\pi}{4}}{\cos\frac{r}{a}\frac{\pi}{2}}\right]x. \quad (31)$$

$$\lim_{x\to 0}G_2\left(\frac{r}{a},x\right)=G_2\left(\frac{r}{a},0\right)-\left[G_2\left(\frac{r}{a},0\right)+\frac{2}{\pi}\left(\frac{a}{r}\right)^{\frac{1}{2}}\frac{\sin\left(1-\frac{r}{a}\right)\frac{\pi}{4}}{\cos\frac{r}{a}\frac{\pi}{2}}\right]x. \quad (32)$$

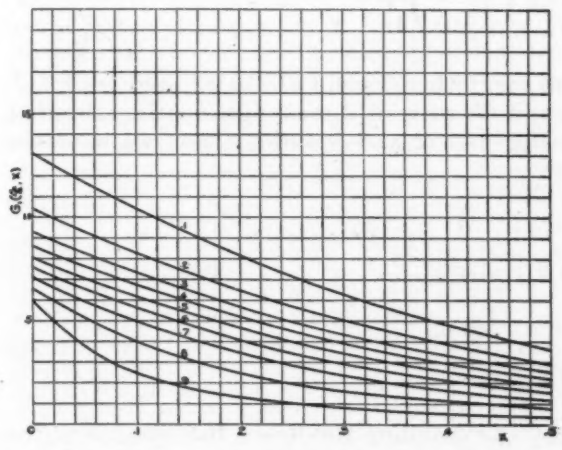

FIG. 7. The function $G_1(r/a, x)$ plotted against x with r/a as parameter.

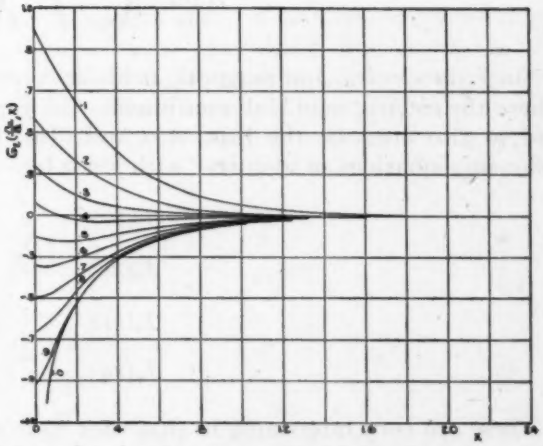

FIG. 8. The function $G_2(r/a, x)$ plotted against x with r/a as parameter.

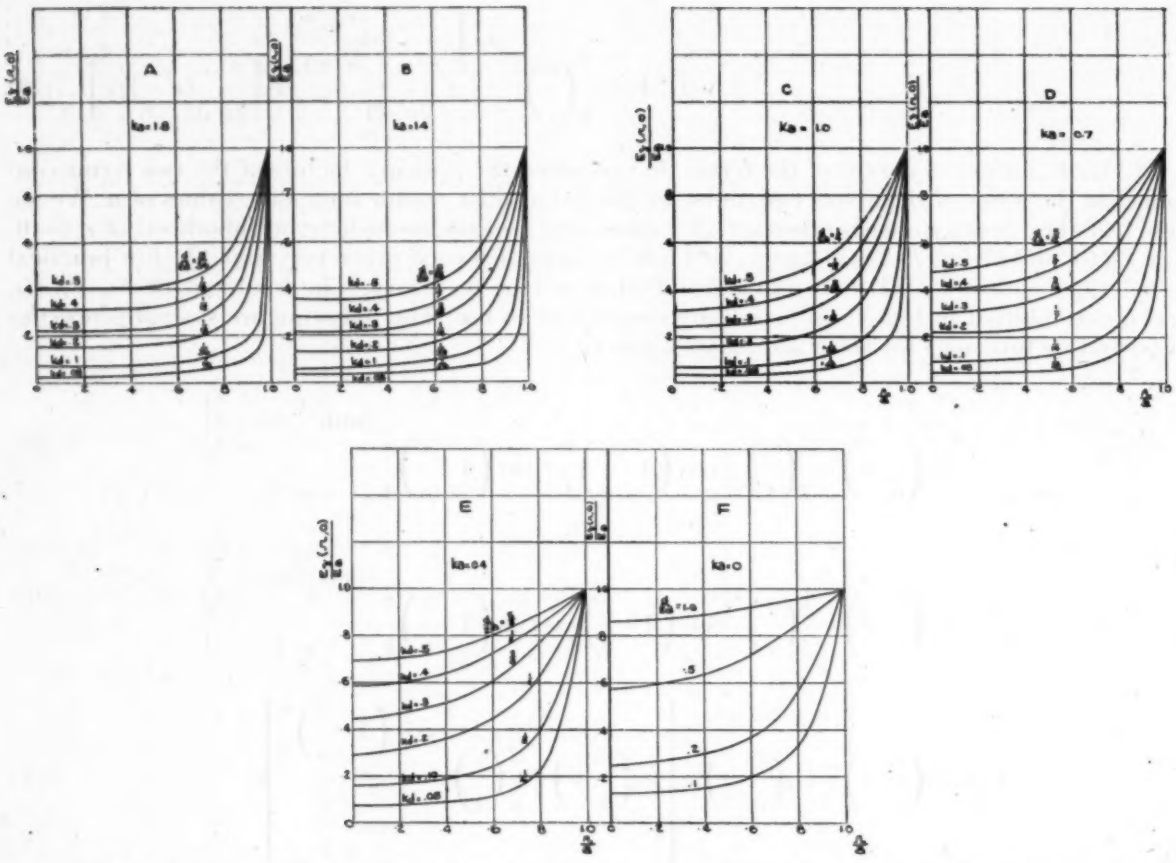

FIG. 9. The relative variation of axial electric field at the center of gap plotted against the relative radius r/a. Each plate corresponding to a fixed value of ka with kd or $d/2a$ as parameter.

$$\lim_{x\to\infty} G_1\left(\frac{r}{a}, x\right) = \frac{2}{\pi}\left(\frac{a}{r}\right)^{\frac{1}{2}} \cos\left(1-\frac{3r}{a}\right)\frac{\pi}{4} e^{-3x}. \tag{33}$$

$$\lim_{x\to\infty} G_2\left(\frac{r}{a}, x\right) = \frac{2}{\pi}\left(\frac{a}{r}\right)^{\frac{1}{2}} \sin\left(1-\frac{3r}{a}\right)\frac{\pi}{4} e^{-3x}. \tag{34}$$

Since the electric and magnetic fields are continuous everywhere except at $r/a=1$, and $z=\pm d/2$, where the electric field is discontinuous, the Eqs. (6) and (7) at $z=d/2$ must agree with each other and so also must be the Eqs. (15) and (16). By setting $z=d/2$ and equating them, we have the following equations of identity: with $r/a>1$,

$$\frac{J_0(kr)}{J_0(ka)} = 2\sum_{n=1}^{\infty} \frac{J_0(R_n r/a)}{R_n J_1(R_n)} \cdot \frac{1}{\cos^2 \alpha_n}. \tag{35}$$

$$\frac{J_1(kr)}{J_0(ka)} = 2\sum_{n=1}^{\infty} \frac{J_1(R_n r/a)}{R_n J_1(R_n)} \cdot \frac{\sin \alpha_n}{\cos^2 \alpha_n}. \tag{36}$$

These are very interesting in that they form one way of expanding the Bessel functions in terms of functions involving the roots of the zeros of Bessel's function of zeroth order.

The above are the equations which can be used for calculations of all the field strength related

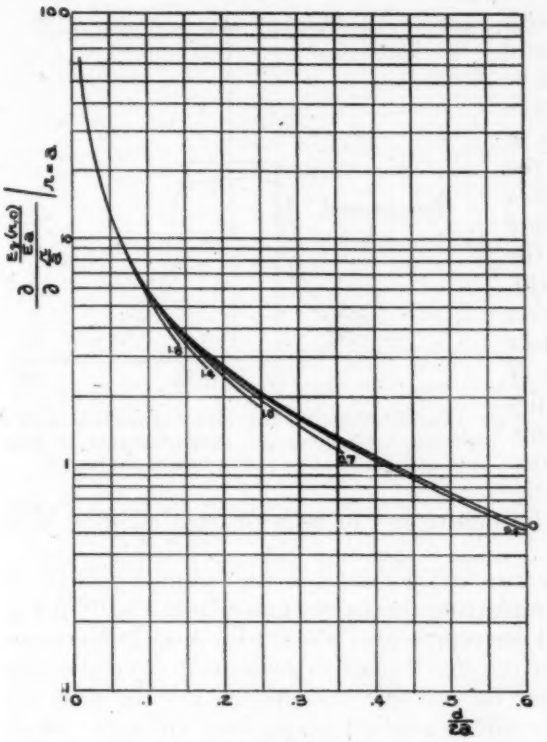

FIG. 10. Rate of axial field variation with respect to relative radius at the center of gap *versus* gap diameter ratio with *ka* and *kd* as parameters.

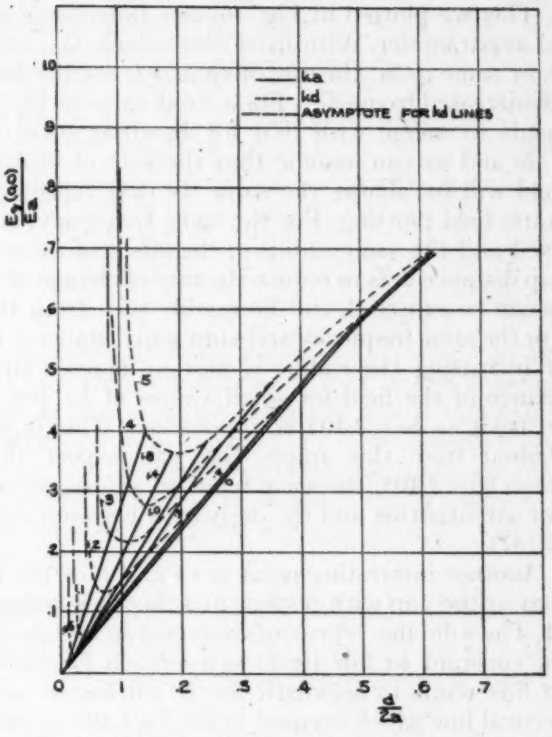

FIG. 11. Relative electric field at the center of the cylinder *versus* gap-diameter ratio with *ka* and *kd* as parameters.

to the axial field at the gap. We will discuss several interesting features based upon the above calculation.

The Radial Variation of Axial Electric Field at the Center of the Gap

It would be too much work to calculate the field throughout the whole space. Perhaps the most interesting thing to know is how the axial electric field, which determines the energy interchange with the electrons, varies along the radial direction. We will calculate this variation at the center of the gap for different sizes of the cylinder and different gap widths. A family of curves of field strength distribution *versus* radius for each value of normalized *ka* are plotted in Fig. 9 with different values of *kd* or $d/2a$ as parameters, *ka* covers the range from 0 to 1.8 and, *kd* covers the range from 0 to 0.5 which are the most likely ranges to be used in micro-wave tubes. For $ka=0$, i.e., the case corresponding to the electrostatic case, we use $d/2a$ alone as parameters. One essential feature of these curves is that since the field drops rapidly at the opening of the gap and then decreases slowly toward the center, the variation with respect to the radius must be zero at the center by reason of symmetry. It is perhaps very interesting to see the rate of variation right at the gap. This is, from (25),

$$\left.\frac{\partial\dfrac{E_z(r,z)}{E_a}}{\dfrac{\partial r}{a}}\right|_{r=a} = -ka\frac{J_1(ka)}{J_0(ka)}+\exp\left(-\frac{d}{2a}\frac{\pi}{4}\right)\left\{\frac{1}{\sinh^2\dfrac{d}{a}\dfrac{\pi}{4}}+\frac{\tanh^{-1}\operatorname{sech}\dfrac{d}{a}\dfrac{\pi}{4}}{2}\right\}$$

$$+\sum_{n=1}^{\infty}\frac{1}{\cos^2\alpha_n}F_1\left[0,\frac{d}{2a}R_n\cos\alpha_n\right]-\frac{2n-\frac{1}{2}}{2n-1}F_1\left[0,\frac{d}{2a}(n-\tfrac{1}{4})\pi\right]. \quad (37)$$

This we plotted in Fig. 10, as a function of $d/2a$ with ka as parameter. With fixed dimensions, i.e., same d and a, or same $d/2a$, the rate of change is smaller for large ka or increased frequency. For a fixed value of ka, the curve tends to merge with that for $ka=0$ at small values of $d/2a$ and we can assume that the rate of change of the field will be almost the same as that represented in a static field plotting. For the same frequency, i.e., with k fixed and the same radius a, the effect of increasing the gap distance d, is to reduce the rate of change of the field, as can be expected, and be readily seen from the curve. For the same frequency and same gap distance d, the effect of increasing the radius is first to increase the rate of change of the field for small values of ka and then decrease it as $ka=2.405$ is approached. This is not quite evident from this graph. One can expect this, since when $ka=2.405$, the wave tends to propagate out without attentuation and the derivative becomes negatively infinite as can be seen from the first term in (37).

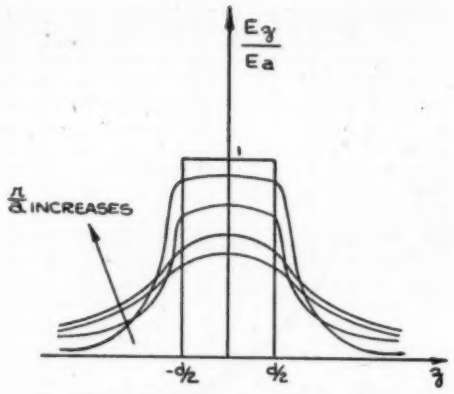

FIG. 12. Sketch of the rélative variation of axial electric field along the axial direction of fixed radius with relative radius r/a as parameters.

Another interesting point is to find how the field varies at the center of the cylinder relative to that at the gap with respect to $d/2a$. This is done by replotting the values taken from Fig. 9 in Fig. 11. The solid line represents constant ka and the dotted line represents constant kd. As $d/2a$ increases, the constant ka line tends to approach $Ez/Ea=1$ and the $ka=0$ lines as asymptote. The constant kd line tends to approach the $ka=0$ line as asymptote on one side and approaches the dash dot vertical line which is equal to $kd/2\times 2.405$ on the other side as another asymptote. The curve shows that the field at the center of the cylinder with fixed kd first decreases with ka at small value of ka, i.e., large $d/2a$ up to a minimum and then increases again as ka further increases. This increase at values approaching $ka=2.405$ shows the tendency for the wave to spread in the cylinder as the cut-off value of the E wave is approached. Examination of curves in Fig. 9 shows that the corresponding values of the field at the center for the same kd is higher for $ka=1.8$ than those for $ka=1.4$ although the rate of change of field is greater at the gap for $ka=1.8$ than that of $ka=1.4$.

The Axial Variation of Axial Electric Field

The axial field variation is interesting to know as it represents the force acting upon the electrons as they move along the axial direction. We can calculate by the above formulae different values of E_z/E_a for different values of z with r fixed. The result as plotted against z would be like that in Fig. 12 with different values of r/a as parameters. The peak at the center can be obtained from the values calculated in the previous section. We can have some general idea of how these curves should vary by examining the above equations, when $d/2a$ is small, which is generally the case. For small values of $d/2a$, we expect the field to stay almost constant within the gap i.e. for $-d/2a<z<d/2a$. This is so from examination of Eq. (25) and the function G_1. For the region outside the gap, we see in Eq. (27), with the aid of Eqs. (31), (32), (33), for $d/2a\ll 1$,

$$F_2(1,\,(d/2a)R_n\cos\alpha_n)\doteqdot F_2(1,\,d/2a)\cdot(n-\tfrac{1}{4})\pi)\doteqdot 0,$$

$$\left.\frac{E_z(r,d/2)}{E_a}\right|_{d/2a\ll 1}=\left[G_1\left(\frac{r}{a},0\right)+\frac{2}{\pi}\left(\frac{a}{r}\right)^{\frac{1}{2}}\frac{\cos\left(1-\frac{r}{a}\right)\frac{\pi}{4}}{\cos\frac{r}{a}\frac{\pi}{2}}\right]\frac{d}{a}\frac{\pi}{4}, \tag{38}$$

$$\left.\frac{E_z(r,z)}{E_a}\right|_{\substack{z/d\gg 1\\ d/2a\ll 1}}=\frac{4}{\pi}\left(\frac{a}{r}\right)^{\frac{1}{2}}\cos\left(1-\frac{3r}{a}\right)\frac{\pi}{4}\exp\left(-\frac{z}{a}\frac{3\pi}{4}\right)\sin\frac{3d\pi}{8a}. \tag{39}$$

When we take the ratio of (39) to (38), for very small value of $d/2a$,

$$\frac{E_z(r,z)}{E_z(r,d/2)}=\frac{\frac{6}{\pi}\cos\left(1-\frac{3r}{a}\right)\frac{\pi}{4}}{\left(\frac{r}{a}\right)^{\frac{1}{2}}G_1\left(\frac{r}{a},0\right)+\frac{2\cos(1-r/a)\frac{\pi}{4}}{\pi\cos\frac{r}{a}\frac{\pi}{2}}}\exp\left(-\frac{z}{a}\frac{3\pi}{4}\right). \tag{40}$$

By Eq. (40), we can plot the distribution curve against z at large distances z, in terms of the field at the edge of the gap of the same radius and it falls exponentially as $e^{(-z/a)(3\pi/4)}$ of a constant times the field at the edge of the gap. This constant increases as r/a decreases and it more than compensates for the decrease of field at the edge of the gap, so that the field at a large distance away from the gap is actually higher for smaller values of r/a, this also being seen from Eq. (39), since the factor in front of the exponential is a decreasing function of r/a. This explains the cross over in plotting the curves as shown by Fig. 12. Notice, Eq. (38) and Eq. (40) are good only for not too small r/a. More terms can be taken from Eq. (27) for smaller r/a.

The Spatial Variation of the Radial Electric Field

We will not attempt to plot all the curves for the radial electric field because they are probably of less interest than the axial field. The distribution curves will have the shape as shown in Fig. 13. Singularity occurs at $r/a=1$ and $z=\pm d/2$.

The Electrostatic Potential, Electrostatic Lens

As a special case, the above equations can be applied to trace the field of the electrostatic lenses which are so commonly used in the electron microscope, cathode-ray tubes, etc. The electric field can be obtained from Eqs. (25) to (28) in which we set $k=0$, $\cos\alpha_n=1$, $\sin\alpha_n=0$. The axial field is already plotted in Fig. 4. Perhaps the electrostatic potential lines are important to know. Let us define the potential difference between the two cylinders as V, the equipotential plane at the mid-point in between the two cylinders being 0 volts, the voltage of the cylinder at the right being $-V/2$ and that at the left being $V/2$, and V will be equal to E_0d. The potential function $\varphi(r,z)$ at any point in the space will be, by integrating (6) for $-d/2<z<d/2$,

$$\frac{\varphi(r,z)}{V}=\frac{1}{V}\int_0^z E(r,z)dz=z/d-(a/d)\sum_{n=1}^{\infty}\frac{J_0(R_nr/a)}{R_n^2J_1(R_n)}2\exp\left(-\frac{d}{2a}R_n\right)\sinh\frac{z}{a}R_n, \tag{41}$$

for $d/2<z<\infty$,

$$\varphi(r,z)=\int_{d/2}^z E(r,z)dz+\varphi(r,d/2),$$

$$\frac{\varphi(r,z)}{V}=\tfrac{1}{2}-\frac{a}{d}\sum_{n=1}^{\infty}\frac{J_0(R_nr/a)}{R_n^2J_1(R_n)}2\exp\left(-\frac{z}{2a}R_n\right)\sinh\left(\frac{d}{2a}R_n\right). \tag{42}$$

The above series is quite convenient to use, since, it converges fairly rapidly, falling as $1/n^2$.

The Magnetic Field and the Equivalent Capacitance

The most interesting thing to know about the magnetic field is the average value right at the opening of the gap, which represents the r.f. current flowing into the cylinder. Let us define the total r.f. current flowing into the cylinder all over the whole circumference as the following, and by Eq. (15).

$$I=\frac{2\pi a}{d}\int_{-d/2}^{d/2}H_\theta(a,z)dz=jE_0d2\pi\left(\frac{\epsilon}{\mu}\right)^{\frac{1}{2}}\frac{a}{d}(kt), \tag{43}$$

where

$$kl=\frac{J_1(ka)}{J_0(ka)}-\sum_{n=1}^{\infty}\frac{1}{R_n^2\cos^3\alpha_n}\cdot\frac{\sin\alpha_n}{\frac{d}{2a}}2\exp\left(-\frac{d}{2a}R_n\cos\alpha_n\right)\sinh\frac{d}{2a}R_n\cos\alpha_n, \tag{44}$$

and ϵ and μ are the dielectric constant and permeability respectively.

Let us define the equivalent susceptance A such that

$$\begin{aligned}A&=I/E_a d=j\cdot 2\pi(\epsilon/\mu)^{\frac{1}{2}}(a/d)(kt)\\&=j(a/d)(kt)/60 \text{ for vacuum.}\end{aligned} \tag{45}$$

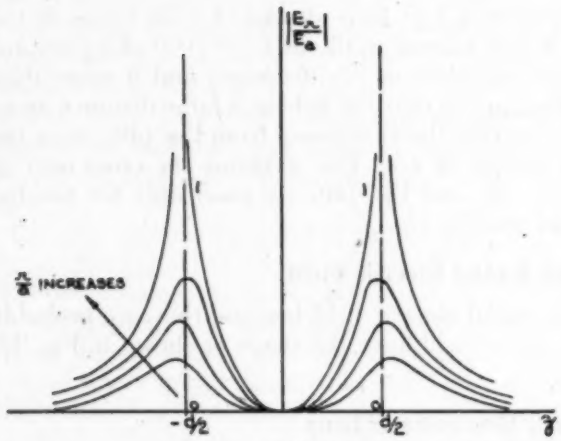

FIG. 13. Sketch of the relative variation of radial electric field along the axial direction of fixed radius with relative radius r/a as parameters.

The value t has the significance of being the equivalent added thickness of the metal cylinders which form the capacitance. For in the resonator as shown in Fig. 14, suppose the metallic wall has the thickness of t' as shown. Then the equivalent capacitance formed by this wall at the gap is approximately $2\pi at'\epsilon/d$ if the wall is thin and the fringing effect is neglected; the capacitive susceptance will be approximately $j\omega 2\pi t'\epsilon/d$ or $j2\pi(\epsilon/\mu)^{\frac{1}{2}}akt'/d$. Thus, in calculating the resonance frequency of the cavity we can consider the combined capacitive susceptance due to the proximity of the metallic wall and that due to energy storage in the cylinder space is loaded to the transmission line as shown in Fig. 15. The net effect of the energy storage in the cylinder space is as if an imaginary thickness has been added to the wall as shown in Fig. 14. This susceptance must be equal in magnitude to the short-circuited inductive susceptance offered by the transmission line, as shown in Fig. 15, which would be the equivalent circuit of Fig. 14. The value of kl, i.e., the normalized length of the line will be below $\pi/2$ or l will be less than $\lambda/4$ such that, with R_0 equal to the characteristic impedance of the line, with $2\pi(\epsilon/\mu)^{\frac{1}{2}}=60$.

$$R_0\tan kl=60d/ka(t+t')=|1/A|,$$

or

$$kl=\tan^{-1}(60/R_0)d/ka(t+t'). \tag{46}$$

The values of kat/d per Eq. (43) are calculated and plotted as in Fig. 16 *versus* $d/2a$. The solid lines are for constant ka, and dotted lines for constant kd. As $d/2a$ decreases, both increase. The solid line is asymptotic to the $d/2a=0$ axis and dotted lines are asymptotic to $kd/2\times 2.405$ lines as indicated by the dash dot lines. This can be expected, since as the cut-off frequency is approached, more energy tends to be stored in the space and finally to be lost through propagation to the space.

To illustrate, let us have the case with $ka=1.4$, $kd=0.1$, $kt'=0.05$, $R_0=60$ ohms and $kat'/d=0.7$. Then from the curve we have $kat/d=1.85$.

Hence, $kl=\tan^{-1}(60/60)\cdot 1/(1.85+0.7)$,

$$kl=21°23'=0.118\pi \quad \text{or} \quad l=0.059\lambda,$$

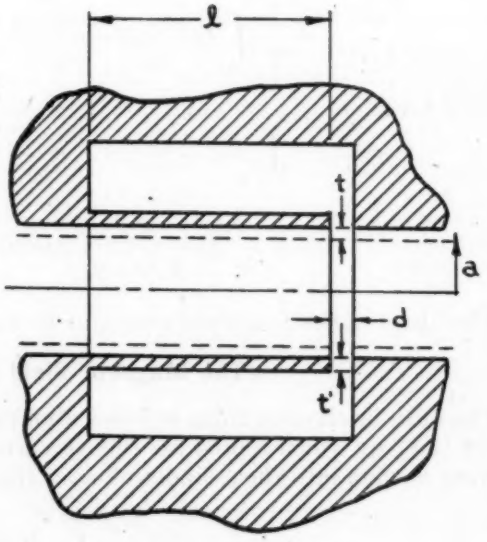

FIG. 14. A resonator.

which is far below $\lambda/4$. If the characteristic impedance is 15 ohms, then,

$$kl = \tan^{-1} 4/1.85 + 0.7) = 57°30'$$

or

$$l = 0.16\lambda.$$

Acknowledgment

The author wishes to thank Professor E. Weber for discussing the problem and also Mr. J. R. Lurye for reading and checking the manuscript.

APPENDIX

Evaluation of the integral

$$E_z(r, z) = \frac{2}{\pi} Ea \int_0^\infty \frac{(\sin hd/2)}{h} \frac{J_0(k^2 - h^2)^{\frac{1}{2}} r)}{J_0(k^2 - h^2)^{\frac{1}{2}} a)} \cos hz dh.$$

Let $jh = x$, and change the integral; then we have

$$E_z(r, z) = \frac{2}{\pi} E_a \int_0^\infty (\quad) dh$$

$$= \frac{1}{2\pi j} Ea \int_0^{j\infty} \frac{e^{\frac{d}{2}x} - \exp\left(-\frac{d}{2}x\right)}{x} \frac{J_0[(k^2 + x^2)^{\frac{1}{2}} r]}{J_0[(k^2 + x^2)^{\frac{1}{2}} a]} \cdot \frac{(e^{zx} + e^{-zx})}{2} dx$$

$$= \frac{1}{4\pi j} \int_{-j\infty}^{j\infty} (\quad) dx$$

$$= \frac{1}{4\pi j} \int_{-j\infty}^{j\infty} \frac{J_0[(k^2 + x^2)^{\frac{1}{2}} r]}{J_0[(k^2 + x^2)^{\frac{1}{2}} a]} \frac{1}{x} \cdot [e^{x(d/2+z)} - e^{-x(d/2+z)} + e^{x(d/2-z)} - e^{-x(d/2-z)}] dx. \quad \text{(A1)}$$

Equation (A1) is a combination of four integrals, each of which contains in the integrand an exponential factor. Each integral has a path of integration along the imaginary axis from $-j\infty$ to $+j\infty$. Let the symbol $\int_\supset$ be the integral along the semicircular path of infinite radius in the right half of the complex plane and $\int_C$ be the corresponding one in the left half of the plane. Let $\int_\supset$ be the complete closed integral from $-j\infty$ to $j\infty$ along the imaginary axis and back to $-j\infty$ along the circular path in the right half of the plane and $\int_\subset$ will be the corresponding one in the left half of the plane. The poles of the integrands occur at $x = 0$, and $x = \pm x_n$ at which $J_0[(k^2 + x_n^2)^{\frac{1}{2}} a]$ equals zero. Let R_n be the roots of $J_0 = 0$, such that

$$x_n a = (R_n^2 - k^2 a^2)^{\frac{1}{2}}$$

the x_n will be real quantities provided that $R_n > ka$. Let us restrict ourselves in such a way that $ka < 2.405$. Then all the poles will be along the real axis as in Fig. A1.

The way to handle the integral is to add the semicircular integral to the right or left depending upon whether the integral vanishes as the radius of the semicircle increases indefinitely. This will be so if the factor $J_0[(k^2 + x^2)^{\frac{1}{2}} r]/xJ_0[(k^2 + x^2)^{\frac{1}{2}} a]$ remains finite as x increases, and we will add a semicircular path to the left if the coefficient of x in the exponential term is positive (as the negative real part of x as x approaches infinity in the left plane will make the integral zero) and to the right if the coefficient of x is negative. To see whether this factor stays finite as x approaches infinity, let us set $x = (\pi/2)\xi \pm jy = A \cdot i^{\pm\rho}$.[3]

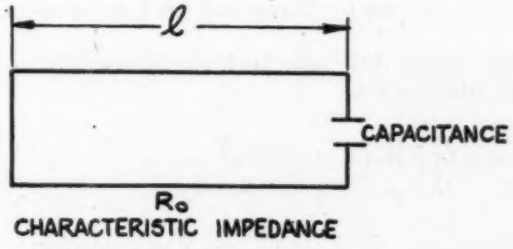

FIG. 15. Equivalent circuit of a resonator.

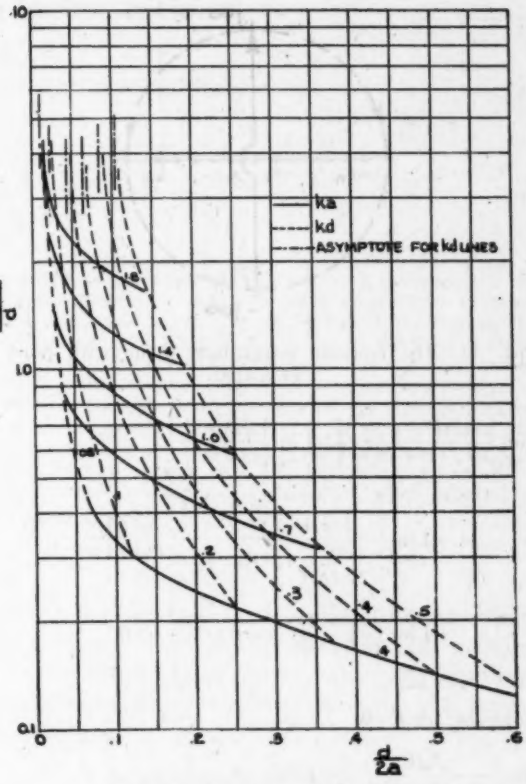

FIG. 16. Equivalent capacitive susceptance *versus* gap-diameter ratio with *ka* and *kd* as paramaters.

[3] E. Jahnke and F. Emde, *Tables of Bessel Functions with Formulae and Curves* (Leipzig, 1939), Third Edition, p. 138.

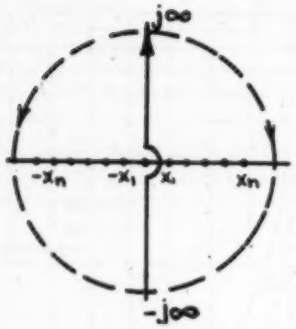

FIG. A1. The contour integration plane with poles as indicated.

$$\lim_{z\to\infty}\left|\frac{J_0[(k^2+x^2)^{\frac{1}{2}}r]}{xJ_0[(k^2+x^2)^{\frac{1}{2}}a]}\right|=\lim_{z\to\infty}\left|\frac{J_0(xr)}{xJ_0(xa)}\right|$$

$$=\lim_{z\to\infty}\left|\frac{\frac{e^{jr}}{(2\pi Ar)^{\frac{1}{2}}j^{\frac{1}{2}(1-\rho)-\xi_r}}\frac{S_0(2Are^{\pm(1+\rho)j})}{S_0(2Aae^{\pm(1+\rho)j})}}{\frac{e^{ja}}{(2\pi Aa)^{\frac{1}{2}}Aj^{\pm\rho_j\frac{1}{2}(1-\rho)-\xi_a}}}\right|$$

$$=\lim_{\substack{z\to\infty\\ y\to\infty\\ A\to\infty}}\left(\frac{a}{r}\right)^{\frac{1}{2}}\frac{e^{-y(a-r)}}{A}=0 \text{ as } a-r>0.$$

However, for $r=0$

$$\lim_{z\to\infty}\left|\frac{J_0(0)}{xJ_0[(k^2+x^2)^{\frac{1}{2}}a]}\right|=\lim_{z\to\infty}\left|\frac{1}{xJ_0[(k^2+x^2)^{\frac{1}{2}}a]}\right|$$

$$=\lim_{\substack{y\to\infty\\ A\to\infty}}\frac{(2\pi a)^{\frac{1}{2}}}{e^{ya}(A)^{\frac{1}{2}}}=0. \quad \text{(A2)}$$

Take the case for $-d/2<z<d/2$. Then $d/2+z>0$, $d/2-z>0$. Therefore we can add to the first and third integrals an additional path of integration on the infinite semicircle to the left of the imaginary axis. Thus, the first integral becomes

$$\frac{1}{4\pi j}\int_{-j\infty}^{j\infty}\frac{J_0[(k^2+x^2)^{\frac{1}{2}}r]}{J_0[(k^2+x^2)^{\frac{1}{2}}a]}\frac{1}{x}e^{x(d/2+z)}dx$$

$$=\frac{1}{4\pi j}\int_{-j\infty}^{j\infty}(\ )+\frac{1}{4\pi j}\int_{C_1}(\ )$$

$$=\frac{1}{4\pi j}\int_{C_1}(\ )$$

$$=\frac{1}{4\pi j}\cdot 2\pi j\,\Sigma \text{ residue of the poles on the negative real axis and zero}$$

$$=\frac{1}{2}\frac{J_0(kr)}{J_0(ka)}-\sum_{n=1}^{\infty}\frac{J_0\left(R_n\frac{r}{a}\right)}{J_1(R_n)}\frac{R_n}{a^2x_n^2}\exp\left(-x_n\left(\frac{d}{2}+z\right)\right). \quad \text{(A3)}$$

Similarly the third integral becomes

$$\frac{1}{4\pi j}\int_{-j\infty}^{j\infty}\frac{J_0[(k^2+x^2)^{\frac{1}{2}}r]}{J_0[(k^2+x^2)^{\frac{1}{2}}a]}\cdot\frac{1}{x}\exp\left(x_n\left(\frac{d}{2}-z\right)\right)$$

$$=\frac{1}{2}\frac{J_0(kr)}{J_0(ka)}-\sum_{n=1}^{\infty}\frac{J_0\left(R_n\frac{r}{a}\right)}{J_1(R_n)}\frac{R_n}{a^2x_n^2}\exp\left(-x_n\left(\frac{d}{2}-z\right)\right). \quad \text{(A4)}$$

The second integral will be evaluated with the integration path added to the right side plane and remembering the closed integral is equal to negative $2\pi j$ times the residues as the sense of rotation of integration is clockwise, then the second integral

$$\frac{1}{4\pi j}\int_{-j\infty}^{j\infty}\frac{J_0[(k^2+x^2)^{\frac{1}{2}}r]}{J_0[(k^2+x^2)^{\frac{1}{2}}a]}\frac{1}{x}e^{-x(d/2+z)}dx$$

$$=\frac{1}{4\pi j}\left\{\int_{-j\infty}^{j\infty}(\ )+\int_{C}(\ )\right\}$$

$$=\frac{1}{4\pi j}\int_{C}(\ )$$

$$=-\frac{1}{4\pi j}\cdot 2\pi j\,\Sigma \text{ residue on the positive real axis}$$

$$=-\frac{1}{2}\sum_{n=1}^{\infty}\frac{J_0\left(R_n\frac{r}{a}\right)}{J_1(R_n)}\frac{R_n}{a^2x_n^2}\exp\left(-x_n\left(\frac{d}{2}+z\right)\right). \quad \text{(A5)}$$

Similarly, the fourth integral becomes

$$\frac{1}{4\pi j}\int_{-j\infty}^{j\infty}\frac{J_0[(k^2+x^2)^{\frac{1}{2}}r]}{J_0[(k^2+x^2)^{\frac{1}{2}}a]}\frac{1}{x}e^{-x(d/2-z)}dx$$

$$=-\frac{1}{2}\sum_{n=1}^{\infty}\frac{J_0\left(R_n\frac{r}{a}\right)}{J_1(R_n)}\frac{R_n}{a^2x_n^2}\exp\left(-x_n\left(\frac{d}{2}-z\right)\right), \quad \text{(A6)}$$

for $-d/2<z<d/2$

$$\frac{E_z(r,z)}{E_a}=\text{sum of (A3) to (A6)}$$

$$=\frac{J_0(kr)}{J_0(ka)}-\sum_{n=1}^{\infty}\frac{J_0\left(R_n\frac{r}{a}\right)}{R_nJ_1(R_n)}\frac{1}{\cos^2\alpha_n}$$

$$\cdot 2\exp\left(-\frac{d}{2a}R_n\cos\alpha_n\right)\cosh\frac{z}{a}R_n\cos\alpha_n. \quad \text{(A7)}$$

For $d/2<z<\infty$, the first and fourth integrals will have an added path of integration to the left side and the second and third will have an added path to the right; the result is

$$\frac{E_z(r,z)}{E_a}=\sum_{n=1}^{\infty}\frac{J_0\left(R_n\frac{r}{a}\right)}{R_nJ_1(R_n)}\frac{1}{\cos^2\alpha_n}$$

$$\cdot 2\exp\left(-\frac{z}{a}R_n\cos\alpha_n\right)\sinh\frac{d}{2a}R_n\cos\alpha_n. \quad \text{(A8)}$$

For $z=d/2$, the third and fourth integrals cancel each other; we have

$$\frac{E_z(r,z)}{E_a}=\frac{1}{2}\frac{J_0(kr)}{J_0(ka)}-\sum_{n=1}^{\infty}\frac{J_0\left(R_n\frac{r}{a}\right)}{R_nJ_1(R_n)}\frac{1}{\cos^2\alpha_n} \quad \text{(A9)}$$

$$\cdot\exp\left(-\frac{d}{a}R_n\cos\alpha_n\right).$$

Convection Currents in a Porous Medium

C. W. HORTON
Underwater Sound Laboratory, Harvard University, Cambridge, Massachusetts
AND
F. T. ROGERS, JR.*
The University of Houston, Houston, Texas
(Received January 15, 1945)

The problem is considered of the convection of a fluid through a permeable medium as the result of a vertical temperature-gradient, the medium being in the shape of a flat layer bounded above and below by perfectly conducting media. It appears that the minimum temperature-gradient for which convection can occur is approximately $4\pi^2h^2\mu/kg\rho_0\alpha D^2$, where h^2 is the thermal diffusivity, g is the acceleration of gravity, μ is the viscosity, k is the permeability, α is the coefficient of cubical expansion, ρ_0 is the density at zero temperature, and D is the thickness of the layer; this exceeds the limiting gradient found by Rayleigh for a simple fluid by a factor of $16D^2/27\pi^2k\rho_0$. A numerical computation of this gradient, based upon the data now available, indicates that convection currents should not occur in such a geological formation as the Woodbine sand of East Texas (west of the Mexia Fault zone); in view of the fact, however, that the distribution of NaCl in this formation seems to require the existence of convection currents, and in view of the approximations involved in applying the present theory, it seems safe tentatively, to conclude that convection currents do exist in this formation and that the expression given above predicts excessive minimum gradients when applied to such a formation.

I. INTRODUCTION

THE problem of the occurrence of convection-currents in a fluid which is heated from below, has been examined by Rayleigh,[1] Jeffreys,[2,3,4] and Low.[5] The solution of the problem involves the finding of the relationship (between the physical parameters of the medium) which, so to speak, separates stability from instability.

Rayleigh solved the problem for a set of boundary conditions that are somewhat artificial; but the work of Jeffreys shows that the introduction of a more nearly realistic set of boundary conditions does not change the limiting relationship by more than a factor of three. The analysis of this paper follows that of Rayleigh, since his method affords a clearer insight into the physical problem.

Refer all measurements to Cartesian coordinates, of which the z-axis is directed vertically upward; let ρ and μ represent the density and viscosity of the fluid respectively, and let k represent the permeability of the porous medium. Let p represent the pressure in the fluid; and let u, v, and w represent the x-, y-, and z-components respectively of the velocity of the fluid. Let g represent the acceleration of gravity. Then, as Muskat has shown,[6] the hydrodynamic equations of motion of the fluid in the porous medium are

$$\left.\begin{aligned} u&=-(k/\mu)(\partial p/\partial x),\\ v&=-(k/\mu)(\partial p/\partial y),\\ w&=-(k/\mu)(\partial p/\partial z+g\rho),\end{aligned}\right\} \tag{1}$$

if the only external force is gravity. It will be supposed that the density, ρ, varies only with temperature and according to the relation

$$\rho=\rho_0(1-\alpha\Theta), \tag{2}$$

where Θ is the temperature and ρ_0 is the density at $\Theta=0$.

Other relationships which must be considered simultaneously with Eqs. (1) and (2) are those of continuity and of thermal conduction. If the fluid is supposed to be incompressible, the equation of continuity becomes

$$\partial u/\partial x+\partial v/\partial y+\partial w/\partial z=0. \tag{3}$$

If h^2 is the thermal diffusivity, the equation for the conduction of heat is

$$D(\Theta)/Dt=h^2\nabla^2\Theta, \tag{4}$$

in which the operator

$$D/Dt=\partial/\partial t+u(\partial/\partial x)+v(\partial/\partial y)+w(\partial/\partial z);$$

t, of course, represents time.

* Now with The Lukas-Harold Corporation (Laboratory), operators of the U. S. Naval Ordnance Plant, Indianapolis. Part of the work of F.T.R. on this problem was done in connection with the Physics Department of The University of Houston, and represents Contribution No. 91 from the Science Divisions of that University.

[1] Rayleigh, Phil. Mag. **32**, 529 (1916).
[2] H. Jeffreys, Phil. Mag. **2**, 833 (1926).
[3] H. Jeffreys, Proc. Roy. Soc. **118A**, 195 (1928).
[4] H. Jeffreys, Proc. Camb. Phil. Soc. **26**, 170 (1930).
[5] A. R. Low, Proc. Roy. Soc. **125A**, 181 (1929).

[6] M. Muskat, *Flow of Homogeneous Fluids* (McGraw-Hill Book Company, Inc., 1937).

II. SOLUTION OF THE PROBLEM

To prepare Eqs. (1)–(4) for solution, first separate Θ into two parts: a steady-state temperature, βz, due to the gradient β; and the deviation, θ, therefrom. That is, let

$$\Theta=\beta z+\theta. \tag{5}$$

Secondly, introduce the potential-function

$$\Omega=p+g\rho_0 z-g\rho_0\alpha\int\beta z dz. \tag{6}$$

Finally, suppose that u, v, w, and θ and their rates of change are small. Then by Eqs. (5) and (6), Eqs. (1) become

$$\left.\begin{aligned} u&=-(k/\mu)(\partial\Omega/\partial x),\\ v&=-(k/\mu)(\partial\Omega/\partial y),\\ w&=-(k/\mu)(\partial\Omega/\partial z)+\Lambda\theta,\end{aligned}\right\} \tag{7}$$

where

$$\Lambda=kg\rho_0\alpha/\mu. \tag{8}$$

Again, Eq. (5) with Eq. (4) yields

$$D\theta/Dt+w\beta=h^2\nabla^2\theta;$$

and by the assumption of smallness as stated above, $D\theta/Dt=\partial\theta/\partial t$, so that this last equation becomes

$$\partial\theta/\partial t+w\beta=h^2\nabla^2\theta. \tag{9}$$

Let us suppose that u, v, w, and θ, and also Ω, are each proportional to

$$e^{ilx}e^{imy}e^{nt}; \tag{10}$$

then Eqs. (7) become

$$\left.\begin{aligned} u&=-i(kl/\mu)\Omega,\\ v&=-i(km/\mu)\Omega,\\ w&=-(k/\mu)(\partial\Omega/\partial z)+\Lambda\theta,\end{aligned}\right\} \tag{11}$$

while the equation of continuity, Eq. (3), becomes

$$ilu+imv+\partial w/\partial z=0. \tag{12}$$

Note that Eqs. (11) and (12) together give

$$\Omega=-(1/(l^2+m^2))(\mu/k)(\partial w/\partial z), \tag{13}$$

and that this Eq. (13) together with the last of Eqs. (11) gives

$$w=(1/(l^2+m^2))(\partial^2 w/\partial z^2)+\Lambda\theta. \tag{14}$$

The equation for the conduction of heat, Eq. (9), thus becomes

$$n\theta+w\beta=h^2(\partial^2/\partial z^2-l^2-m^2)\theta. \tag{15}$$

The treatment of the analogous problem for a simple fluid by Jeffreys is based upon the fact that the stable condition is distinguished from the unstable condition by the mathematical condition that $n=0$. Then w is eliminated from Eqs. (14) and (15). The resulting fourth-order equation in θ (sixth-order for the problem of the simple fluid) is solved subject to the boundary-conditions discussed by Jeffreys in references (2) and (3). These boundary-conditions yield a sequence of characteristic (eigen-) numbers, the smallest of which specifies the relation between the physical parameters for critical instability.

To continue with the solution of the present problem, note that if the fluid has free surfaces at both top and bottom, and if the media above and below the fluid are perfect conductors, then both w and θ will be zero at both the bottom ($z=0$) and the top ($z=D$) of the fluid layer. A reasonable assumption, then, is that w and θ are proportional to $\sin sz$, where $s=r\pi/D$ and r is an integer. If this assumption be adopted, Eq. (14) becomes

$$w=-(s^2/(l^2+m^2))w+\Lambda\theta, \tag{16}$$

and Eq. (15) becomes

$$n\theta+w\beta=-h^2(l^2+m^2+s^2)\theta. \tag{17}$$

Eqs. (16) and (17) will be consistent if and only if

$$n=[-\beta\Lambda(\sigma-s^2)-h^2\sigma^2]/\sigma, \tag{18}$$

where

$$\sigma=l^2+m^2+s^2. \tag{19}$$

Eq. (18) indicates that if β is positive, n is negative, so that any convective disturbance will decrease in amount exponentially with time; i.e., convection currents cannot occur. On the other hand, if the fluid is heated from below so that β is negative, say $-\beta'$, n can be positive and convection currents may develop.

If $\beta=-\beta'$, $\beta'>0$, n will be positive if

$$\beta' g\alpha(\sigma-s^2)>h^2\mu\sigma^2/k\rho_0. \tag{20}$$

This is similar to the condition for positive n,

$$\beta' g\alpha(\sigma-s^2)>h^2\mu\sigma^3, \tag{21}$$

derived by Rayleigh for a simple fluid.

To complete the solution of the present problem, note that Eq. (18) indicates that if l^2+m^2 is very small or very large, n is negative; that is, the value of σ for which n is just zero is the value for which the numerator has a maximum with respect to σ. Thus the critical condition between stability and instability ($n=0$) is characterized by

$$\beta'\Lambda(\sigma-s^2)-h^2\sigma^2=0 \tag{22}$$

and

$$\beta'\Lambda-2h^2\sigma=0; \tag{23}$$

the Eq. (23) is the derivative of Eq. (22) with respect to σ. These two equations require that

$$\left.\begin{aligned} \sigma &= 2s^2 \\ \text{and} \qquad l^2+m^2 &= s^2. \end{aligned}\right\} \tag{24}$$

For a given s, therefore, the necessary condition for the formation of convection currents is (by Eqs. (22) and (24))

$$\beta'\Lambda > h^2\sigma^2/s^2 = 4h^2s^2. \tag{25}$$

Finally, the minimum value of $s=r\pi/D$ is π/D; so from Eq. (25), the result appears that convection currents may develop only for temperature-gradients

$$\beta' > 4\pi^2h^2\mu/kg\rho_0\alpha D^2. \tag{26}$$

This criterion, Eq. (26), for the formation of convection currents in a fluid in a porous medium may be compared with the equivalent condition developed by Rayleigh for the formation of convection currents in a simple fluid:

$$\beta' > 27\pi^4h^2\mu/4g\alpha D^4. \tag{27}$$

The minimum temperature-gradient necessary for the formation of convection currents in a porous medium is greater than that required for convection currents in the free fluid by the factor

$$(16/27)(D^2/\pi^2k\rho_0). \tag{28}$$

It should be noted that this ratio varies as D^2, where D is the thickness of the fluid layer, and so may become quite large.

III. AN APPLICATION OF GEOPHYSICAL INTEREST; DISCUSSION

An interesting application of this theory can be made to the problem of a subterranean inclined sand-layer containing a fluid, which layer is bounded above and below by impervious layers. The accuracy is limited, in this application, by conceivable inaccuracies in Eq. (26) (which has not been subjected to explicit experimental tests, and which has not been refined by analyses of the types of Jeffreys and of Low), by the simplifying approximations used in deriving Eq. (26), and by numerical uncertainties in the values of the parameters appearing in Eq. (26).

Let T be the thickness of the sand-layer, and let ϕ be the angle made with the horizontal by the plane of the layer. If T is not large, the temperature may be considered as constant across its width; then only the components of the temperature-gradient and of the acceleration of gravity *along* the inclined length enter the computations. Thus β' and g are reduced each by the factor $\sin\phi$. Let H be the inclined length of the layer. It should be noted in this connection that thickness is measured normally to the temperature-gradient, whereas in the analysis (Sec. I and II) this dimension was taken to be parallel to the temperature-gradient; this involves no change of formulae, for H merely corresponds directly with D. With these modifications of notation, Eq. (26) should be applicable.

As a numerical example, consider the Woodbine sand-formation of East Texas. Plummer and Sargent[7] give the following data for the region west of the Mexia Fault zone. In this area the Woodbine sand is 250 feet thick; and it has a uniform dip of 75 feet per mile, so that $\sin\phi = 0.0142$; it is abruptly terminated at its lower end by a fault-plane. The reciprocal temperature-gradient in this region is 50 feet per degree fahrenheit, so that $\beta'_{vert} = 3.64\times10^{-4}$ degrees centigrade per cm. H varies between 34 and 48 miles; and its mean value will be used here as 5.4×10^6 cm. Taking $\mu=1$ centipoise, $\rho_0=1$ g/cm^3, $D=H$, $\alpha=8.5\times10^{-6}$ per degree C, and $h^2=0.009$ for sandy soil,[8] Eq. (26) specifies as the minimum value of the permeability for which convection currents may develop

$$k_{min} = 20 \text{ darcys.}$$

Muskat quotes several values for the permeability of the Woodbine sand, these values being in the neighborhood of 1 darcy. The implication of the present simple analysis and of the data listed above, therefore, is that convection currents should not occur in this portion of the Woodbine sand.

This conclusion concerning the existence of convection currents in the Woodbine sand west of the Mexia Fault zone, based as it is upon the rather limited accuracy of Eq. (26) (see the first paragraph of Sec. III), appears to be at variance with other evidence bearing upon the problem. One of the authors[9] has examined the distribution of NaCl in this region of the Woodbine sand. From geological considerations the

---

[7] F. B. Plummer and E. C. Sargent, Univ. Texas Bull., No. 3138 (1931).
[8] F. Birch, Editor, Geol. Soc. Am. Spec. Paper No. 36.
[9] C. W. Horton, Am. Assoc. Pet. Geol. Bull., **28**, No. 11, p. 1635 (1944).

assumption that the source of NaCl is seepage along the fault-plane mentioned above is very probable. If this assumption be true, the distribution of NaCl can be explained by diffusion provided an "effective coefficient of diffusion" of 150 cm²/day be admitted. The great excess of this 150 cm²/day over the normal value of ½ to 1 cm²/day would seem, therefore, to argue for the existence of some NaCl-transport mechanism other than diffusion, a mechanism which is presumably convection currents.

If this interpretation of the NaCl distribution is correct, it may be tentatively concluded (a) that convection currents exist in the Woodbine sand west of the Mexia Fault zone, and (b) that Eq. (26) predicts excessive temperature-gradients for the existence of convection currents when applied to subterranean sand-layers.

Pigment Dispersion Methods for Electron Microscopy

H. C. O'Brien, Jr.
*St. Joseph Lead Company, Monaca, Pennsylvania**
(Received February 12, 1945)

A method of preparing a pigment dispersion for electron microscopy is described, wherein the pigment, such as zinc oxide, is first wet with water and is then dispersed in a solution of cellulose acetate. Another method is described in which mechanical or chemical damage of the particles is avoided by the use of an electrostatic dispersion apparatus.

A NUMBER of various types of pigment dispersion methods are now in use for electron microscopy. Certain fine powdered materials are successfully dispersed in water from which they may be settled out upon the surface of the conventional collodion membranes of specimen screens by drying. In the majority of instances, however, the surface tension effects upon the drying of water suspensions tend to agglomerate the material in clumps as the concentration increases by evaporation. Several wetting and dispersing agents have been employed to combat this effect, but none is very satisfactory. Almost all of these materials contain some non-volatile constituents which, in sufficient amounts, may remain to mar the particle outlines and haze the film.

The effect of agglomeration of pigment particles on drying of the suspension is not limited to the use of water, but also occurs with most non-aqueous materials such as the commonly used 2 percent collodion in amyl acetate. Fuller, Brubaker, and Berger[1] have effectively removed this difficulty by using, as described in their pigment mounting technique, the solvent, isopropyl acetate.

Suitable cellulose acetate solvents having the proper characteristics are scarce. It would appear that one important property of isopropyl acetate is that it has a many-fold water tolerance over amyl acetate. It has been found that 2-nitropropane in combination with a small percentage of acetone which has infinite water tolerance may be used with some success. Further we have found that a continuous film of cellulose acetate may be formed including particles of pigment which are actually dispersed in water. The advantages of such a technique are apparent in considering the lyophilic nature of most pigments. In this technique .01 gram of pigment is placed upon a clean glass plate. Just sufficient

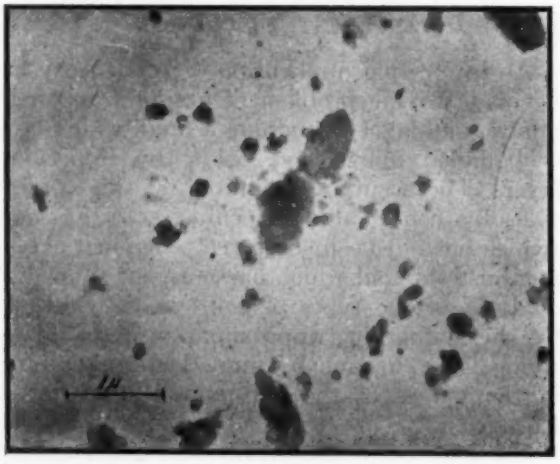

FIG. 1. Film including clay dispersion, methyl ethyl ketone method.

* Buhl Foundation Research Project, University of Pittsburgh.

[1] M. C. Fuller, D. G. Brubaker and R. W. Berger, J. App. Phys. 15, 201 (1944).

1 percent STABLEX-B (a latex stabilizer) in distilled water is added to form a paste. This is worked with a spatula until the pigment is dispersed. Several drops of methyl ethyl ketone containing 1 percent castor oil are added and worked with the spatula. This solvent has a water tolerance of eight times that of isopropyl acetate. Two drops of jellied cellulose acetate in methyl ethyl ketone are then added and the paste further worked with the spatula. Several cc of methyl ethyl ketone solvent are then added and worked until a smooth suspension is obtained. A drop of this is then cast upon water. The film formed may be somewhat uneven, but is continuous and the proper areas for screens may be chosen by the technician (Fig. 1). The castor oil is added as a plasticizer to strengthen the film of cellulose acetate and to increase the wetting of such pigments as zinc oxide (Fig. 2). The film produced with castor oil has elasticity and is much less brittle than without. Films made up in this manner, including water dispersions, seem to be less affected by electrostatic charging. Successful dispersions of many materials may also be made without the 1 percent STABLEX-B solution. In such case, the castor oil may be used, independent of the methyl ethyl ketone, as a wettant in the first step of the procedure.

When pigment preparations are desired to demonstrate particle form that would be broken up by mulling or the less severe work of a spatula some method other than liquid dispersion and inclusion in a film is required. While inclusion may restrain the movement of particles by electron bombardment the surrounding film somewhat decreases the resolution. It also obviously precludes the possibility of dispersing particles with coatings or foreign material which might be soluble in the film forming materials. While good dispersions may not be obtained, in order to demonstrate such pigments, air, or electrostatic dusting methods have been tried.[2]

FIG. 2. Zinc oxide demonstrated by the methyl ethyl ketone method.

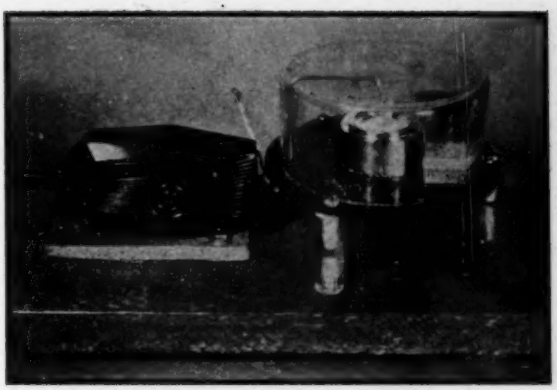

FIG. 3. Vibrator and pigment dusting machine.

Since electrostatic dusting is the more effective, experiments were made upon the effect of a continuous-wave, high voltage, alternating current on pigment particles. Adjustable, horizontal, pinhead electrodes, insulated by polystyrene, were set up on a microscope stage. Pigment was dusted on one electrode after placing a film of rubber over the metal and a 60-cycle a.c. voltage was applied across the electrodes. The powder dusted on the rubber film was observed under low power of the ordinary microscope while the voltage was slowly increased by means of a variable transformer. When the induced voltage on any particle exerted sufficient force, the particle would repel from the rubber. In this type of dusting an interchange of many particles occurred between the electrodes. A relation was found to exist between the size of the particle and the voltage necessary to disturb it. When the voltage was increased to 10,000, large agglomerates were thrown about as readily as the smaller particles.

A dispersion device utilizing the principle of this observation was constructed. It consists of a high voltage transformer and variable control auto transformer which furnish 0 to 10,000 volts (60 cycle) a.c. A relay is placed in the secondary circuit to turn off the power in case an arc or short should occur. The dispersion chamber (Fig. 3) consists of a 4½″ diameter, 2″ deep, inverted glass beaker resting upon a Bakelite

[2] W. A. Ladd, Columbian Carbon Company.

FIG. 4. Surface coating calcium carbonate illustrated by electrostatic method.

form. In the center of the platform a brass cup with inclined walls forms one electrode; while

FIG. 5. Zinc oxide demonstrated by the electrostatic method.

extending partially into the concavity of the bottom electrode, a metallic vibrating button, about $\frac{1}{4}''$ in diameter, forms the other. The button is soldered onto a wire rod which is powered at 7200 vibrations per minute by an a.c. electromagnet outside the chamber. Within the brass bottom electrode is a methyl methacrylate resin, concave, pigment chamber. The insulation of this cup permits a more intense field without arcing and subsequent ionization and decharging of the pigment particles.

In operation, pigment is placed within the insulating cup and the voltage applied slowly to a predetermined value. The vibrating button is turned on and the oxide begins to dust within the chamber. The vibrator changes the field area and intensity, vibrating somewhat horizontally as well as vertically. This keeps the oxide agitated, actually breaks up some of the large agglomerates, and helps create air currents within the chamber. The dispersed dust is collected on films on 200-mesh screens placed upon a plastic platform. The platform is mounted on sponge rubber to reduce vibration and is placed within the chamber next to the brass cup. When the voltage is kept to a correct minimum, a satisfactory specimen is obtained (Fig. 4).

The advantages of this type method are: the negligible amount of work done on the pigment, the removal of the danger of contamination and chemical action from solvents, plasticizers and dispersing media, the simplicity and ease of control of the forces involved, and the fact that the sample particles lie on and not within the cast film, which permits a sharper resolution (Fig. 5).

Acknowledgment is made of the helpful cooperation of the Buhl Foundation.